Multi-skyrmion solutions of a sixth order skyrme model

Floratos, Ioannis

Multi-Skyrmion Solutions of a Sixth Order Skyrme Model

Ioannis Floratos

Centre for Particle Theory

Department of Mathematical Sciences

A Thesis presented for the degree of Doctor of Philosophy

at the University of Durham

England

August 2001

Dedicated to my parents, Ketty and Giorgos, and to my brother, Dionysis

Multi-Skyrmion Solutions of a Sixth Order Skyrme Model

Ioannis Floratos

Ph.D. Thesis, August 2001

Abstract

In this Thesis, we study some of the classical properties of an extension of the Skyrme model defined by adding a sixth order derivative term to the Lagrangian.

In chapter 1, we review the physical as well as the mathematical motivation behind the study of the Skyrme model and in chapter 2, we give a brief summary of various extended Skyrme models that have been proposed over the last few years. We then define a new sixth order Skyrme model by introducing a dimensionless parameter λ that denotes the mixing between the two higher order terms, the Skyrme term and the sixth order term.

In chapter 3 we compute numerically the multi-skyrmion solutions of this extended model and show that they have the same symmetries with the usual skyrmion solutions. In addition, we analyse the dependence of the energy and radius of these classical solutions with respect to the coupling constant λ. We compare our results with experimental data and determine whether this modified model can provide us with better theoretical predictions than the original one.

In chapter 4, we use the rational map ansatz, introduced by Houghton, Manton and Sutcliffe, to approximate minimum energy multi-skyrmion solutions with $B \leq 9$ of the $SU(2)$ model and with $B \leq 6$ of the $SU(3)$ model. We compare our results with the ones obtained numerically and show that the rational map ansatz works just as well for the generalised model as for the pure Skyrme model, at least for $B \leq 5$.

In chapter 5, we use a generalisation of the rational map ansatz, introduced by Ioannidou, Piette and Zakrzewski, to construct analytically some topologically non-trivial solutions of the extended model in $SU(3)$. These solutions are spherically symmetric and some of them can be interpreted as bound states of skyrmions. Finally, we use the same ansatz to construct low energy configurations of the $SU(N)$ sixth order Skyrme model.

Contents

Declaration

This thesis summarises the research work carried out by the author from May 1998 to July 2001 at the Centre of Particle Theory at the Department of Mathematical Sciences of the University of Durham, England. No part of this thesis has been submitted for any other degree in this or any other University.

Chapter 1 and sections 2.1 and 2.2 of chapter 2 serve as introductory material for which no claim of originality is made. The remainder of chapter 2 and chapters 3, 4 and 5 are believed to be original work, unless stated. Section 2.3 of chapter 2 and chapters 3 and 4 originate from *'Multi-Skyrmion Solutions for the Sixth Order Skyrme Model'* [1] which was written in collaboration with B. Piette. Chapter 5 is based on *'Spherically Symmetric Solutions of the 6th Order $SU(N)$ Skyrme Models'* [2] which was also written in collaboration with B. Piette.

Acknowledgements

I wish to take this opportunity to thank all the people who have helped at various stages, and in many different ways, in the preparation of this thesis.

First of all, I am indebted to my supervisor, Dr Bernard Piette, for his guidance and support during my four year stay in Durham. I would also like to thank him for his encouragement and patience, especially in the early stages of my research.

I am also grateful to my parents and to my brother. Their constant moral and financial support has been invaluable to me and without it I would have been unable to complete my studies.

My special thanks go also to Prof. Wojtek Zakrzewski for many fruitful discussions, Prof. D. Ghikas for help and guidance, and everyone that I had the pleasure to work with. In no order of preference: Tom, Nuno and the rest of the topological solitons group, Christos Charmousis for endless debates on mathematics and football, Sharry for everything, Lars for arguments on operating systems, Imran, Linda, Matt, Vinay, Stuart, Clare, Medina, Anastasia, Babis, Steve, Apostolis and all the people of the CPT group in Physics and Maths. I also acknowledge the Department of Mathematical Sciences for travel grants.

I am also grateful to Katelia Vassiliou for turning a broad mathematical text into a readable document and for endless corridor discussions.

As my housemate for two years, fellow physicist and above all friend for nine long years, George Tzamtzis deserves my special gratitude.

These acknowledgments would not have been complete without my thanking also Panos P., George S. (for midnight sessions), Thani & Matthew, Christos S. for all the morning coffee breaks, Dimitris S., Leonidas, Andreas A., Andreas P., Eleana, Kostas V., the Founder and the rest of the Hellenic Society for making my stay in Durham as enjoyable as possible.

Chapter 1

Solitons in particle physics

1.1 Introduction and outline

In the past few decades, particle physics has undergone a series of major developments that have drastically changed our understanding of the fundamental laws that govern Nature. In particular, experiments at high energies have revealed the existence of new particle states, resulting in a different picture of the subatomic world. Quarks and leptons are now considered as the building blocks of matter, whereas particles like the proton or neutron, which were previously regarded as elementary, are now believed to have a structure and to consist of quarks. Parallel to that, it has been realised that within the theoretical framework the dynamics of these particles can be described by quantum field theories that exhibit local gauge symmetries. The successful application of these ideas not only resulted in a correct quantum theory for electromagnetism (QED), but also enabled us to unite electromagnetic and weak interactions into one theory, the *electroweak model*, bringing new interest into the possible unification of the four forces. In addition, the use of mathematical tools like perturbation theory and renormalisation group, has provided us with a way to compare theoretical predictions with experiment, both qualitatively and quantitatively. As a result of this progress, quantum field theory is now firmly established as the appropriate mathematical language to describe particle interactions.

Recently, there has been increasing interest in the study of quantum field theory beyond the perturbation scheme. Non-trivial classical solutions, such as instantons, monopoles and solitons, are now considered as an important class of objects that have found many applications not only in particle physics, but in other areas like condensed matter physics. Among others, an idea that has attracted a lot of attention, is the possible description of particles, in particular nucleons, as topological

solitons. The foundations of this idea were placed by T.H.R. Skyrme [3] almost forty years ago, although at that time his suggestions were greeted with great scepticism. Skyrme's original motivation was to describe nucleons as extended objects rather as point-like ones. For this purpose he proposed a non-linear theory for nuclear interactions where particles like the proton emerge as topological solitons.

In general, integrable solitons are defined in the literature as waves of non linear character with localized finite energy. They are solutions of non-linear partial differential equations and they have particle-like behaviour, *i.e.* they interact strongly with each other but they continue to retain their identity after every interaction. This, and other remarkable properties of these solutions, originate from a number of conservation laws that characterise such non-linear theories. In a similar manner, topological solitons also behave as particles and their stability is due to their non-trivial topology. They are also characterised by the conservation of the so-called topological charge. Skyrme's ingenious suggestion was to identify this topological charge with the baryon number, a quantum number that was introduced to particle physics by experimental observations, but for which there has been no satisfactory theoretical explanation for its conservation.

Despite the above attractive features of the Skyrme model, this theory has been largely overshadowed by the success of pertubative gauge field theories. In recent years, however, after the realisation that nuclear interactions can be considered the low energy limit of strong interactions, there has been a renewal of interest in the Skyrme model. In particular, Quantum Chromodynamics (QCD), the theory that describes strong interactions, is of a non-perturbative character at the low-energy regime and hence, different mathematical methods are required for its study. As it has been shown recently [4, 5, 6], QCD simplifies greatly under certain approximations and the resulting effective theory surprisingly resembles the Skyrme model. This revived Skyrme's suggestions and to the present day the Skyrme model has been established as the strongest candidate for the low energy limit of QCD.

There are, however, reasons to believe that the Skyrme model is the simplest effective theory that one can consider. Its phenomenological predictions are within 30% accuracy [7] and to improve them, various extended Skyrme models have been proposed [8, 9, 10, 11, 12, 13]. In what follows we will explore these ideas further. Our investigation starts with a brief summary of the physical motivation that lies

behind the study of the Skyrme model. We then present the Skyrme model and its properties in greater detail. This will provide us with the necessary background for the next chapters.

In chapter 2 we review the most characteristic extended Skyrme models that have been studied over the last few years. We then define a new sixth order Skyrme model that we study in the remainder of this thesis. In the same chapter we also introduce the physical quantities that we will help us determine the quality of our model's theoretical predictions. In chapter 3 we study multi-skyrmion solutions of the sixth order Skyrme model and discuss their symmetries and some of their classical properties [1]. We argue that the only possible way to obtain these solutions is by using advanced numerical methods. Our results show that our extended model has similar properties to the original Skyrme model. However, when we compare these results with the experimental values, we find that in some cases the sixth order Skyrme model provides us with better theoretical predictions than the original model. In chapter 4 we use a different, semi-analytical approach and we approximate the solutions of the model using the rational maps ansatz that has been recently introduced by Houghton et al. [14] and the harmonic map ansatz introduced by Ioannidou et al. [15]. The results of this chapter are compared with the numerical solutions of chapter 3 and we show that this ansatz works quite well, and in some cases even better for the extended Skyrme model [1]. Finally, chapter 5 explores the possibility of constructing analytically exact solutions in $SU(N)$ that have spherical symmetry [2]. We find that this construction only works for the $SU(N)$ Skyrme model and for the $SU(3)$ extended model. Nevertheless, we show that by using a generalisation of the harmonic map ansatz, one can still construct low energy configurations of the $SU(N)$ sixth order Skyrme model which correspond to bound states of skyrmions.

1.2 Low energy limit of QCD

In this section we review some of the most important ideas that have led to the establishment of the Skyrme model as the strongest candidate theory for the low energy limit of strong interactions. For this purpose, we will follow closely Witten's approach [5] (for a brief summary see also chapter 9 of [16]).

1.2.1 QCD formalism

Initially, nuclear (or strong) interactions were thought to involve protons and neutrons, *i.e.* nucleons, and they were considered responsible for the binding of the nuclei. However, experiments revealed that nucleons are just the lightest among a spectrum of particles which are now called *baryons*. Moreover, as we have mentioned previously, it has been shown experimentally that all these particles, including the proton and the neutron, have rich internal structure and can no longer be considered as elementary. Hence, it became evident that a different, more fundamental theory was needed in order to explain all these results.

In 1964 Gell-Mann and Neeman [17] introduced a model where baryons can be interpreted as bound states of three elementary particles, called *quarks*. They assumed that these particles are fermions, *i.e.* they have spin one half, and in order to explain the full spectrum of baryons known at that time, they considered three different types (*flavours*) of quarks: up (u), down (d) and strange (s). Recent experimental discoveries revealed the existence of another three flavours: charm (c), bottom (b) and top (t). In this context the proton and the neutron can be thought of as bound states of uud and udd respectively. Since we traditionally describe baryons as particles with integer electric charge, we have to assume that quarks have fractional electric charge. Moreover, the carriers of the nuclear force, which we refer to as *mesons*, can be considered as bound states of one quark and one anti-quark ($q\bar{q}$). This description is compatible with the experimental picture where these particles obey Bose-Einstein statistics, *i.e.* they have integer spin.

The quark model had enormous success in the interpretation of the spectrum of baryons and mesons. It also managed to predict correctly the existence of heavier particles which were later discovered experimentally. However, it created one serious theoretical problem. The Δ^{++} state, with electric charge $+2$ and spin $3/2$, was considered as a bound state described by three identical quarks, namely uuu. Since Δ^{++} has zero orbital angular momentum, the three quarks all have parallel spins and there are indistinguishable. As a result, we have an undesired violation of the Pauli principle. A solution to this problem was given [18, 19] with the introduction of a new quantum number called *colour*. In the simplest case, one can assume that quarks are characterised by three primary colours: red, green and blue. By assigning a different colour label to each u quark in the Δ^{++} state, we can avoid

the violation of the Pauli principle. In addition, since this quantum number is unobserved experimentally, we require that all baryons are colour singlets, *i.e.* their are colourless. The introduction of colour is equivalent to the assumption that the quark fields exhibit a local gauge symmetry, namely $SU(3)_c$. This is similar to Quantum Electrodynamics where the charged fermionic fields are described by the Lagrangian

$$L_{QED} = \bar{\psi}(i\gamma^\mu D_\mu - m)\psi - \frac{1}{4}F_{\mu\nu}F^{\mu\nu}. \tag{1.1}$$

The covariant derivative D_μ is defined using the gauge field A_μ as

$$D_\mu\psi = (\partial_\mu - ieA_\mu)\psi, \tag{1.2}$$

where e is the electric charge, *i.e.* the coupling constant of electromagnetic interactions, and

$$F_{\mu\nu} = \partial_\mu A_\nu - \partial_\nu A_\mu. \tag{1.3}$$

The Lagrangian (1.1) is invariant under $U(1)$ gauge transformations, *i.e.* transformations of the type $\psi \to e^{ia}\psi$.

The colour hypothesis solves many theoretical problems in its description of quarks as fields which are symmetric under transformations of the $SU(3)_c$ group. However, there a few important phenomenological questions that need to be answered. Firstly, there is no experimental evidence of free quark states. Thus, a correct theory for strong interactions must somehow confine quarks into baryons. Secondly, experiments revealed that, quite surprisingly, quarks behave as if they were free at short distances. In other words, strong interactions are weak at high energies. This last property, which is referred to in the literature as *asymptotic freedom*, seemed to create serious obstacles to the theoretical visualisation of strong interactions. However, when it was proven [20, 21, 22, 23] that theories with non-Abelian local gauge symmetries, like $SU(3)_c$, are asymptotically free, it became evident that quark fields can be thought of as representations of the groups $SU(3)_c$ and $SU(N_f)$ where N_f is the number of flavours. Thus, in analogy to QED, strong interactions or Quantum Chromodynamics (QCD), can be formulated by the Lagrangian

$$L_{QCD} = \sum_\alpha \bar{q}_a^\alpha(i\gamma^\mu D_\mu - m_\alpha)q_a^\alpha - \frac{1}{4}G_{\mu\nu}G^{\mu\nu}, \tag{1.4}$$

where $\alpha = 1, .., N_f$ is the flavour index, $a = 1, 2, 3$ is the colour index and m_α is the quark mass. The covariant derivative D_μ is now given by,

$$D_\mu q_a^\alpha = \left(\delta_{ab}\partial_\mu - ig(\frac{\lambda_i}{2})_{ab}A_{\mu i}\right) q_a^\alpha, \tag{1.5}$$

where λ_i are the Gell-Mann matrices and g is the colour coupling constant. Moreover,

$$G^i_{\mu\nu} = \partial_\mu A^i_\nu - \partial_\nu A^i_\mu + g\, f^{ijk} A^j_\mu A^k_\nu, \tag{1.6}$$

where f^{ijk} are the structure constants of the $SU(3)_c$ symmetry group. The Lagrangian (1.4) describes the propagation of massive quarks q_a^α and the interactions between them. The quanta of these interactions are massless and they are called *gluons*. However, in contrast to QED where the carriers of the electromagnetic interactions, the photons, have no electric charge, the gluons have colour and hence, they can be considered as self-interacting fields.

QCD is, at the moment, at the frontier of high energy particle physics. Although it manages to bring together a number of interesting ideas, it is still a very complicated theory and is very difficult to treat systematically. Since a detailed discussion of these topics goes beyond the main subject of this thesis, we will not go into further details. Instead, we will refer the reader to general bibliography like [24, 25, 26, 27] and references therein. In what follows, we will only concentrate on the possible applications of the Skyrme model in connection to QCD.

1.2.2 The $1/N_c$ expansion of QCD

As we have mentioned in the previous section, QCD is an asymptotically free theory, *i.e.* the strong coupling constant g is small at high energies – or equivalently at short distances – and hence, it is possible to apply perturbation theory to extract qualitative results. However, at low energies – the regime that interests us – g is large and it can no longer be used as an expansion parameter. In fact, in this limit, QCD is a zero parameter theory and conventional perturbation theory does not work. In the absence of an obvious free parameter, one has to look for a 'hidden' parameter that can be used for a perturbation expansion. For this purpose one can consider quantities that are normally fixed to a specific value, like the space time dimensions. Such methods have been known to work quite well for problems

that appear in Atomic or Statistical Physics. Before we illustrate how they can be applied to QCD, let us first consider a simple example that we find instructive and was first discussed by Witten [28].

In Atomic Physics, the hydrogen atom is described by the Hamiltonian

$$H = \frac{p^2}{2m} - \frac{e^2}{r}. \tag{1.7}$$

In general, one can derive the ground state energy using perturbation expansion around the potential energy. However, this method cannot be used in the case of the Hamiltonian (1.7) since the parameter e^2 in the potential $V = -e^2/r$ cannot be characterised as small. The reason is that e has dimensions and its value depends on our choice of units. This can be made clearer if we consider the following transformation $r \to r/me^2$ and $p \to p \cdot me^2$. Then (1.7) is given by

$$H = m\,e^4 \left(\frac{p^2}{2} - \frac{1}{r}\right). \tag{1.8}$$

We see that the parameter e^2 is now scaled out as an overall factor and the hydrogen atom can be equally described by the parameter-free Hamiltonian

$$\tilde{H} = \left(\frac{p^2}{2} - \frac{1}{r}\right). \tag{1.9}$$

Hence, in the absence of an obvious expansion parameter, one has to look for an implicit one and in the case of the hydrogen atom the most suitable candidate is the number of dimensions. In particular, if we assume that the Hamiltonian (1.7) describes a system in N dimensions instead of 3, then the Schrödinger equation for the wavefunction $\psi = \psi(r)$ will read

$$\left[-\frac{1}{2m}\left(\frac{d^2}{dr^2} + \frac{N-1}{r}\frac{d}{dr}\right) - \frac{e^2}{r}\right]\psi(r) = E\psi(r). \tag{1.10}$$

Under the transformation $\psi \to r^{-(N-1)/2}\psi$ equation (1.10) becomes

$$\left[-\frac{1}{2m}\frac{d^2}{dr^2} + \frac{(N-1)^2}{8m\,r^2} - \frac{e^2}{r}\right]\psi(r) = E\psi(r), \tag{1.11}$$

and by rescaling r as: $r = (N-1)^2 r'$, we have

$$\frac{1}{(N-1)^2}\left[-\frac{1}{2m(N-1)^2}\frac{d^2}{dr'^2} + \frac{(N-3)}{8m(N-1)\,r'^2} - \frac{e^2}{r'}\right]\psi(r') = E\psi(r'). \tag{1.12}$$

Equation (1.12) describes a particle that has effective mass $m_{eff} = m(N-1)^2$ and moves in the effective potential

$$V_{eff} = \frac{N-3}{N-1}\,\frac{1}{8\,m\,r'^2} - \frac{e^2}{r'}. \tag{1.13}$$

For large N the effective mass m_{eff} becomes significantly large and we can reasonably assume that the particle is located at the absolute minimum of the effective potential. In other words, the energy of the ground state will be

$$E = -\frac{1}{2}me^4 \frac{4}{(N-1)^2}. \tag{1.14}$$

For $N = 3$ we have that $E = -\frac{1}{2}me^4$ which is the expected result for the minimum energy of the hydrogen atom.

Having demonstrated the idea of using implicit parameters in order to obtain correct qualitative results in a parameter-free theory, let us return to QCD which is our primary interest. As we have mentioned previously, in the low-energy limit, QCD does not have any parameter that can be used for a perturbation expansion. However, as 't Hooft indicated [4], one can generalise QCD from 3 to N_c number colours and consider the $SU(N_c)$ gauge theory. In the large N_c limit, QCD simplifies greatly and it is possible to perform an expansion in powers of $1/N_c$. Like in the simple example of the hydrogen atom, one hopes that the resulting theory might be qualitatively and quantitatively close to the $N_c = 3$ theory.

Let us give a brief review of the results obtained under the large N_c approximation by starting from a typical low order Feynman diagram that describes the gluon contribution to the one-loop gluon vacuum polarization [5] and it is shown in Figure 1.1.

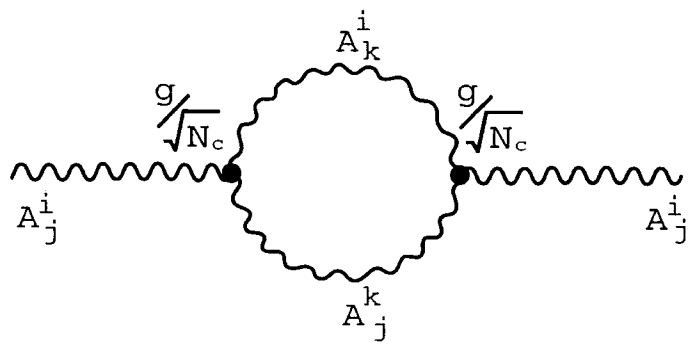

Figure 1.1: Gluon contribution to the one-loop gluon vacuum polarisation. The gluon field A^i_j has one upper colour index like the quark field q^i and one lower colour index like the anti-quark field $\bar{q}_j$.

By observing Figure 1.1 carefully, it is easy to see that the internal gluon loop is

independent of the initial and final states, even where these are specified. As a result, we will have N_c different possibilities of the intermediate contribution, introducing a factor of N_c in the diagram. Another factor associated with this Feynman diagram comes from the interaction vertices, *i.e.* the points where a gluon state is separated into two gluons or two gluons are united into one state. Each vertex has a coupling constant factor and since the diagram in Figure 1.1 has two vertices, we will have a factor equal to the square of the coupling constant. If we want QCD to have a smooth limit for $N_c \to \infty$ then we must choose the coupling constant to be $g/\sqrt{N_c}$. The combination of all the factors associated with the Feynman diagram of Figure 1.2 gives: $N_c\,(g/\sqrt{N_c})^2 = g^2$ which is independent of the number of colours.

One of the most important results of this approximation is that a certain class of diagrams, the so-called planar diagrams, are the only ones that 'survive' for large N_c whereas all the remaining diagrams vanish. To illustrate this, let us consider two higher order Feynman diagrams which are shown in Figure 1.2.

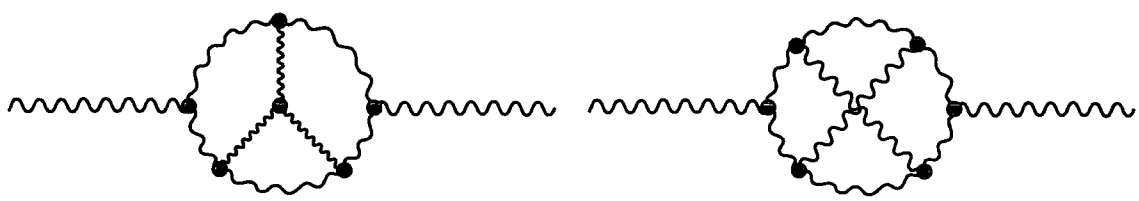

(a) (b)

Figure 1.2: Planar (a) and non-planar (b) Feynman diagrams.

Each diagram in Figure 1.2 has six vertices which contribute a factor of $(g/\sqrt{N_c})^6$. The left diagram (Figure 1.2.a) has three closed colour loops which are self-contracted and thus, they contribute a total factor of N_c^3. As a result, the diagram 1.2.a is of order $N_c^3(g/\sqrt{N_c})^6 = g^6$ and it is independent of N_c. On the other hand, the right diagram of Figure 1.2 has only one large closed colour loop that contributes a factor of N_c. This diagram is called non-planar as it is impossible to draw it on the plane without line crossings. The total factor of the non-planar diagram is $N_c(g/\sqrt{N_c})^6 = g^6/N_c^2$ and it vanishes like $1/N_c^2$ for large N_c.

Hence, we have obtained the first 'selection' rule for the large N_c approximation

of QCD: Non-planar diagrams are suppressed and the only non-vanishing diagrams are the planar ones, *i.e.* diagrams like Figure 1.2.a.

A second 'selection' rule concerns Feynman diagrams that involve quark loop contributions to the gluon propagator. For instance, consider the diagram shown in Figure 1.3. Unlike Figure 1.1, diagrams of the type 1.3 do not have any closed colour

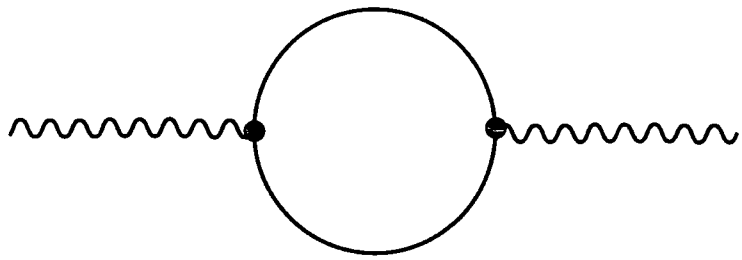

Figure 1.3: One quark loop contribution diagram to the gluon propagator.

loops and because they have two vertices, they are of order $(g/\sqrt{N_c})^2 = g^2/N_c$. We therefore conclude that diagrams with internal quark loops are also suppressed.

All the above results can be summarised in the following statement: For large N_c the dominant diagrams are the planar diagrams with only one quark loop which runs to the edge of the diagram, *i.e.* it is not an internal quark loop. The summation of these diagrams is equivalent to deriving an exact solution for QCD at low energies and clearly this is a very difficult problem. However, a few qualitative results can be extracted from the low energy limit of QCD. In particular, as it has been suggested by 't Hooft [4] and Witten [5], for $N_c \to \infty$, mesons are free, stable and non-interacting. Their decay amplitudes are of order $1/\sqrt{N_c}$, whereas the meson-meson scattering amplitudes are of order $1/N_c$. To find these amplitudes one needs to perform a summation over tree diagrams which involve physical mesons and not quarks and gluons [5].

Another important observation made by Witten [5] is that for large N_c, QCD can be regarded as a weakly coupled field theory of mesons. Such theories sometimes exhibit additional states whose masses diverge like $1/c$ where c is a weak coupling constant. These states are topological solitons and the most typical example of them is the 't Hooft-Polyakov monopole that was found to exist as a solution of non-Abelian gauge theories. In a similar manner, in the large N_c approximation of

QCD, baryons have mass of order N_c, which can be rewritten as $1/(1/N_c)$. Since $1/N_c$ is the 'coupling constant' of QCD for interactions among mesons, we can assume that baryons are the topological solitons of QCD at low energies. This last qualitative result is responsible for the revival of the Skyrme model as the simplest candidate theory for an effective low energy limit of QCD.

Besides Witten's observation, Skyrme's ideas have found additional support in later efforts to derive an effective mesonic Lagrangian directly from QCD [1]. In particular, by assuming spontaneous chiral symmetry breaking and by using functional integration methods and the large N_c diagramatic analysis, the following effective Lagrangian has been obtained

$$L_{eff}(U) = -\frac{F_\pi^2}{16} Tr(L_\mu L^\mu) + L_{WZ} + V_0, \tag{1.15}$$

where $F_\pi = \sqrt{N_c} f_\pi$ is the pion decay constant, L_{WZ} is the Wess-Zumino term which is proportional to

$$L_{WZ} \propto \epsilon^{\mu\nu\lambda\rho\sigma} Tr(L_\mu L_\nu L_\lambda L_\rho L_\sigma), \tag{1.16}$$

and $L_\mu = U^{-1}(\partial_\mu U)$ is the left chiral current. The first term in (1.15) is the simplest chiral Lagrangian and is referred to in the literature as the *non-linear σ model.*

The potential V_0 implies an expansion in powers of the chiral currents, resulting in terms of order four and higher in L_μ. It turns out that in the lowest order approximation the additional term coming from V_0 is the term that Skyrme has used in his effective meson Lagrangian. However, the determination of the exact form of V_0 requires the summation of all planar diagrams in the $N_c \to \infty$ approximation and as previously mentioned, to the present day this is an unresolved problem.

Let us close our review of the physical motivation behind the study of the Skyrme model by noting that the effective Lagrangian (1.15) suggests that the Skyrme model is the simplest candidate low energy theory of QCD and by extending it to higher orders it is possible to improve its predictions. In the following chapters we will explore such generalisations in further detail.

[1] For further details see section 9.3 of reference [16] and references therein.

1.3 The Skyrme model

In the previous section we presented the theoretical developments in particle physics that have led to the revival of Skyrme's suggestions. In this section we would like to pay tribute to the Skyrme model itself and expose its most important properties by mainly focusing on the mathematical motivation behind the study of such models.

1.3.1 The sine-Gordon model in (1+1) dimensions

Studying the dynamics of non-linear field theories like the Skyrme model is a highly non-trivial task since it is very difficult to obtain exact solutions, even at a classical level. In general, it is common practice in physics, as well as in mathematics, when one is dealing with such complicated models, to consider first a reduced version of the problem in fewer dimensions. This approach has often provided us with a qualitative insight of the properties that characterise the full theory. In our case, a very useful toy model, that can be classically solved exactly, is the sine-Gordon model which is the (1+1) dimensional analogue of the Skyrme model.

The sine-Gordon model is described by the Lagrangian

$$\mathcal{L}_{SG} = \frac{1}{2}\left[\left(\frac{\partial}{\partial_t}\phi\right)^2 - \left(\frac{\partial}{\partial_x}\phi\right)^2\right] - (1-\cos\phi), \tag{1.17}$$

where the angular variable ϕ is $\phi = \phi(x,t)$. For a fixed time t, the classical field corresponds to mappings from $\mathbb{R}^1 \mapsto S^1$. From (1.17) we obtain the following Euler-Lagrange equation

$$\left(\frac{\partial^2}{\partial_t^2}\phi\right) - \left(\frac{\partial^2}{\partial_x^2}\phi\right) + \sin\phi = 0, \tag{1.18}$$

which is referred to as the sine-Gordon equation. This equation has various types of solutions. Since we are interested in solutions with finite energy we require that ϕ satisfies the following boundary conditions

$$\phi(x,t) \to 0(\mathrm{mod}2\pi), \qquad \text{when} \qquad |x| \to \infty. \tag{1.19}$$

The energy for any given field configuration is

$$\mathcal{E} = \int_{-\infty}^{+\infty} dx \left[\frac{1}{2}\left(\frac{\partial}{\partial_t}\phi\right)^2 + \frac{1}{2}\left(\frac{\partial}{\partial_x}\phi\right)^2 + (1-\cos\phi)\right]. \tag{1.20}$$

In the simplest case we can assume that ϕ takes the same value, say zero, at $x = \pm\infty$. In this case, a non-trivial solution for the sine-Gordon equation, which satisfies the boundary (1.19), has the form [29]

$$\phi(x,t) = 4 \arctan\left[\frac{\sqrt{1-u^2}}{u}\frac{\sin(u(t-t_0))}{\cosh(\sqrt{1-u^2}(x-x_0))}\right], \tag{1.21}$$

where u is a real constant with $0 < u < 1$. This class of solutions is the well known breather and its profile is shown in Figure 1.4.

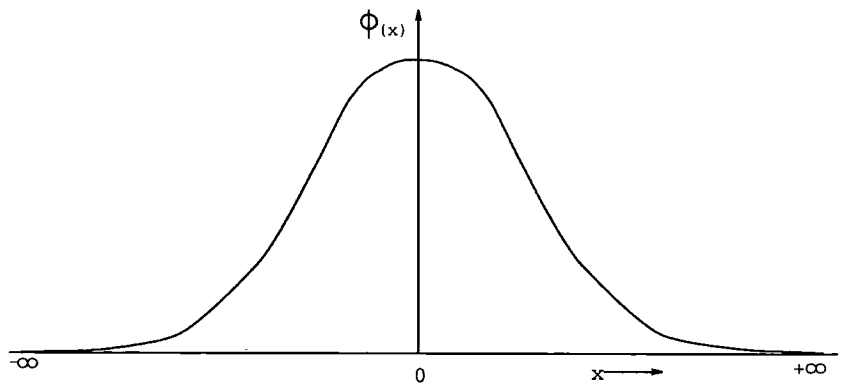

Figure 1.4: Breather solution of the sine-Gordon model for a given t.

However, there is another class of solutions where the field, or equivalently the angular variable $\phi(x,t)$, takes two different values at $\pm\infty$, *i.e.* $\phi(-\infty) = 0$ and $\phi(+\infty) = 2\pi$. In other words, ϕ has two different vacuum states. It is very easy to check that this solution has the form [29, 16]

$$\phi(x,t) = 4 \arctan\left[\exp\left(\frac{(x-x_0)-u(t-t_0)}{\sqrt{1-u^2}}\right)\right], \tag{1.22}$$

where $0 < u < 1$ and its profile is shown in Figure 1.5. This solution is referred to in the literature as the one-soliton or the 2π-kink solution and it describes a localised field configuration at $x = x_0$ which moves without dissipation, *i.e.* without changing shape or size.

The two types of solutions, the breather and the one-soliton solution, cannot be transformed to each other by any continuous deformation. This implies that the solution space of the sine-Gordon equation (1.18), with the boundary conditions (1.19), has distinct components or else classes of solutions. The latter indicates that for the sine-Gordon model there exists a conserved quantity –the topological charge–

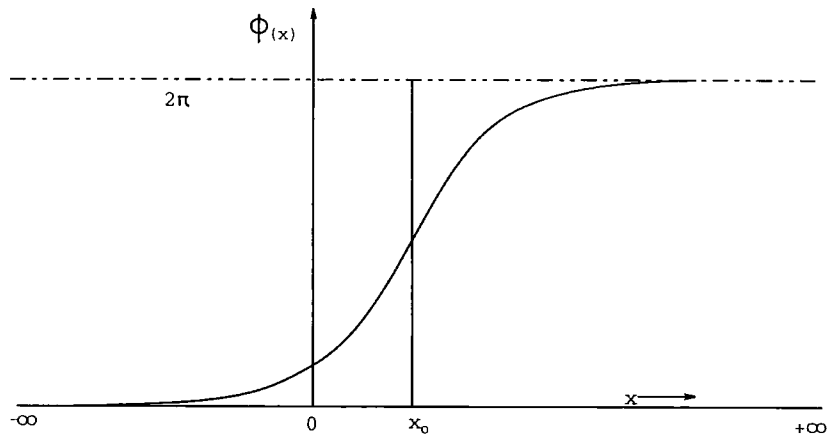

Figure 1.5: One-soliton or 2π-kink solution of the sine-Gordon model for a given t.

that follows from the conservation of a current J^μ with $\mu = 0, 1$. The explicit form of this current is

$$J^\mu = \frac{1}{2\pi}\,\epsilon^{\mu\nu}\,\frac{\partial}{\partial_\nu}\,\phi \tag{1.23}$$

and the conservation law is $\partial_\mu J^\mu = 0$. This implies that for the topological charge $Q(t)$ we have

$$Q(t) = Q(0), \tag{1.24}$$

where $Q(t)$ is given by

$$Q(t) = \int_{-\infty}^{+\infty} dx\, J^0 = \frac{1}{2\pi}\int_{-\infty}^{+\infty} dx \frac{\partial\phi}{\partial x} = \frac{1}{2\pi}\Big(\phi(+\infty, t) - \phi(-\infty, t)\Big). \tag{1.25}$$

An important remark that can be made at this point is that the existence of the current J_μ is not due to the invariance of the Lagrangian (1.17) under any symmetry transformation. Hence, J^μ is not a Noether current.

Let us now classify the solutions of the sine-Gordon model in terms of their topological properties. As we have mentioned previously, any field configuration of the sine-Gordon model at a fixed time t corresponds to mappings from $\mathbb{R}^1$ to S^1. However, under the boundary conditions (1.19), the two points at infinity, *i.e.* $x = \pm\infty$, can be mapped to one single point, the 'north' or 'south' pole of the circle S^1. Hence, we will have that any field configuration will be a map from $S^1 \mapsto S^1$. From expression (1.25) it is easy to see that the topological charge of the breather solution is equal to zero. Topologically this can be simply visualised if we assume

that it describes a closed loop which does not cover the whole S^1 circle.[2] As a result, these maps can be continuously transformed to a single point on S^1 and hence, their topology is trivial.

On the other hand, the one-soliton solution (1.22) has topological charge $Q = 1$. In terms of topology, this solution corresponds to a closed loop that wraps around the whole circle S^1 once and which cannot be transformed under any continuous deformation to a single point on S^1. Thus, it can be characterised as a topologically non-trivial solution.

Finally, it is possible to construct a third type of solution of the sine-Gordon model which is non-static and is also topologically non-trivial. It describes a field configuration with $\phi(-\infty, t) = 0$ and $\phi(+\infty, t) = 4\pi$. The profile of this configuration is shown in Figure 1.6.

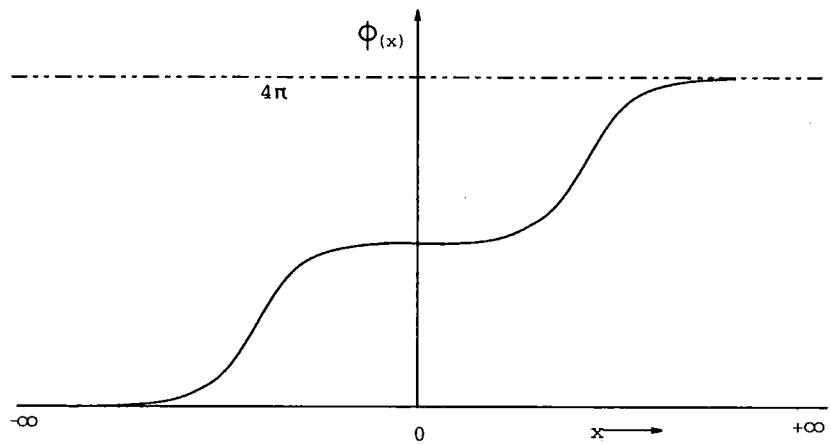

Figure 1.6: Two-soliton or two-kink solution of the sine-Gordon model for a given t.

This solution has topological charge $Q = 2$ and corresponds to maps which wrap around the circle S^1 twice and cannot be continuously transformed either to the breather solution nor to the one-soliton solution.

In general, we can always construct multi-soliton solutions of the sine-Gordon model by adding non-trivial field configurations. For example, if we add two different field configurations with topological charge Q_1 and Q_2 then we obtain a third configuration with topological charge $Q_3 = Q_1 + Q_2$. This last configuration is also a non-trivial solution of the sine-Gordon model, *i.e.* it is a topological soliton. This

[2]Due to the topology of these solutions, the topological charge is often referred to in the literature as the winding number.

implies that the solutions of the sine-Gordon model have particle-like behaviour; their 'quantum' number – the topological charge – is additive and hence, it is possible to have annihilation of solitons. In particular, if we consider a soliton solution ϕ_1: $\phi_1(-\infty) = 0$ and $\phi_1(+\infty) = n\,2\pi$, $n \in \mathbb{N}$, with topological charge Q_1 and the corresponding anti-soliton solution $\bar{\phi}_1$: $\bar{\phi}_1(-\infty) = n\,2\pi$ and $\bar{\phi}_1(+\infty) = 0$ with topological charge $\bar{Q}_1 = -Q_1$ then the addition of these two configurations will give us a soliton with topological charge $Q = 0$ which is just the breather solution.

There is a rather convenient way to summarise all the above results: The set of distinct classes of solutions of the sine-Gordon model, which satisfy the boundary conditions (1.19), forms a group, the *first homotopy group* that we denote as $\pi_1(\Phi)$. This group is an additive group. In other words the set $\{\mathcal{Q}_i\}$ obeys the following composition law

$$\mathcal{Q}_1 \oplus \mathcal{Q}_2 = \mathcal{Q}_3, \tag{1.26}$$

where $\mathcal{Q}_i$ are elements of $\pi_1(\Phi)$, *i.e.* they are distinct classes of solutions and we will refer to them as *homotopy classes.* The additive property (1.26) of $\pi_1(\Phi)$ implies that two different homotopy classes can be added together and give a third homotopy class. Since is can be shown that for the sine-Gordon model, $\pi_1(S^1)$ is isomorphic to $\mathbb{Z}$, this additive action is equivalent to that of simple integer numbers. This isomorphism can be defined through the homotopic variable $\mathbf{Q}$ as

$$\mathbf{Q} : \pi_1(S^1) \mapsto \mathbb{Z}. \tag{1.27}$$

As it can be shown [16] that $\mathbf{Q}$ is equal to

$$\mathbf{Q} = \frac{1}{2\pi} \int_0^{2\pi} d\xi \frac{\partial \phi}{\partial \xi}, \tag{1.28}$$

we have that the homotopic variable $\mathbf{Q}$ is equivalent to the topological charge Q given by (1.25).

1.3.2 Three dimensional Skyrme model

In the light of the non-trivial results obtained for the sine-Gordon model, let us now consider the higher dimensional theory, *i.e.* the Skyrme model in (3+1) dimensions. In its original form [3], the Skyrme model is described by the Lagrangian

$$\mathcal{L}_{Skyrme} = \frac{\epsilon}{4\pi^2}\left(k^2 Tr\,(L_\mu L_\mu) - \frac{1}{2} Tr\,[(L_\mu L_\mu)^2 - (L_\mu L_\nu)^2]\right), \tag{1.29}$$

with the summation convention

$$L_\mu L_\mu = L_0 L_0 - L_i L_i. \tag{1.30}$$

In (1.29), L^a_μ are the left chiral currents and the constants ϵ and k are parameters of the model which can be fitted from experimental data[3]. There exists an equivalent form of the Lagrangian (1.29) that we will use in what follows

$$\mathcal{L}_{Skyrme} = \frac{{F_\pi}^2}{16} Tr(\partial_\mu U \partial^\mu U^\dagger) + \frac{1}{32a^2} Tr[(\partial_\mu U)U^\dagger, (\partial_\nu U)U^\dagger]^2, \tag{1.31}$$

where again F_π and a are the parameters of the model. The first term in (1.31) is the non-linear σ model whereas the second term was introduced by Skyrme and we will refer to it as the fourth order Skyrme term. Moreover, the chiral field U is $U = U(\vec{x}, t)$ and for a fixed time t corresponds to maps $\mathbb{R}^3 \mapsto SU(N_f)$, where N_f is the number of quark flavors. As $SU(N_f)$ is isomorphic to S^3, we will have that

$$U(\vec{x}) : \ \mathbb{R}^3 \mapsto S^3. \tag{1.32}$$

In analogy to the sine-Gordon model, we would like to impose boundary conditions to U so that any field configuration will have finite energy. These conditions are

$$U(\vec{x}, t) \to M \qquad \text{as} \qquad |\vec{x}| \to \infty, \tag{1.33}$$

where M is any constant $N_f \times N_f$ matrix and without loss of generality we can choose it to be the identity matrix I . The boundary (1.33) implies that the space $\mathbb{R}^3$ is compactified to S^3 and hence, $U(\vec{x}, t) : \ S^3 \mapsto S^3$.

Topological charge

Since the corresponding homotopy group of the Skyrme model, $\pi_3(S^3)$, is isomorphic to $\mathbb{Z}$, we will have that each homotopy class, or equivalently each distinct class of solutions, will be characterised by a topological charge, B, that takes integer values. To construct a topological charge associated with a field configuration one can use a general algorithm as proposed by Isham[4]. In the case of the Skyrme model, this topological charge is given by the following expression

$$B = \frac{1}{24\pi^2} \int_{\mathbb{R}^3} d\vec{x} \ \varepsilon^{ijk} \, Tr\Big[(\partial_i U)U^\dagger (\partial_j U)U^\dagger (\partial_k U)U^\dagger\Big]. \tag{1.34}$$

[3]The experimental fitting of these parameters will be shown in detail in the following chapter.

[4]For a review on this construction see section 2.3 of reference [16].

Like in the sine-Gordon model, the topological charge (1.34) does not follow from the invariance of the Lagrangian (1.31) under symmetry transformations and therefore it is not a Noether charge. Instead, the conservation of B is due to the non-trivial topology of the solutions of the Skyrme model.

As we have mentioned previously, Skyrme's suggestion was to interpret the topological charge B as the baryon number. In general, this quantum number has been introduced by particle physicists in order to justify the absence of certain types of interactions among baryons. For instance, if we assume that every baryon is characterised by an integer baryon number B, then decays like

$$p \rightarrow e^{+} \pi_0, \tag{1.35}$$

are forbidden[5]. The conservation of B also implies that since the proton p is the lightest state among baryons, it must be stable against collapse which is in accordance with experimental observations.

Even though the baryon number characterises strong interactions, it has not been possible to relate it to the strong coupling constant g, as it has been done with the electric charge in QED. Hence, the conservation of B does not follow 'naturally' from the invariance of the QCD Lagrangian under local gauge transformations. Skyrme's idea to identify the topological charge of the Skyrme model with the baryon number is quite appealing and until now it is the only theoretical explanation we have for the conservation of B.

The Hobart-Derrick theorem

Let us now examine the stability of the static solitonic solutions of the Skyrme model. To do so we can use the Hobart-Derrick theorem [30, 31] which provides us with a necessary condition for a solution of any field equation to be stable against collapse.

Let $\phi_1(\vec{x})$ be a static solution of an Euler-Lagrange equation derived from the variational principle

$$\delta \Phi[\phi_1] = 0. \tag{1.36}$$

[5]Electrons e^{-}, positrons e^{+} and in general leptons, together with mesons have zero baryon number.

If we consider a scale transformation κ such that

$$\vec{x} \to \kappa\,\vec{x} \qquad \text{and} \qquad \phi_1(\vec{x}) \to \phi_\kappa = \phi(\kappa\,\vec{x}), \tag{1.37}$$

then the variational principle (1.36) reads

$$\delta\,\Phi[\phi_\kappa] = \left.\frac{\partial\,\Phi[\phi(\kappa\vec{x})]}{\partial\kappa}\right|_{\kappa=1} \cdot\,\delta\kappa = 0. \tag{1.38}$$

If we assume that the functional $\Phi[\phi(\kappa\vec{x})]$ is a function of κ, *i.e.* $\Phi = \Phi(\kappa)$, then the condition

$$\left.\frac{d\,\Phi(\kappa)}{d\kappa}\right|_{\kappa=1} = 0, \tag{1.39}$$

ensures the existence of static solutions of the equation (1.36).

Let us now apply this theorem to the non-linear σ model, *i.e.* the first term in the Lagrangian (1.31), which is of order two and has energy given by

$$E_{(2)} = \int d^D x\,\left[-Tr(\partial_\mu U \partial^\mu U^\dagger)\right], \tag{1.40}$$

where we have assumed that the number of dimensions is D. If we consider a scale transformation k of the type (1.37) then it is very easy to check that

$$E_{(2)}(\kappa) = \kappa^{2-D}\,E_{(2)}. \tag{1.41}$$

By applying the Hobart-Derrick theorem, *i.e.* condition (1.39), to the energy functional (1.41) we have

$$\left.\frac{\partial\,E_{(2)}(\kappa)}{d\kappa}\right|_{\kappa=1} = (2-D)E_{(2)} = 0. \tag{1.42}$$

This last condition is only satisfied for $D = 2$. In other words, for $D \geq 3$ the σ model admits no static solitonic solutions. To ensure the stability of these solutions we need to require the positive definiteness of the second variation of the energy functional, *i.e.* we need to ensure that $\delta^2 E[\phi] > 0$. The latter is equivalent to the condition

$$\left.\frac{\partial^2 E(\kappa)}{\partial\kappa^2}\right|_{\kappa=1} > 0. \tag{1.43}$$

For the energy of the σ model (1.41) we have that

$$\left.\frac{\partial^2 E_{(2)}(\kappa)}{\partial \kappa^2}\right|_{\kappa=1} = (2-D)(1-D)E_{(2)}. \tag{1.44}$$

We see that for $D = 2$, which is the only case where the σ model has static solutions, we have that $\delta^2 E_{(2)}[\phi] = 0$. The latter implies that in order to ensure the stability of these static solutions, we need to include further terms in (1.40) with different scaling behaviour.

Let us now consider the energy functional of the full Skyrme model (1.31) which under a scale transformation κ will be given by

$$\mathcal{E}_{SK}(\kappa) = \kappa^{2-D}\mathcal{E}_{(2)} + \kappa^{4-D}\mathcal{E}_{(4)}, \tag{1.45}$$

where $\mathcal{E}_{(4)}$ denotes the contribution of the fourth order Skyrme term. The first derivative of (1.45) with respective to κ is

$$\left.\frac{\partial \mathcal{E}_{SK}(\kappa)}{\partial \kappa}\right|_{k=1} = (2-D)\mathcal{E}_{(2)} + (4-D)\mathcal{E}_{(4)}. \tag{1.46}$$

If we want to ensure the existence of static solutions we must require

$$(2-D)\mathcal{E}_{(2)} + (4-D)\mathcal{E}_{(4)} = 0. \tag{1.47}$$

Notice that for $D = 3$, condition (1.47) implies that $\mathcal{E}_{(2)} = \mathcal{E}_{(4)}$.

To determine the stability of these solutions we need to calculate the second derivative of the energy functional $\mathcal{E}_{SK}$, *i.e.*

$$\left.\frac{\partial^2 \mathcal{E}_{SK}(\kappa)}{\partial \kappa^2}\right|_{k=1} = (2-D)(1-D)\mathcal{E}_{(2)} + (4-D)(3-D)\mathcal{E}_{(4)}, \tag{1.48}$$

and by using (1.47) we have that

$$\left.\frac{\partial^2 \mathcal{E}_{SK}(\kappa)}{\partial \kappa^2}\right|_{k=1} = 2(D-2)\mathcal{E}_{(2)}. \tag{1.49}$$

For $D \geq 3$ we have that

$$\left.\frac{\partial^2 \mathcal{E}_{SK}(\kappa)}{\partial \kappa^2}\right|_{k=1} > 0. \tag{1.50}$$

Hence, we can conclude that the (3+1) dimensional Skyrme model admits stable solitonic solutions under scale transformations. From the above, we also see that the addition of a Skyrme-like term of order higher than four will also lead to stable solutions.

Topological bound on the energy

Let us close our review of the Skyrme model by noting that it is possible to obtain a bound on the energy of a corresponding solution. To achieve this we need to rewrite the energy of the model as a perfect square plus the topological charge, *i.e.*

$$E_{SK} = -\int d\vec{x}\, Tr\left(\frac{F_\pi}{4}(\partial_\mu U)U^\dagger - \frac{\sqrt{2}}{8a}\left[(\partial_\mu U)U^\dagger, (\partial_\nu U)U^\dagger\right]\right)^2 + \frac{(3\sqrt{2})F_\pi\,\pi^2}{2a}B \geq 0, \tag{1.51}$$

where B is the topological charge given by expression (1.34). From (1.51) it is easy to see that

$$E_{SK} \geq |B| \tag{1.52}$$

This inequality, which has been introduced by Bogomol'nyi [32], implies that the energy of a given field configuration in any homotopy class has a lower bound. Skyrme himself obtained a similar estimate for the energy when he was studying field configurations with $B = 1$ [33].

Chapter 2

Generalisation of the Skyrme model

2.1 Introduction

In the previous chapter we saw that the Skyrme model, in its original form, is considered as a non linear field theory with great mathematical interest in its own right. Its properties are quite fascinating, even at the classical level, and developing methods to investigate them systematically is a difficult and challenging problem.

However, from the physical point of view, the main motivation to study the Skyrme model comes from its possible applications to particle physics. In particular, as was emphasised previously, this model is established as a candidate theory for nuclear interactions. Its most attractive feature is that it can provide us with a qualitative understanding of strong interactions at low energies. It is also the only model that can offer a rather simple interpretation of the baryon number and its conservation law.

Nevertheless, despite the success of the Skyrme model in the description of baryons, this theory is only an approximation and improving its theoretical predictions is always an important issue. As we shall see in what follows, one possible way to achieve this improvement, is to modify the Skyrme Lagrangian by considering additional higher order terms. However, before we discuss such generalisations in greater detail, let us first stress the fact that since the Skyrme model is by itself an effective theory, generalising it (or extending it), is an arbitrary procedure. Hence, in order to consider the most appropriate generalisation, it will prove useful to identify first all the theoretical requirements that must be satisfied by a Skyrme-like Lagrangian.

We start with a short historical remark. Describing the low energy limit of strong interactions using an effective meson Lagrangian is a problem that existed prior to

QCD. Over the years, numerous models have been proposed, with the Skyrme model offering the most radical approach. From the modern perspective, however, nuclear interactions are thought of as a manifestation of quark dynamics in the low energy regime. Hence, if these effective theories are thought to originate from QCD, then they must have certain properties. In particular, besides Lorentz invariance that is present in any consistent physical theory, one also needs to require the so called *chiral invariance*. This symmetry is characteristic of the low energy limit of QCD where all interactions are dominated by the light flavour quark fields (u, d). Since the masses of these quarks are only a few percent $(0.5 - 1\%)$ of the average hadron mass (typically of order 1 GeV), they can be considered massless. Assuming this approximation, QCD is then invariant under transformations of the symmetry group

$$SU(N_f)_L \otimes SU(N_f)_R, \tag{2.1}$$

where N_f is the number of quark flavours and L, R distinguish between left and right rotations respectively. Any effective meson theory that is thought to describe correctly the low energy limit of QCD must also exhibit the same chiral symmetry (2.1).

In addition, Witten's [5] observation[1] that baryons behave as solitons in the limit as the number of colours goes to infinity ($N_c \to \infty$), provides us with a further constraint: a meson Lagrangian must admit stable solitonic solutions. These solutions can then be thought of as particles that originate from a theory that involves mesons only.

It is remarkable that the Skyrme model – that appeared before QCD – can incorporate quite successfully all the above restrictions in a rather simple way. The Skyrme Lagrangian given in (1.31) can also be expressed using the right, R_μ, chiral currents in the following compact form

$$\mathcal{L}_{Sk} = -\frac{F_\pi^2}{16} Tr R_\mu R^\mu + \frac{1}{32a^2} Tr[R_\mu, R^\nu][R_\nu, R^\mu], \tag{2.2}$$

where $R_\mu = (\partial_\mu U)U^{-1}$ and U is the Skyrme field. The coefficient F_π is the pion decay constant and a is a dimensionless parameter that is left free in order to tune the model's predictions appropriately.

It can be shown that the first term in (2.2) is a unique quadratic combination of R_μ with chiral invariance. The second term, which was imposed by Skyrme

[1] See section 1.2.2 of chapter 1.

to stabilise the solitonic solutions, is also chiral invariant and ensures the positive definiteness of the energy. Moreover, it is the only fourth order term that leads to a positive definite Hamilotonian and to a second degree differential equation for the Skyrme fields. Although the latter property is not justified by any underlying physical symmetry, it contributes to the simplicity of the model especially when one tries to quantise it using a semiclassical approach [6].

The above features of the Skyrme model have established it as a strong candidate for a meson theory. Nevertheless, as we have mentioned previously, it has been suggested that this model does not give the complete picture but rather an approximation. For example, Aitchison et al. [34] constructed an effective model as an expansion of the derivatives of the chiral fields. Their calculations showed that good agreement with the low energy experimental $\pi - \pi$ scattering data can be achieved by a Skyrme type Lagrangian that also includes further fourth order terms:

$$\mathcal{L}_{(Aitchison)} = \alpha \mathcal{L}_{Sk} + Tr\{\beta\,(R_\mu R^\mu)^2 + \gamma\,\partial_\mu \partial^\mu U\,\partial_\mu \partial^\mu U^{-1}\}, \tag{2.3}$$

where α, β and γ are coefficients that can be tuned phenomenologically. A similar Lagrangian is also known to occur when one attempts to derive an effective theory directly from QCD, like in the chiral bosonisation method by Adrianov [35] and Adrianov and Novozhilov [36].[2] These extra fourth order terms, however, destabilise the soliton and a possible way to resolve this problem is to extend the Skyrme Lagrangian by adding a sixth order term. Even though the particular form of this extra term is unknown, it is reasonable to require that the new model must satisfy the same constraints as the original one.

We see therefore, that including higher derivative terms to the Skyrme model is supported not only by mathematical interest, but also by physical arguments. Of course, at this point the question of renormalisability arises; the Skyrme model is not a renormalisable theory and including higher order terms makes the situation even worse. Nevertheless, since the properties of such models and their extensions are not fully exploited even at the classical level, a further study is needed before they can be used as effective field theories for the low energy limit of strong interactions.

In what follows we will focus our attention to extended Skyrme models and investigate their static properties. However, we will not take into consideration

[2] A detailed discussion on this and other similar methods can be found in section 9.3.3 of [16].

the fourth order destabilising terms of (2.3). This is because their presence leads to a higher degree differential equation which is very difficult to solve even using numerical methods. Instead, we will restrict ourselves to possible extensions of the original Skyrme Lagrangian which is relatively simpler. Such models have been studied before for B=1 and in the following sections we will give a short review of the most characteristic ones. We will then be able to define a similar generalised Skyrme model that we will study extensively in the next chapters.

2.2 Extended Skyrme models

The Skyrme model, in its simplest form, is described by the Lagrangian (2.2) or equivalently (1.31) where the field $U(\vec{x},t)$ takes values in $SU(N)$ and satisfies the boundary condition

$$U \to I \qquad \text{as} \qquad |\vec{x}| \to \infty, \tag{2.4}$$

where I is the unit matrix. In this notation, any field configuration which corresponds to mappings from S^3 to $SU(N)$ is characterised by the conservation of the topological current

$$B^{\mu} = \frac{1}{24\pi^2}\ \varepsilon^{\mu ijk}\, Tr(R_i\ R_j\ R_k). \tag{2.5}$$

The topological charge, which is associated with this current and as we have seen, can be interpreted as the baryon number, is given by

$$B = \frac{1}{24\pi^2}\int_{R^3} d\vec{x}^{\,3}\ \varepsilon^{ijk}\, Tr(R_i\ R_j\ R_k). \tag{2.6}$$

The lowest energy solution of the Skyrme model is a single soliton ($B = 1$) which we will refer to as the *skyrmion* and we will identify it with the nucleon. For this special case the field U takes values in $SU(2)$ and can be described by the hedgehog ansatz,

$$U = exp\,[i\,\tau\,\hat{\mathbf{r}}\,f(r)], \tag{2.7}$$

where τ are the Pauli matrices and $f(r)$ is an unknown profile function that depends only on r and can be determined numerically. The boundary condition (2.4) for the field U then becomes

$$f(0) = \pi \qquad \text{and} \qquad f(\infty) = 0, \tag{2.8}$$

and the baryonic current density (2.5) reads

$$B^0 = -\frac{1}{2\pi^2}\left(\frac{\sin^2 f}{r^2}\right)\frac{\partial f}{\partial r} \quad \text{and} \quad B_i = 0. \tag{2.9}$$

The hedgehog ansatz (2.7) was initially proposed by Skyrme [3] in order to describe the single skyrmion as a spherically symmetric configuration. As we shall see with greater detail in the following chapter, this particular ansatz describes an actual solution of the Skyrme model.

All generalisations of the Skyrme model that have been studied in the past have focused only on the single skyrmion solution. Hence, for the next three sections we will assume that the field U is described by the ansatz (2.7).

2.2.1 Introducing ω-mesons

In [8], Adkins and Nappi have argued that since the mass of the nucleon is of order 1 GeV, the Skyrme model can include more mesons like the ω or ρ mesons that have mass relatively smaller than the baryon mass. For simplicity, in their choice of Lagrangian they ignored the fourth order Skyrme term and only considered an ω vector meson field coupled to the non-linear σ model in the following way:

$$\begin{aligned}\mathcal{L}_{A\&N} &= -\frac{1}{4}(\partial_\mu\omega_\nu - \partial_\nu\omega_\mu)(\partial^\mu\omega^\nu - \partial^\nu\omega^\mu) + \frac{1}{2}m_\omega^2\,\omega_\mu\omega^\mu + \delta\,\omega_\mu B^\mu \\ &\quad + \frac{{F_\pi}^2}{16}Tr R_\mu R^\mu + \frac{1}{8}F_\pi^2 m_\pi^2\,(Tr\,U - 2),\end{aligned} \tag{2.10}$$

where ω_μ is the ω field with mass m_ω. F_π is the pion decay constant which is also present in the Skyrme model (2.2). Similarly δ is the decay constant of the ω-meson[3]. Both F_π and δ are left as free parameters of the model in order to determine the quality of its predictions. Moreover, the last term in the Lagrangian (2.10) is the chiral symmetry breaking term and the term $\delta\,\omega_\mu B^\mu$ describes the coupling of the ω field with the pion field.

The most interesting property of this model, is that the extra ω meson field stabilises the soliton solution like in the Skyrme model. As Adkins and Nappi indicated [8], this can be understood much easier if we eliminate ω_μ from the Lagrangian using the corresponding Euler-Lagrange equation:

$$\left[\left(\frac{d}{dr}\right)\left(r^2\frac{d}{dr}\right) + r^2 m_\omega^2\right]\omega_\mu(r) = \delta r^2 B_\mu(r), \quad \text{with} \quad B_0(r) \neq 0,\ B_i(r) = 0. \tag{2.11}$$

[3]In particular, this constant is related to the decay rate Γ_ω of the process $\omega \to \pi^+\pi^-\pi^0$.

The ω field can then be expressed as

$$\omega_\mu(r) = \int_0^\infty dr' \frac{1}{2m_\omega r\, r'} \left(e^{-m_\omega |r-r'|} - e^{-m_\omega |r+r'|} \right) \delta r'^{\,2} B_\mu(r'). \tag{2.12}$$

Hence, the interaction between the two fields – chiral and ω– is described by a term which is chiral invariant and has the form

$$\mathcal{L}_{6\,(A\&N)} \sim \left[Tr\,(B_\mu) \right]^2 . \tag{2.13}$$

Using a simple scaling argument[4], it is easy to prove that this term tends to stabilise the soliton in a similar way like the Skyrme term. Moreover, although the term (2.13) is of order six in derivatives of the pion fields U, we see from expression (2.9) that the Lagrangian (2.10) – or equivalently the action – is only up to second power of $\partial f/\partial r$. Thus, the Euler-Lagrange equation for the field U is second order and the new model has similar features as the original one.

After performing a semiclassical quantisation as in [7], one can calculate various physical quantities like the constant F_π or the magnetic moment μ of the proton and neutron. The values of these quantities are close to those predicted by the Skyrme model and in some cases improved when compared to the experimental ones [8].

We see therefore that by introducing ω-mesons in the Lagrangian (2.10), Adkins and Nappi were led to a sixth order model that preserves the simplicity and the properties of the original Skyrme model.

2.2.2 The Skyrme model and the NN potential

In a different approach, Jackson et al. [9] tried to reproduce qualitatively the low energy Nucleon-Nucleon (NN) interactions using the Skyrme model. In their analysis, they consider a two-skyrmion configuration that can be approximated using the *product ansatz*, defined as,

$$U_{B=2} = U_1(\mathbf{r} - \mathbf{r_1}) \cdot U_2(\mathbf{r} - \mathbf{r_2}), \tag{2.14}$$

where the field $U\,(\mathbf{r} - \mathbf{r_a})$ is the hedgehog field that is described by expression (2.7) and minimises the energy of the single skyrmion configuration ($B = 1$). This ansatz is considered to work quite well when the two skyrmions are well separated, *i.e.* when $|r_1 - r_2| \to \infty$. However, for small distances numerical calculations show that

[4]For example using the Hobart-Derrick theorem introduced in section 1.3.2 of chapter 1.

the total energy of this configuration is almost three times the energy of the single skyrmion and clearly this is not a bound state. Nonetheless, in this section we are mainly interested in the qualitative description of the two-skyrmion interactions and for this purpose the ansatz (2.14) can be considered as a rather good approximation.

Traditionally, interactions between two nucleons at low energies can be described in terms of the pseudo-scalar π, the pseudo-vector ω and the vector ρ mesons. In this context, both the scalar and ω mesons contribute to the central NN potential. In order to distinguish between their effects, one also needs to study the $N\overline{N}$ interactions. This is because the pseudo-scalar π mesons lead to attraction in both NN and $N\overline{N}$ interactions whereas the ω mesons have a similar effect only in the $N\overline{N}$ channel. In the Skyrme model, these hedgehog-antihedgehog ($N\overline{N}$) configurations can be constructed quite easily by replacing one of the fields U by $U^\dagger$ in the ansatz (2.14). However, as Jackson et al. indicate [9], when one tries these calculations in the Skyrme model, then the repulsive contribution in the central potential is not characteristic of an ω meson exchange at all. To understand this in greater detail, let us give a short review of their analysis.

The product ansatz (2.14) consists of two separate fields, U_1 and U_2. When the right chiral current R_μ acts on the field $U_{B=2}$ we have

$$\begin{aligned} R_\mu = (\partial_\mu U_{B=2})U_{B=2}^{-1} &= \big(\partial_\mu(U_1 \cdot U_2)\big)(U_1 \cdot U_2)^{-1} \\ &= (\partial_\mu U_1)U_2\,U_2^{-1}U_1^{-1} + U_1(\partial_\mu U_2)U_2^{-1}U_1^{-1} \\ &= (\partial_\mu U_1)U_2\,U_2^{-1}U_1^{-1} + U_1 R_\mu^2 U_1^{-1}, \end{aligned} \tag{2.15}$$

where R_μ^a denotes the right chiral current of the field U_a. If we plug this ansatz into the Lagrangian of the Skyrme model (2.2) then the fourth order Skyrme term will give us three different types of term. Firstly we will have terms where all R_μ act on one field. Their contribution is in the total energy of this specific field and nowhere else. In the second type of term one R_μ will act on one field and three on the second field. Although these terms lead to a repulsion in the NN system, they can only be considered as correction terms for the scalar meson exchange. The remaining terms, where we have two R_μ acting on each field, are the ones that contribute to the interaction. However, their behaviour does not indicate any repulsive force coming from an ω meson exchange. In general, as Jackson et al. argue [9], when an even number of R_μ act on each field then we get an attractive channel, whereas when we

have an odd number of R_μ acting on each field, then the contribution is repulsive. We see therefore that the fourth order term in the Skyrme Lagrangian (2.2) is not adequate to describe the NN interactions correctly. Hence, an extra term needs to be added. In order for this term to provide us with the desired contribution in the central NN potential, it must be of order six so that we can have an odd number (three) of R_μ acting on each field. The term that was suggested in [9] was,

$$\mathcal{L}_{6(Jack.)} \sim Tr[B_\mu B^\mu]. \tag{2.16}$$

This sixth order term is identical to the term that Adkins and Nappi found (2.13) within a numerical factor and hence, it has the same properties: it is chiral invariant, it stabilises the soliton and leads to a second order variation equation. Thus this new extended model shares the same benefits as the original. However, while proceeding further in their investigation, Jackson et al. suggested that the coefficient of the fourth order Skyrme term must be negative in order to simulate correctly the effects of the scalar mesons. This of course, does not ensure the positive definiteness of the energy and hence, we will not consider it as a valid possibility. We will only emphasise the fact that the terms $\mathcal{L}_{6(A\&N)}$ (2.13) and $\mathcal{L}_{6(Jack.)}$ (2.16) are almost identical even though they were adopted in a different context.

2.2.3 A systematic approach for all orders

In the previous two sections we saw that Adkins and Nappi [8], and Jackson et al. [9] generalised the Skyrme model using terms only up to sixth order. They claimed that these are the only higher order terms which lead to an action which is second order in terms of the derivatives of the fields. Thus, one cannot add more terms without destroying the simplicity of the original model.

However, Marleau [10, 11, 37, 12] managed to overcome this difficulty and construct a model that includes all order terms of the pion fields. His work is the most characteristic example of a Skyrme model with infinite number of terms and in what follows we will give a brief account of it.

As we have mentioned a number of times before, there are no theoretical restrictions in the form of the extra terms and so their choice can be arbitrary as long as the condition of chiral invariance is satisfied. Keeping this in mind, we start our calculations by noting that the right chiral fields R_μ can be written in the hedgehog

ansatz in the following simple form,

$$R_m = i\tau_k l_{km}(\alpha, \beta, \gamma), \tag{2.17}$$

where

$$l_{ij}(\alpha, \beta, \gamma) = (\delta_{ij} - \hat{r}_i\hat{r}_j)\alpha + \hat{r}_i\hat{r}_j\beta - \epsilon_{ijk}\hat{r}_k\gamma \tag{2.18}$$

and

$$\alpha = \frac{\sin f(r)\cos f(r)}{r}, \qquad \beta = f'(r) \quad \text{and} \quad \gamma = \frac{\sin^2 f(r)}{r}.$$

It is easy to prove that the following properties hold

$$l_{im}(\alpha_1, \beta_1, \gamma_1)l_{jm}(\alpha_2, \beta_2, \gamma_2) = l_{ij}(\alpha_1\alpha_2 + \gamma_1\gamma_2, \beta_1\beta_2, 0) \tag{2.19}$$

and

$$l_{kk} \equiv l_{kk}(\Gamma, \Delta, 0) = (N-1)\Gamma + \Delta, \tag{2.20}$$

where N is the number of dimensions, *i.e.* $N = 3$, and

$$\Gamma = \alpha^2 + \gamma^2 = \frac{\sin^2 f}{r^2} \quad \text{and} \quad \Delta = \beta^2 = f'^2. \tag{2.21}$$

If we rewrite the Skyrme Lagrangian (2.2) in the following more general form

$$\mathcal{L}_{Sk} = \underbrace{c_2\, Tr R_\mu R^\mu}_{\mathcal{L}_2} + \underbrace{c_4\, Tr[R_\mu, R^\nu][R_\nu, R^\mu]}_{\mathcal{L}_4}, \tag{2.22}$$

where $c_2 = F_\pi^2/16$ and $c_4 = 1/32a^2$, then using the properties (2.19), (2.20) and expression (2.21) we have that the σ model term $\mathcal{L}_2$ is given by,

$$\mathcal{L}_2 = c_2\, Tr R_\mu R^\mu = c_2\, l_{kr} Tr(\tau_k\tau_r) = 2\, c_2\, [(N-1)\Gamma + \Delta]. \tag{2.23}$$

Any term that is constructed as the trace of a product of R_μ's will always give a product of antisymmetric tensors (ϵ^{ijk}) which will contract with each other. The result will then be given in terms of Kronecker's deltas, $\delta^{kr}\ldots\delta^{pi}\delta^{jq}$, which when multiplied by $l_{kr}\ldots l_{pq}l_{ij}$ will give $l_{kk}\ldots l^{(2)}_{pp}$. The term $l^{(2)}_{pp}$ denotes the mixing between indices, *i.e.* $\delta^{pi}\delta^{jq}l_{pq}l_{ij} = l^{(2)}_{pp}$.

In general, we have that

$$l^{(n)}_{kk} = l_{kk}(\Gamma^n, \Delta^n, 0) = (N-1)\Gamma^n + \Delta^n. \tag{2.24}$$

Having declared all the important properties of l_{kk}'s, we can proceed to the evaluation of the Skyrme term,

$$\begin{aligned}\mathcal{L}_4 &= c_4\, Tr[R_\mu, R^\nu][R_\nu, R^\mu] = c_4\, l_{km} l_{rm} l_{pn} l_{qn}\, Tr[\tau_k, \tau_p][\tau_q, \tau_r] \\ &= -4c_4\, l_{kr} l_{pq}\, \epsilon^{kpa}\epsilon^{qrb} Tr(\tau_a \tau_b) = -8c_4 l_{kr} l_{pq}\, (\delta^{kq}\delta^{pr} - \delta^{kr}\delta^{pq}) \\ &= 8c_4\, (l_{kk} l_{pp} - l^{(2)}_{kk}) = 8c_4\, (N-1)\, \Gamma\, [(N-2)\Gamma + \Delta]. \end{aligned} \tag{2.25}$$

As expected, both terms (2.23) and (2.25) are of order f'^2 (*i.e.* they are proportional to Δ) and hence, the corresponding Euler-Lagrange equation will be of second order. These results are the same as those obtained from conventional calculations and thus, this verifies the validity of this notation.

Proceeding further, we consider a sixth order term which can be constructed according to Marleau [10] as

$$\mathcal{L}_6 = c_6\, Tr[R_\mu, R^\nu][R_\nu, R^\lambda][R_\lambda, R^\mu]. \tag{2.26}$$

It can be shown that for the hedgehog ansatz this term is equivalent to (2.13) and (2.16) within a numerical constant. Evaluating it explicitly we have,

$$\begin{aligned}\mathcal{L}_6 &= c_6\, l_{kr} l_{pq} l_{ij}\, Tr[\tau^k, \tau^i][\tau^j, \tau^p][\tau^q, \tau^r] \\ &= 16\, c_6\, l_{kr} l_{pq} l_{ij}\, \epsilon^{kia}\epsilon^{jpb}\epsilon^{qrc}\epsilon^{abc} \\ &= 16\, c_6\, l_{kr} l_{pq} l_{ij}\, (\delta^{kj}\delta^{ip}\delta^{qr} - \delta^{kj}\delta^{ir}\delta^{pq} + \delta^{kp}\delta^{ir}\delta^{qj} \\ &\qquad\qquad -\delta^{kp}\delta^{ij}\delta^{qr} + \delta^{kr}\delta^{ij}\delta^{pq} - \delta^{kr}\delta^{ip}\delta^{qj}) \\ &= 16\, c_6\, (2l^{(3)}_{kk} - 3l^{(2)}_{kk} l_{pp} + l_{kk} l_{pp} l_{ii}) \\ &= 16\, c_6\, (N-1)(N-2)\, \Gamma^2\, [(N-3)\Gamma + 3\Delta]. \end{aligned} \tag{2.27}$$

This term is also of order f'^2 as required. Comparing the three results (2.23), (2.25) and (2.27) obtained so far, we observe that they seem to obey a general pattern, given by,

$$\mathcal{L}_{2n} \propto \Gamma^{n-1}\, [(N-n)\Gamma + n\Delta]. \tag{2.28}$$

where the index $2n$ denotes the order of a specific term.

For a given order $2n$ one can always consider the general form,

$$\mathcal{L}_{2n} = c_{2n}\, Tr \underbrace{[R_\mu, R^\nu][R_\nu, R^\lambda] \ldots [R_\omega, R^\mu]}_{n \text{ commutators}}. \tag{2.29}$$

However, explicit calculations of such higher order terms show that they are not proportional to f'^2. For example, if we calculate the 8^{th} order term we find,

$$\begin{aligned}\mathcal{L}_{8a} &= c_8\, Tr[R_\mu, R^\nu][R_\nu, R^\lambda][R_\lambda, R^\rho][R_\rho, R^\mu] = \\ &= 32\, c_8\, (N-1)(N-2)\, \Gamma^2\, [(N-3)\Gamma^2 + 2\Gamma\Delta + \Delta^2]. \end{aligned} \tag{2.30}$$

If we want to restrict ourselves to the pattern (2.28) then we need to eliminate Δ^2 (or the f'^4) from (2.30). A possible way to do this, is by constructing another 8^{th} order term given by,

$$\begin{aligned}\mathcal{L}_{8b} &= c_8 \Big(Tr[R_\mu, R^\nu][R_\lambda, R^\rho]\Big)\Big(Tr[R_\nu, R^\lambda][R_\rho, R^\mu]\Big) \\ &= 64\, c_4\, (N-1)\, \Gamma^2\, [(N-2)\Gamma^2 + 2\Delta^2]. \end{aligned} \tag{2.31}$$

Using an appropriate linear combination of (2.30) and (2.31) we get

$$\begin{aligned}\mathcal{L}_8 &= 2\,\mathcal{L}_{8a} - \frac{1}{2}\,(N-2)\,\mathcal{L}_{8b} \\ &= 32\, c_8\, (N-1)(N-2)\, \Gamma^3\, [(N-4)\Gamma + \Delta]. \end{aligned} \tag{2.32}$$

From this last result we see that not only was Δ^2 eliminated but in addition the 8^{th} order term constructed in this special way, is consistent with the pattern (2.28).

In general , for every order $2n$ one can consider $[\frac{n}{2}]$ types of linearly independent terms where $[z]$ denotes the integer part of z. These terms are constructed as

$$\begin{aligned}\mathcal{L}_{na} &= c_n\, Tr(f_\mu^\nu f_\nu^\lambda f_\lambda^\rho f_\rho^\sigma f_\sigma^\omega \dots f_\eta^\mu), \\ \mathcal{L}_{nb} &= c_n\, Tr(f_\mu^\nu f_\lambda^\rho)\; Tr(f_\nu^\lambda f_\rho^\sigma f_\sigma^\omega \dots f_\eta^\mu), \\ \mathcal{L}_{nc} &= c_n\, Tr(f_\mu^\nu f_\lambda^\rho)\; Tr(f_\nu^\lambda f_\sigma^\omega)\; Tr(f_\rho^\sigma f_\omega^\xi \dots f_\eta^\mu), \\ &\vdots \end{aligned} \tag{2.33}$$

where we have defined $f_\mu^\nu = [R_\mu, R^\nu]$ for simplicity. The linear combination of these terms that eliminates all powers of Δ^n for $n > 1$ will always be consistent with the pattern (2.28). This last property has been proven in the general case by Marleau in [12] where it was also shown, using the properties of the Pauli matrices τ_a, that all terms $\mathcal{L}_{2n}$ for $n > 3$ and $n \equiv$ odd are identically zero.

At this point there is one important comment that needs to be made. Every extra term comes with an unknown coefficient that denotes its strength and in principle it can be tuned phenomenologically. In an all orders model, however, we have an

infinite number of these unknown coefficients and tuning them is very difficult. To resolve this problem one can link these coefficients to the coefficients of the Skyrme model. This has been done in various ways [10, 12, 38, 39]. The original Skyrme model can then be thought of as the first and second order of an expansion series of one initial function. This idea is quite interesting and has been investigated with great detail by Marleau [11, 12, 38].

As a concluding remark we note that while generalised Skyrme models including all order terms are not entirely justified physically, they do possess some very interesting mathematical properties which need to be explored further.

2.3 A general sixth order Skyrme model

2.3.1 Definition of the model

In the light of the above, we define in this section a generalised Skyrme model that is of order six in derivatives of the pion fields and is described by the Lagrangian,

$$\mathcal{L} = \frac{{F_\pi}^2}{16} Tr R_\mu R^\mu + \frac{1}{32a^2} Tr[R_\mu, R^\nu][R_\nu, R^\mu] + c_6 Tr[R_\mu, R^\nu][R_\nu, R^\lambda][R_\lambda, R^\mu]. \tag{2.34}$$

The unknown coefficient c_6 denotes the strength of the sixth order term and will be left as a free parameter of the model like a. The extra term we have considered here, is similar to expressions (2.13), (2.16) and identical to (2.27) that Marleau has used in his extension of the Skyrme model. It is the most general term of order six that preserves chiral invariance and also leads to an Euler-Lagrange equation that does not involve derivatives of order higher than two.

All the studies of generalised Skyrme models that we have seen so far, have focused on the properties of a single skyrmion (*i.e.* B=1) where the Skyrme field U takes values in $SU(2)$. Our analysis, however, is going to be much more general. In particular, in the following chapters we will investigate the properties of multi-skyrmion configurations (*i.e.* $B > 1$) of the model (2.34). For these configurations the hedgehog ansatz (2.7) is no longer a minimum energy solution and hence, we will not use it to describe the field U. Instead, we will assume that U has the most general form, $U = U(\vec{x}, t)$, and is $SU(N)$ valued. The topological charge is given by the general expression (2.6).

In addition, we will only focus our attention on static solutions and hence, we will also assume that U does not depend on time, *i.e.* $U = U(\vec{x})$. In this perspective, the energy of the model is given by,

$$E = -\int d\vec{x}^{\,3}\left(\frac{F_\pi^{\,2}}{16} Tr R_\mu R^\mu + \frac{1}{32a^2} Tr[R_\mu, R^\nu][R_\nu, R^\mu] + c_6\, Tr[R_\mu, R^\nu][R_\nu, R^\lambda][R_\lambda, R^\mu]\right). \quad (2.35)$$

If we consider the transformation

$$\vec{x} \to \vec{x}\,\frac{\sqrt{2}}{(aF_\pi)}\sqrt{1+\sqrt{1+\kappa}}\,, \quad (2.36)$$

where $\kappa = 192 c_6 F_\pi^2 a^4$, then we can rewrite the energy (2.35) in the following convenient form

$$E = -\Lambda \int d\vec{x}^{\,3}\left(\frac{1}{2} Tr R_i^2 + \frac{1-\lambda}{16} Tr[R_i, R_j]^2 + \frac{1}{96}\lambda\, Tr[R_i, R_j][R_j, R_k][R_k, R_i]\right), \quad (2.37)$$

where

$$\Lambda = \frac{F_\pi}{(4\sqrt{2}a)}\sqrt{1+\sqrt{1+\kappa}} \qquad \text{and} \qquad \lambda = \frac{\kappa}{(1+\sqrt{1+\kappa})^2}. \quad (2.38)$$

The parameter Λ is the energy scale of the model and λ is a numerical constant. Using this notation, we can also define the dimensionless energy expressed in the so-called topological units,

$$\tilde{E} = -\frac{1}{12\pi^2}\int d\vec{x}^{\,3}\left(\frac{1}{2} Tr R_i^2 + \frac{1-\lambda}{16} Tr[R_i, R_j]^2 + \frac{1}{96}\lambda\, Tr[R_i, R_j][R_j, R_k][R_k, R_i]\right). \quad (2.39)$$

The advantage of this parameterisation is that $\lambda \in [0, 1]$ describes the mixing between the Skyrme term and the sixth order term. When $\lambda = 0$ our model reduces to the usual pure Skyrme model while when $\lambda = 1$ the Skyrme term vanishes and the model reduces to what we refer to in what follows as the pure *Sk6 model*. This last model is similar to the model that Adkins and Nappi have studied.

The Euler-Lagrange equations derived from (2.37) for the static solutions are given by

$$\partial_i \left(R_i - \frac{1}{4}(1-\lambda)\Big[R_j,[R_j,R_i]\Big] - \frac{1}{16}\lambda\Big[R_j,[R_j,R_k][R_k,R_i]\Big] \right) = 0. \tag{2.40}$$

Moreover the following inequality holds for every configuration

$$\tilde{E} \geq \sqrt{1-\lambda}\ B. \tag{2.41}$$

When $\lambda = 0$ this inequality is the Bogomol'nyi bound which we have introduced in chapter 1 and provides us with a lowest energy bound for any field configuration of the Skyrme model. However, when $\lambda = 1$, the inequality (2.41) just shows the positive definiteness of the energy of the pure Sk6 model.

2.3.2 Fitting the parameters of the model

Our extended model depends on three parameters: F_π, a and c_6. To determine the values of these parameters one can evaluate different physical quantities. As our analysis will be purely classical, we will use the total energy (2.37) and the isoscalar mean square matter radius given by [7]

$$R^2 \equiv < r^2 >_{I=0} = \frac{\int_0^\infty dr\, r^4\, \rho_B(r)}{\int_0^\infty dr\, r^2 \rho_B(r)}, \tag{2.42}$$

where

$$\rho_B(r) = 4\pi\, B^0(r). \tag{2.43}$$

Notice that after performing the scaling (2.36) we can define the matter radius evaluated in dimensionless units as

$$\tilde{R} = \frac{1}{\sqrt{2}\sqrt{1+\sqrt{1+\kappa}}}\, aF_\pi\, R. \tag{2.44}$$

To illustrate how we can determine the unknown parameters, let us consider first the original Skyrme model and set $c_6 = 0$ in the Lagrangian (2.34). This is equivalent to setting $\lambda = 0$ in the energy (2.37). Then the unit energy, Λ, is only a function of F_π and a

$$\Lambda_{Skyrme} = \frac{F_\pi}{4a}. \tag{2.45}$$

Using expressions (2.37) and (2.39) we have that

$$\Lambda_{Skyrme} = E/(12\pi^2\tilde{E}). \tag{2.46}$$

The dimensionless energy $\tilde{E}$ can be computed numerically by minimising expression (2.39). For the simplest configuration, where $B = 1$, we have that $\tilde{E} = 1.232$. This is the case of the single skyrmion that is identified with the nucleon. If we consider that the static energy E is the mass of the proton or neutron, *i.e.* $E \simeq 939$MeV, we can obtain a value for Λ_{Skyrme} from expression (2.46). The free parameter a is then determined by fixing F_π to its experimental value, *i.e.* for $F_\pi = 186$MeV we get $a = 7.22577$. Using these values for a and F_π, one can compute other physical quantities like the matter radius (2.42) and compare them with experimental data. Although in this approach our results are incomplete, since we did not consider any quantum corrections, we can still estimate the quality of the model's predictions.

Similarly, the pure Sk6 model (*i.e.* when $\lambda = 1$) also depends on two parameters, F_π and c_6. In this case the transformation (2.36) and the unit energy Λ (2.38) will read

$$\vec{x} \to 4\left(3\frac{c_6}{F_\pi^2}\right)^{\frac{1}{4}}\vec{x} \qquad \text{and} \qquad \Lambda_{Sk6} = \frac{1}{2}\left(3\,c_6\,F_\pi^6\right)^{\frac{1}{4}}. \tag{2.47}$$

By inputting the mass of the nucleon, one can also obtain a value for the unknown coefficient c_6.

In the general case, where both higher orders are present, we see from expressions (2.39) and (2.44) that $\tilde{E}$ and $\tilde{R}$ are functions of λ only. Thus, instead of determining the values of the parameters a and c_6 in the $B = 1$ case as we had done for the pure Skyrme and pure Sk6 models, we can calculate the ratio of the energy and matter radius for different solutions. Since these ratios are dimensionless, they can be compared directly with the experimental ratios which are also dimensionless.

In the following chapter we will evaluate the energy and radius of multi-skyrmion solutions for the general model and evaluate these two quantities with the corresponding value for the single skyrmion. We will then compare them directly to the experimental ratio,

$$\frac{E_B}{E_{B=1}} = \frac{\tilde{E}_B(\lambda)}{\tilde{E}_{B=1}(\lambda)} \quad \text{and} \quad \frac{R_B}{R_{B=1}} = \frac{\tilde{R}_B(\lambda)}{\tilde{R}_{B=1}(\lambda)}. \tag{2.48}$$

The advantage of this approach is that by varying the strength of the extra sixth order term one can gain an understanding of the effect that it has on the

general behaviour of the model. As we shall see, this behaviour changes for different multi-skyrmion solutions.

Chapter 3

Numerical solutions

3.1 Introduction

Understanding the properties of the Skyrme model is strongly related to obtaining solutions for the corresponding Euler-Lagrange equations. To the present day, however, despite the significant theoretical progress that has been achieved in the field, we have no knowledge of any analytical solution of these differential equations. They are of such complexity, that we lack the appropriate mathematical tools to treat them systematically, even in the case of the simple fourth order Skyrme model, let alone its generalisations.

In general, there are very few non-linear models that can be solved exactly. They are usually referred to as integrable models and they exist in (1+1) as well as in (2+1) and (3+1) dimensions. Their solutions can be obtained explicitly by applying a number of techniques like the inverse scattering method and the Bäcklund transformation among others. Unfortunately, none of these methods seem to work for the Skyrme model as the model is non-integrable. The only exception is when we restrict ourselves to $(1 + 1)$ dimensions where the Skyrme model reduces to the well known sine-Gordon model. As we have seen in chapter 1, this simplified model is a fully integrable model with well known analytical solutions. However, our main interest lies in $(3+1)$ dimensions where our results can be directly applied to particle physics. In this case the Skyrme model is non-integrable and in the absence of analytical solutions one has to rely on numerical methods for studying its properties.

Solving the Skyrme equations numerically, is a problem that can be approached in two different ways. One can either try to solve the general Euler-Lagrange equations – in our case equations (2.40) – directly, using numerical methods or try to

approximate the Skyrme fields first, by imposing a symmetry for a given configuration. Although the latter simplifies the differential equations greatly, the numerical results obtained in this way are only an approximation and not an actual solution of the model. This semi-analytical approach will be studied in detail in the following chapters.

In this chapter we will focus our attention on the first approach and we will try to compute static solutions of the general sixth order Skyrme model, defined by the Lagrangian (2.34). For what follows, we will not consider any approximations of the Skyrme fields and thus our results will correspond to true solutions of the model. Our investigation will start from the single skyrmion solution ($B = 1$). Since this configuration has been studied previously, it provides us with an excellent testing ground for our methods. We will then study the properties of multi-skyrmion configurations with $B = 2..5$ and determine the quality of our model's theoretical predictions. For this purpose we will use the energy and matter radius ratios, that were defined in the previous chapter in (2.48), and compare our results with experimental data. This will also help us to understand the effect of the additional sixth order term that we have considered in the Skyrme model.

We would like to emphasise that this approach is a difficult and time-consuming problem. Not only does it require a significant amount of computer power but one must always be careful when estimating the accuracy of the results. The numerical methods that we have used throughout this and the following chapters are quite advanced and in Appendix A we discuss them in some detail.

3.2 The ϕ-formulation

In the previous chapter we introduced our sixth order Skyrme model using the unitary field $U = U(\vec{x})$. We noted that in the most general case U takes values in $SU(N)$. However, as we have already mentioned, obtaining the solutions of this model numerically is a rather complicated procedure and for this reason we will restrict ourselves to $SU(2)$. In this case, it is more convenient to use the four-component vector ϕ which is related to U by

$$U = \phi_0 I + i \vec{\tau} \cdot \vec{\phi}, \tag{3.1}$$

where I is the unit matrix and $\vec{\tau}$ are the Pauli matrices. The boundary condition (2.4) then becomes $|\phi|^2 = 1$, *i.e.* we assume that ϕ is a unit vector. In this notation, the dimensionless energy $\tilde{E}$ is given by

$$\begin{aligned}\tilde{E} &= \frac{1}{12\pi^2}\int_R |\phi_\mu|^2 + \frac{1-\lambda}{2}\Big(|\phi_\mu|^4 - (\phi_\mu\cdot\phi_\nu)^2\Big) \\ &\quad + \frac{\lambda}{6}\Big(|\phi_\mu|^6 - 3\,|\phi_\mu|^2\,(\phi_\nu\cdot\phi_\kappa)^2 + 2\,(\phi_\mu\cdot\phi_\nu)(\phi_\kappa\cdot\phi_\mu)(\phi_\nu\cdot\phi_\kappa)\Big). \quad (3.2)\end{aligned}$$

To derive the Euler-Lagrange equations, we minimise the above expression after we have added a Lagrange multiplier to impose the constraint $|\phi|^2 = 1$. We have,

$$\begin{aligned}&\phi_{\mu\mu}\left(1 + (1-\lambda)\,|\phi_\nu|^2 + \frac{1}{2}\lambda\,|\phi_\nu|^2|\phi_\kappa|^2 - \frac{1}{2}\lambda\,(\phi_\nu\cdot\phi_\kappa)^2\right) + |\phi_\mu|^2\cdot\phi \\ &+(1-\lambda)\left((\phi_\nu\cdot\phi_{\nu\mu})\,\phi_\mu - (\phi_{\mu\mu}\cdot\phi_\nu)\,\phi_\nu - (\phi_\mu\cdot\phi_\nu)\,\phi_{\nu\mu} + |\phi_\mu|^4\,\phi - (\phi_\mu\cdot\phi_\nu)^2\phi\right) \\ &+\lambda\Big(\phi_\mu\,(\phi_\nu\cdot\phi_{\nu\mu})\,|\phi_\kappa|^2 - \phi_\mu\,(\phi_\nu\cdot\phi_\kappa)\,(\phi_\nu\cdot\phi_{\kappa\mu}) - \phi_\nu\,(\phi_\mu\cdot\phi_{\mu\kappa})\,(\phi_\nu\cdot\phi_\kappa) \\ &\quad -\phi_\nu\,(\phi_\nu\cdot\phi_{\kappa\kappa})\,|\phi_\mu|^2 - \phi_{\nu\kappa}\,(\phi_\nu\cdot\phi_\kappa)\,|\phi_\mu|^2 + \phi_{\nu\mu}\,(\phi_\kappa\cdot\phi_\mu)\,(\phi_\nu\cdot\phi_\kappa) \\ &\quad +\phi_\nu\,(\phi_\kappa\cdot\phi_{\mu\mu})\,(\phi_\nu\cdot\phi_\kappa) + \phi_\nu\,(\phi_\kappa\cdot\phi_\mu)\,(\phi_\nu\cdot\phi_{\kappa\mu}) \\ &\quad +\frac{1}{2}\left[|\phi_\mu|^6 - 3\,|\phi_\mu|^2\,(\phi_\nu\cdot\phi_\kappa)^2 + 2\,(\phi_\mu\cdot\phi_\nu)(\phi_\kappa\cdot\phi_\mu)(\phi_\nu\cdot\phi_\kappa)\right]\phi\Big) = 0. \quad (3.3)\end{aligned}$$

As before, λ is a dimensionless parameter with $\lambda \in [0,1]$. Let us remind the reader that when $\lambda = 0$, expressions (3.2) and (3.3) correspond to the pure Skyrme model and when $\lambda = 1$ they refer to the Sk6 model. In what follows, we will solve the above equations numerically, by treating λ as a free parameter.

3.3 The single-skyrmion solution

When we were studying the Skyrme model and its possible modifications in chapter 2, we have seen that in the simplest case, where $B = 1$, the field U is spherically symmetric and can be described by the hedgehog ansatz (2.7). There we have argued that this ansatz describes an actual solution of the model. To show that this is true, one needs to plug (2.7) directly to the Euler-Lagrange equations of the Skyrme model. Then the angular part of the resulting equations vanishes and one is left with a one-dimensional equation that depends only on the radius r. Therefore,

the solution for the single skyrmion is invariant under rotations with respect to all axes and hence, it is spherically symmetric. By performing the same calculations for our sixth order model (3.3) one can prove that it is also spherical symmetric for any value of $\lambda \in [0,1]$. In all these cases the solutions can be described by the hedgehog ansatz which in the ϕ-formulation is given by,

$$\phi = \begin{pmatrix} \sin f(r)\, \sin\theta\, \sin\varphi \\ \sin f(r)\, \sin\theta\, \cos\varphi \\ \sin f(r)\, \cos\theta \\ \cos f(r) \end{pmatrix}, \tag{3.4}$$

where r, θ and φ are the usual spherical coordinates. $f(r)$ is the unknown profile function that satisfies the boundary conditions $f(0) = \pi$ and $f(\infty) = 0$ and is determined numerically. Plugging (3.4) into (3.2) we have that

$$\begin{aligned} \tilde{E}_{B=1} &= \frac{1}{3\pi}\int dr\Big(f_r^2 r^2 + 2\sin^2 f\,(1+(1-\lambda)f_r^2) \\ &\quad +(1-\lambda)\frac{\sin^4 f}{r^2} + \lambda\frac{\sin^4 f}{r^2} f_r^2\Big). \end{aligned} \tag{3.5}$$

The Euler-Lagrange equation for the function $f(r)$ is an ordinary differential equation, given by

$$\begin{aligned} & f_{rr}\left(1+2\,(1-\lambda)\frac{\sin^2 f}{r^2} + \lambda\frac{\sin^4 f}{r^4}\right) + \frac{2}{r} f_r\left(1-\lambda\frac{\sin^4 f}{r^4}\right) \\ & +\frac{\sin 2f}{r^2}\left((1-\lambda)f_r^2 - 1 + \frac{\sin^2 f}{r^2} + \frac{\sin^2 f}{r^2}\left(\lambda f_r^2 - 1 + \lambda\right)\right) = 0. \end{aligned} \tag{3.6}$$

To solve this equation one can use different methods but since it is a one dimensional problem (*i.e.* it only depends on r) we have used the shooting method because it is the fastest and it gives very accurate results. In Figure 3.1 we give the profile function f and the energy density obtained for the two extreme cases: the pure Skyrme and the pure Sk6 model. We see that the two profile functions are very similar and the energy density seems to be more 'spread out' for the pure Sk6 model. In addition, the total energy given in dimensionless units decreases when λ increases, taking the minimum value when $\lambda = 1$. This is shown in Figure 3.2 where we have plotted the λ dependence of the energy and matter radius of the solutions. In the same Figure we also see that in contrast to the energy, the radius increases with λ. All these effects, however, are due to our choice of parameters and

given a different parameterisation, we would have obtained different results. The real quantities one has to investigate are the energy and radius ratios (2.48) which we will study in the next sections.

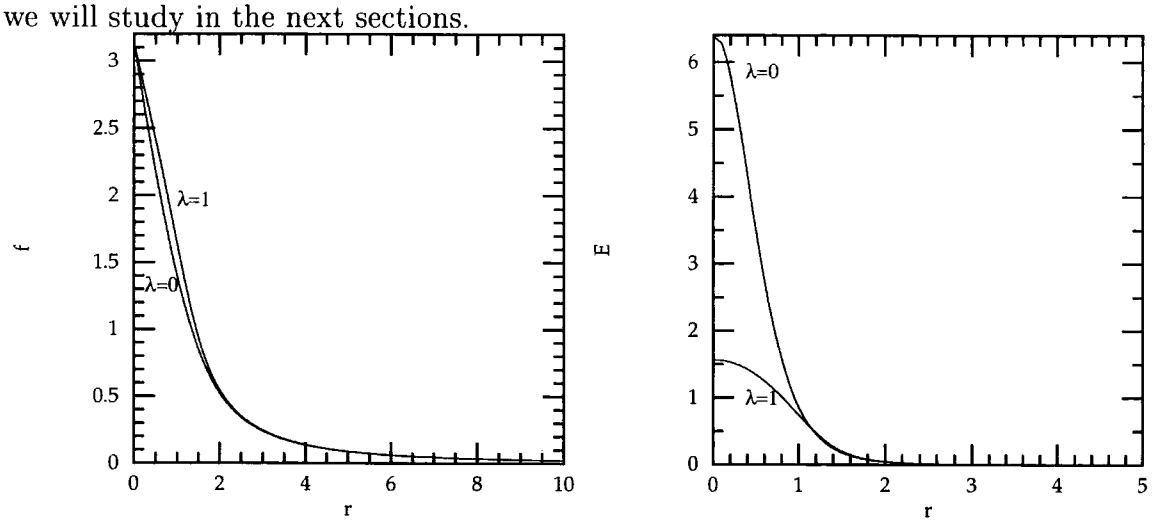

Figure 3.1: Profile function f and energy density of the single skyrmion solution for the pure Skyrme model, $\lambda = 0$, and the pure Sk6 model, $\lambda = 1$.

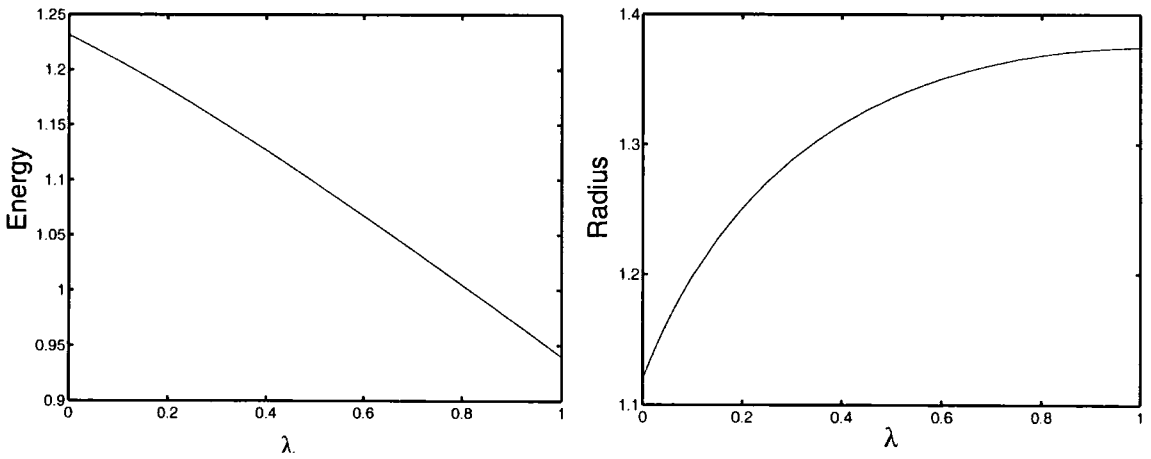

Figure 3.2: $\tilde{E}(\lambda)$ and $\tilde{R}(\lambda)$ for the $B = 1$ solutions.

As a final remark, let us note that the symmetry of a given configuration, if any, can be identified by plotting surfaces of constant baryon density. In this way we have a picture of the shape of each specific solution. For example, as we already

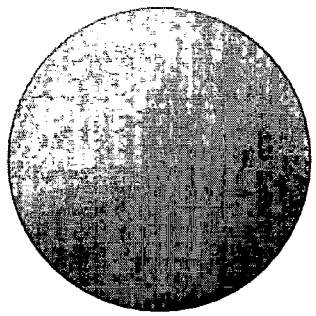

Figure 3.3: Baryon density isosurface for $B = 1$.

know, when $B = 1$ the solutions of our model are radially symmetric and hence, the surface of constant baryon density will have the shape of sphere like in Figure 3.3.

3.4 The $B = 2$ case

Besides the single skyrmion, it is widely accepted that the bound state of two skyrmions ($B = 2$) in the Skyrme model also exhibits a characteristic symmetry. This has been suggested both analytically [40], using qualitative arguments, and numerically [41] where it was shown that the global minimum-energy configuration for $B = 2$ is axially symmetric. To give a brief description of the numerical approach that was used in [41], we mention that the initially considered system consisted of two skyrmions placed in the most attractive channel. As we have seen in the previous chapter, when two skyrmions are well separated, they can be described quite well using the product ansatz, given in (2.14). To obtain the minimum energy solution, these skyrmions where brought together adiabatically and the results showed that the system relaxed to an axially symmetric configuration. This has also been proven in greater accuracy using a more advanced numerical code [42] and recently using a different numerical method, based on the *simulated annealing* technique [43].

In the case of the general sixth order Skyrme model, which interests us here, the $B = 2$ configuration is also axially symmetric for different values of the parameter λ. To prove this, we have solved equations (3.3) numerically. Our solutions have the same symmetry as the ones of the pure Skyrme model and hence, we can argue

that the axial symmetry of the $B = 2$ bound state is not disturbed by the additional sixth order term we have considered. The latter can also be shown by plugging an axially symmetric ansatz, expressed in cylindrical coordinates, into equations (3.3). Like in the hedgehog ansatz, the angular dependence vanishes and the system is invariant under rotations with respect to one axis, *i.e.* is axially symmetric.

The axially symmetric ansatz, that reduces equations (3.3) to a two-dimensional system, is given by

$$\phi = \begin{pmatrix} \sin f \, \sin g \, \sin(2\varphi) \\ \sin f \, \sin g \, \cos(2\varphi) \\ \sin f \, \cos g \\ \cos f \end{pmatrix}, \tag{3.7}$$

where $\varphi = \text{atan}(y/x)$. The two profile functions, $f(\rho, z)$ and $g(\rho, z)$ are functions of the usual axial coordinates, ($\rho = \sqrt{x^2 + y^2}$, z), and they satisfy the following boundary conditions:

$$\begin{array}{rrrrrr} f(0,0) & = \pi & f(\rho \to \infty, z \to \infty) & = 0 & f_\rho(0,z) & = 0 \\ g(0, z<0) & = 0 & g(0, z>0) & = \pi & g_R|_{R\to\infty} & = 0, \end{array} \tag{3.8}$$

where $R^2 = r^2 + z^2$.

Substituting (3.7) into (3.2) we get

$$\begin{aligned} E \;=\; \frac{1}{6\pi} \int \Bigg\{ & \left[(f_\rho^2 + f_z^2) + \sin^2 f \, (g_\rho^2 + g_z^2) + \frac{4}{\rho^2} \sin^2 f \, \sin^2 g \right] \\ & + (1-\lambda) \left[\frac{4}{\rho^2} \sin^2 f \sin^2 g \left[f_\rho^2 + f_z^2 + \sin^2 f (g_\rho^2 + g_z^2) \right] + \sin^2 f \, (f_\rho g_z - f_z g_\rho)^2 \right] \\ & + \lambda \left[\frac{4}{\rho^2} \sin^4 f \, \sin^2 g \, (f_\rho g_z - f_z g_\rho)^2 \right] \Bigg\} \, \rho \, d\rho dz. \end{aligned} \tag{3.9}$$

The corresponding Euler-Lagrange equations are given by

$$\left(f_{\rho\rho}+f_{zz}+\frac{1}{\rho}f_{\rho}\right)-\frac{2}{\rho^2}\sin 2f\,\sin^2 g-\frac{1}{2}\sin 2f\,(g_{\rho}^2+g_z^2)$$
$$+(1-\lambda)\Bigg\{\frac{4}{\rho^2}\sin^2 f\,\sin 2g\,(f_{\rho}g_{\rho}+f_zg_z)+\frac{1}{\rho}\sin^2 f\,\left(f_{\rho}g_z^2-f_zg_{\rho}g_z\right)$$
$$+\frac{1}{2}\sin 2f\,(f_{\rho}g_z-f_zg_{\rho})^2+\frac{4}{\rho^2}\sin^2 f\,\sin^2 g\left(f_{\rho\rho}+f_{zz}-\frac{1}{\rho}f_{\rho}\right)$$
$$+\frac{4}{\rho^2}\sin 2f\,\sin^2 g\left[\frac{1}{2}(f_{\rho}^2+f_z^2)-\sin^2 f\,(g_{\rho}^2+g_z^2)\right]+\sin^2 f\Big\{f_{\rho\rho}g_z^2+f_{zz}g_{\rho}^2$$
$$-2f_{z\rho}g_zg_{\rho}+f_{\rho}g_zg_{z\rho}-f_zg_{\rho\rho}g_z-f_{\rho}g_{zz}g_{\rho}+f_zg_{\rho}g_{\rho z}\Big\}\Bigg\}$$
$$+\lambda\Bigg\{\frac{8}{\rho^2}\sin^2 f\,\sin 2f\,\sin^2 g\,(f_{\rho}g_z-f_zg_{\rho})^2+\frac{4}{\rho^2}\sin^4 f\,\sin^2 g\Big(f_{\rho\rho}g_z^2+f_{\rho}g_zg_{z\rho}$$
$$-2f_{z\rho}g_{\rho}g_z-f_zg_{\rho\rho}g_z+f_{zz}g_{\rho}^2+f_zg_{\rho}g_{\rho z}-f_{\rho}g_{zz}g_{\rho}-\frac{1}{\rho}(f_{\rho}g_z^2-f_zg_{\rho}g_z)\Big)$$
$$-\frac{4}{\rho^2}\sin 2f\,\sin^2 f\,\sin^2 g\,(f_{\rho}g_z-f_zg_{\rho})^2\Bigg\}=0 \qquad (3.10)$$

and

$$\left(g_{\rho\rho}+g_{zz}+\frac{1}{\rho}g_{\rho}\right)+\frac{\sin 2f}{\sin^2 f}\,(f_{\rho}g_{\rho}+f_zg_z)+\frac{2}{\rho^2}\sin 2g$$
$$+(1-\lambda)\Bigg\{\frac{4}{\rho^2}\sin^2 f\,\sin 2g\,\left(g_{\rho}^2+g_z^2\right)+\frac{4}{\rho^2}\sin^2 g\left(2\sin 2f\,(f_{\rho}g_{\rho}+f_zg_z)\right.$$
$$\left.+\sin^2 f\left(g_{\rho\rho}+g_{zz}-\frac{g_{\rho}}{\rho}\right)\right)+\frac{1}{\rho}\left(f_z^2g_{\rho}-f_{\rho}f_zg_z\right)+f_z^2g_{\rho\rho}+f_{\rho}^2g_{zz}$$
$$-\frac{2}{\rho^2}\sin 2g\Big\{f_{\rho}^2+f_z^2+\sin^2 f\,\left(g_{\rho}^2+g_z^2\right)\Big\}+f_zf_{z\rho}g_{\rho}-f_{\rho\rho}g_zf_z+f_{\rho}f_{\rho z}g_z-2f_{\rho}g_{z\rho}f_z$$
$$-f_{zz}g_{\rho}f_{\rho}\Bigg\}+\lambda\Bigg\{\frac{4}{\rho^2}\sin^2 f\,\sin 2g\,(f_zg_{\rho}-f_{\rho}g_z)^2+\frac{4}{\rho^2}\sin^2 f\,\sin^2 g\Big[f_zf_{z\rho}g_{\rho}+f_z^2g_{\rho\rho}$$
$$-f_{\rho\rho}f_zg_z-2f_{\rho}f_zg_{z\rho}+f_{\rho}f_{\rho z}g_z+f_{\rho}^2g_{zz}-f_{zz}f_{\rho}g_{\rho}-\frac{1}{\rho}\left(f_z^2g_{\rho}-f_{\rho}f_zg_z\right)\Big]$$
$$-\frac{2}{\rho^2}\sin^2 f\,\sin 2g\,(f_{\rho}g_z-f_zg_{\rho})^2\Bigg\}=0. \qquad (3.11)$$

In Figure 3.4 we have plotted the profile functions $f(\rho,z)$ and $g(\rho,z)$ and the profiles of the energy and matter radius for the pure Sk6 model, *i.e.* for $\lambda=1$. Moreover, in Figure 3.5, we present the λ dependence of the energy and radius ratios for the $B=2$ configuration obtained after solving equations (3.10) and (3.11).

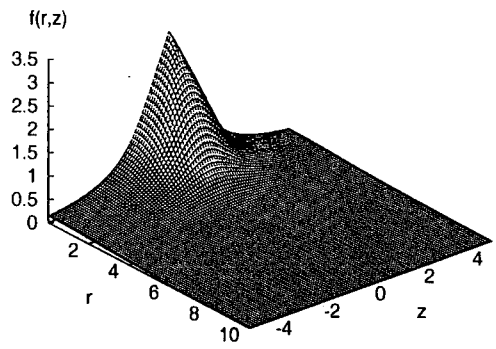

(a) Profile function $f(r, z)$

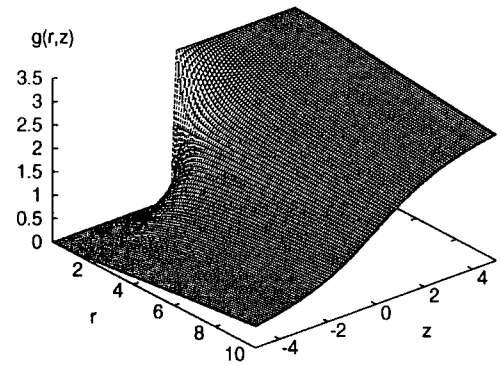

(b) Profile function $g(r, z)$

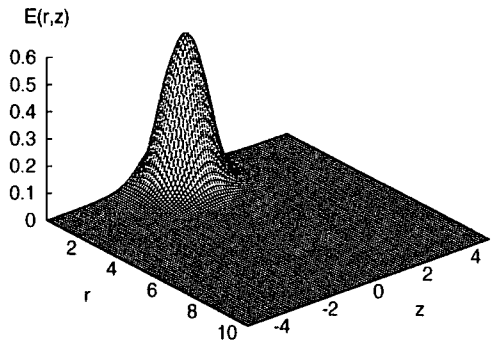

(c) Energy profile $\tilde{E}(r, z)$

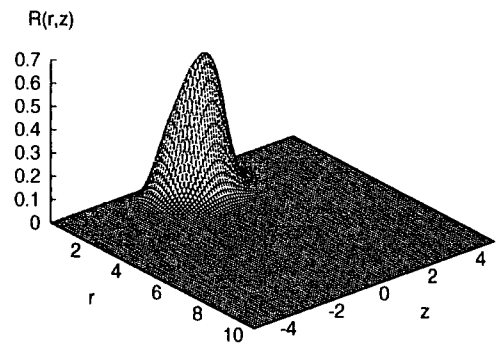

(d) Matter radius profile $\tilde{R}(r, z)$

Figure 3.4: Profile function (a) f and (b) g, and profiles of (c) the energy $\tilde{E}$ and (d) the matter radius $\tilde{R}$ for the axially symmetric $B = 2$ solution of the pure Sk6 model.

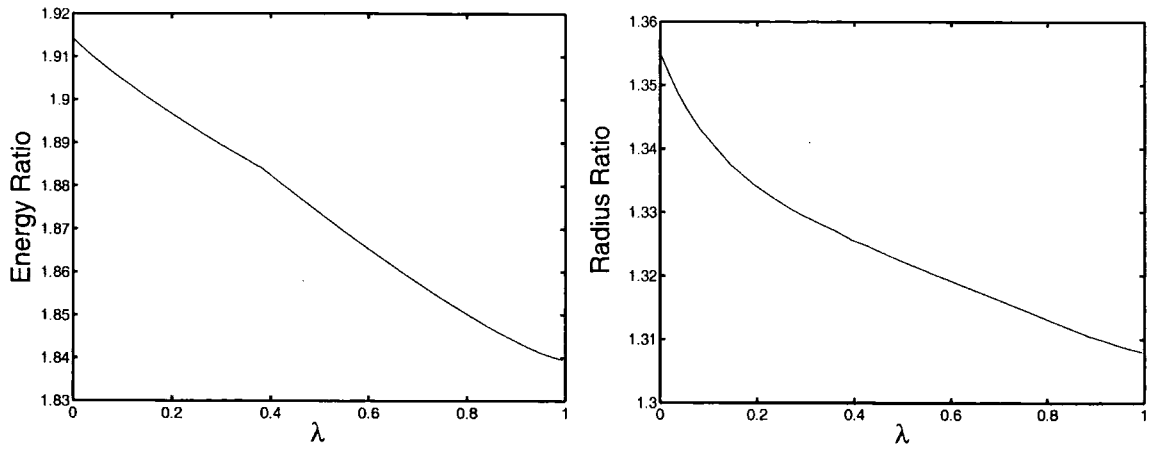

Figure 3.5: $\tilde{E}(\lambda)$ and $\tilde{R}(\lambda)$ ratio of $B = 2/B = 1$ for the numerical solutions.

We see that when λ increases the energy and radius ratios both decrease, taking their minimum value when $\lambda = 1$, *i.e.* when our model reduces to the pure Sk6 model. Hence, we argue that the additional sixth order term results in larger binding energy and in a spatially smaller configuration, and both effects are stronger when this term becomes dominant (*i.e.* when $\lambda \to 1$).

As expected, the symmetry of the $B = 2$ configuration does not change with λ and in the next section we show in Figure 3.9 the baryon density of this solution for the pure Sk6 model (*i.e.* λ=1). We see that it has the shape of a torus like in the case of the pure Skyrme model [42, 41, 43].

3.5 Configurations with $B > 2$

For configurations with topological charge larger than two we can no longer reduce the system of equations using a symmetry and hence, we have solved the three-dimensional equations (3.3) directly. To estimate the accuracy of our numerical method, we have considered the $B = 2$ case and we have compared the solutions of equations (3.3) with the ones obtained from the reduced system of equations (3.10) and (3.11). The advantage of having a reduced two-dimensional system is that it enables us to use much larger grids and thus to get much more accurate results. The difference between the value of the total energy computed in these two different ways was less than 0.1%, validating the accuracy of our methods[1].

[1]See Appendix A for further details.

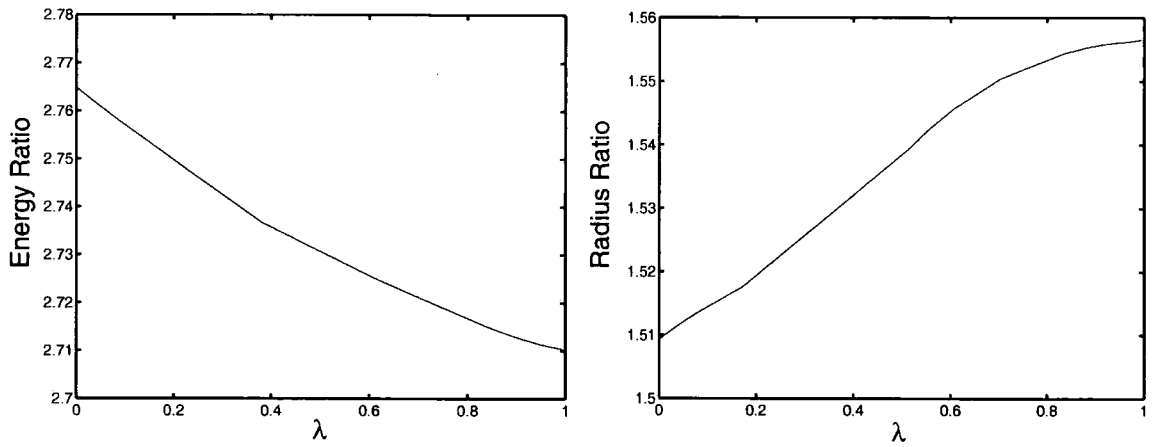

Figure 3.6: $\tilde{E}(\lambda)$ and $\tilde{R}(\lambda)$ ratio of $B = 3/B = 1$ for the numerical solutions.

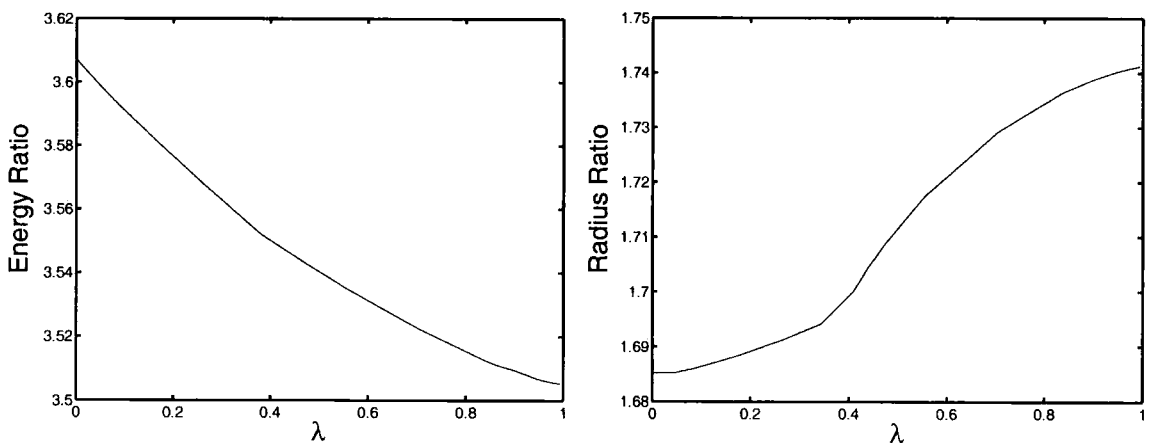

Figure 3.7: $\tilde{E}(\lambda)$ and $\tilde{R}(\lambda)$ ratio of $B = 4/B = 1$ for the numerical solutions.

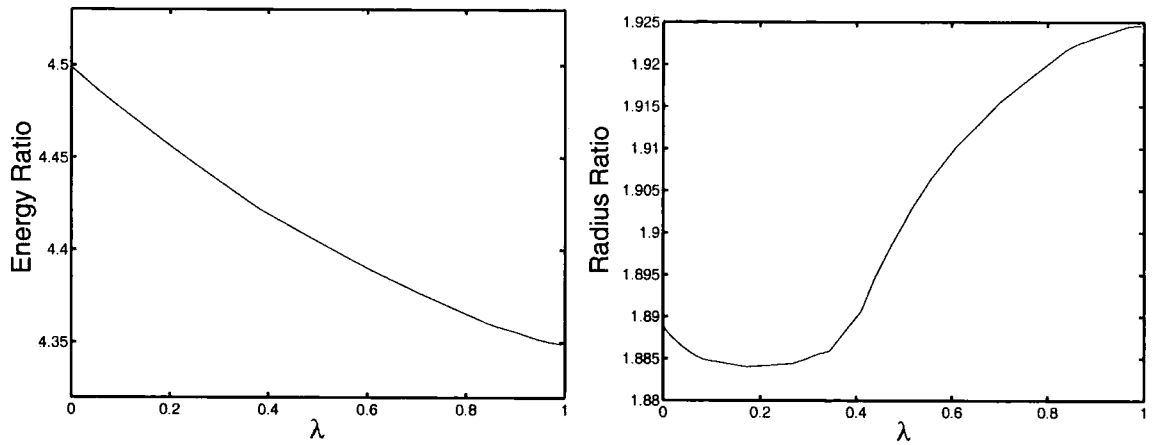

Figure 3.8: $\tilde{E}(\lambda)$ and $\tilde{R}(\lambda)$ ratio of $B = 5/B = 1$ for the numerical solutions.

As in the previous two sections, we present in Figures 3.6, 3.7 and 3.8 the λ dependence of the energy and radius ratios for the $B = 3..5$ multi-skyrmion solutions. We see that in each case the energy ratio decreases when the coefficient of the sixth order term increases ($\lambda \to 1$) while on the other hand, the radius ratio increases thus making the multi-Skyrmion solution broader in all cases. Comparing these graphs with the corresponding ones of the $B = 2$ solution, we see that the behaviour of the energy ratio is similar for all cases, whereas the radius ratio for $B = 2$ is the only one that decreases with λ.

For the solution with $B = 5$, we also observe that there is a small local minimum when $\lambda \simeq 0.2$ but the effect is so small it could be a numerical artifact. However, we believe that the general behaviour of the solution can be trusted.

Alongside the energy and radius ratios, in Figure 3.9 we present surfaces of constant baryon density for the pure Sk6 model. The symmetries of these multi-skyrmion solutions are the same as the ones obtained for the pure Skyrme model [42, 43]. We have already discussed the axial symmetry of the $B = 2$ skyrmion. The solutions for the $B = 3$ and $B = 4$ skyrmions have the shape of a tetrahedron and a cube respectively while the $B = 5$ skyrmion solution has a D_{2d} symmetry. We can therefore argue that our extended model retains the symmetries of the original Skyrme model at least for solutions with $B \leq 5$.

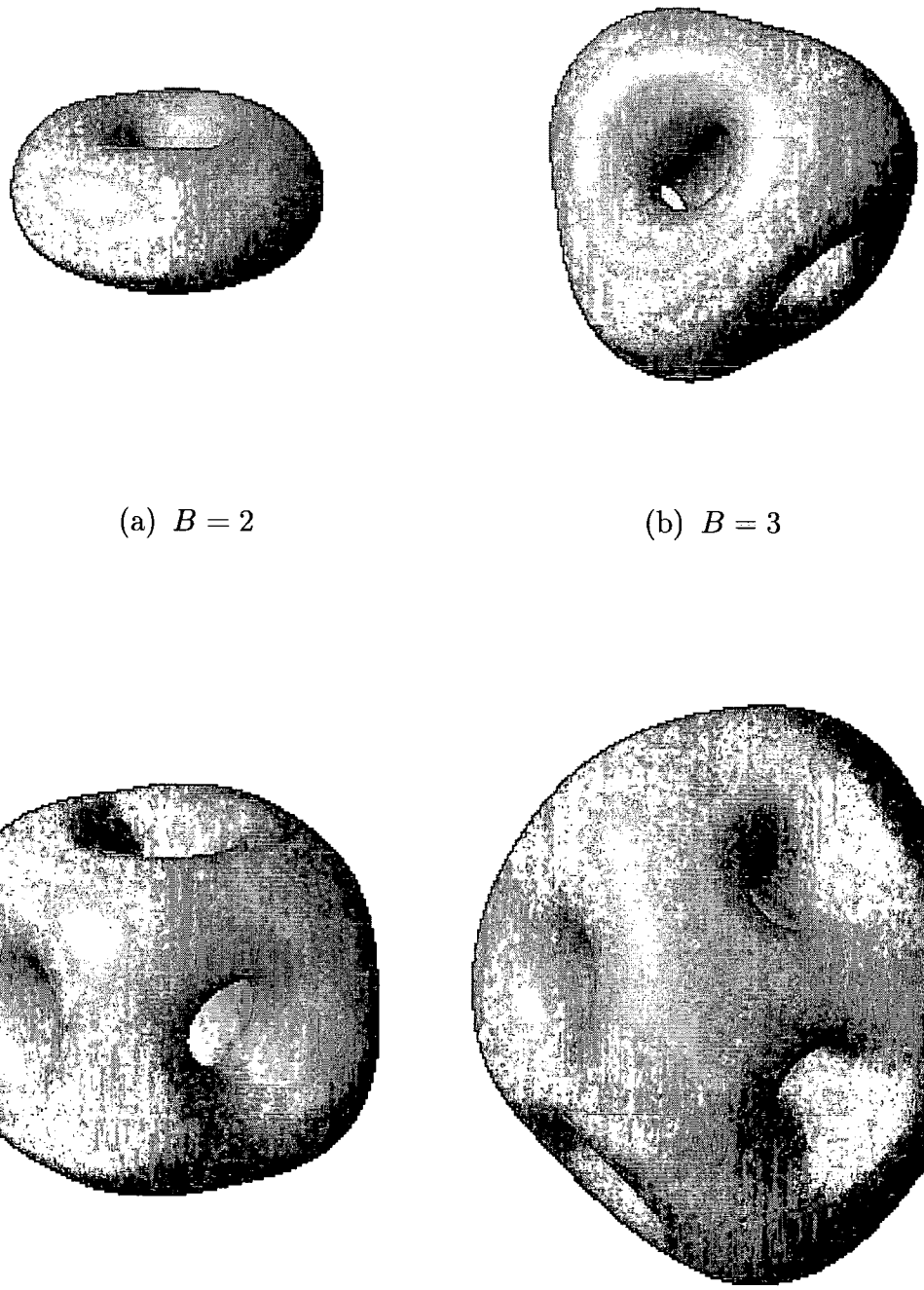

(a) $B = 2$ (b) $B = 3$

(c) $B = 4$ (d) $B = 5$

Figure 3.9: Baryon density isosurface for (a) $B = 2$, (b) $B = 3$, (c) $B = 4$ and (d) $B = 5$ with symmetries of a torus, a tetrahedron, a cube and D_{2d} respectively. All configurations are presented to scale.

3.6 Comparison with experimental data

Although our investigation so far has been restricted to a purely classical level and thus it has excluded all quantum effects, we would like to compare our results with the corresponding experimental values. This will help us determine whether the modification of the Skyrme model, which we have considered in our analysis, can improve – even qualitatively – the theoretical predictions of the Skyrme model.

Since we have already identified the skyrmion with the nucleon (proton or neutron), the multi-skyrmion configurations we have examined thus far, can be thought of as representations of light nuclei. Having associated the topological charge B with the baryon number, any solution of the model will describe a nucleus with mass number $A = B$. Moreover, in our numerical search, we have claimed that the solutions we have obtained, are global minima of the corresponding configuration. Thus, we will assume that the value of the total energy we have computed corresponds to isotopes with minimum mass.

Evaluating the experimental values of the energy ratio of light nuclei with the proton (or neutron) is a straightforward procedure. These masses were determined long ago and one can find their exact values in a number of nuclear physics textbooks. In our comparison we have used the tables of reference [44] [2].

In contrast to the energy, determining the matter radius is a difficult task. Traditionally, information about the structure of stable nuclei has been obtained using direct reactions of ion beams onto target nuclei. Recently, with the availability of radioactive ion beams, it was also possible to study more exotic nuclei, *i.e.* more unstable nuclei like all isotopes of He, Li and Be. Since the details of these experiments are not our primary concern, we refer the reader to the pioneering papers by Tanihata et al. [45, 46] and to the work of Egelhof [47], where an overview of this subject, together with more recent results is presented. For our purposes, it is sufficient to give a brief summary of the method that was used. Like in all scattering processes, the main quantity that was measured in these experiments was the total cross section σ of the interaction between the projectile nuclei and the various target nuclei. To estimate a value for σ one can use the change of intensity of the ion beam before and after the scattering. Then the matter radius of the projectile nucleus R_P

[2] More recently obtained values could be more accurate than the ones found in [44]. However, the difference is too small to affect quantities like the energy ratio which we compute here.

can be determined by the following relation [47]

$$\sigma = \pi \left(R_P + R_T \right)^2, \tag{3.12}$$

where R_T is the matter radius of the target nuclei. Expression (3.12) is rather simple and to get more accurate results one needs to use further, more complicated, analysis. However, using this naive approach it is possible to gain a deeper understanding of the nuclear structure. For example, from the results of [45, 46, 47], it appears that the matter radius becomes significantly large for exotic unstable nuclei, *i.e.* for nuclei with very small binding energy. This large radius is not the result of a deformed core but it is created by a 'halo' of a low density neutron distribution. Such properties of exotic nuclei are quite interesting and suggest that the nuclear structure is much richer than previously thought.

Returning to our theoretical approach, in Tables 3.1 and 3.2 we give the experimental values of the energy E and matter radius R and compare them with the energy and radius we computed numerically. We notice that the predicted values for the energy are always smaller than the experimental ones and the addition of the sixth order term makes the energy ratio even smaller. The difference in the pure Skyrme model is of order 5% for the ratio $E_{B=2}/E_{B=1}$ (*i.e.* the ratio of the energy of the deuteron with the proton) and it increases for large B. This is also true for the pure Sk6 model where the error increases with B. On the other hand, the addition of the sixth order term makes the multi-Skyrmion solution broader, except when $B = 2$. However, it is clear that in this case the predicted values are still much smaller than the experimental ones.

For the radius ratio, the largest error is obtained for the deuteron ($B = 2$) and when B increases, the theoretical values seem to improve. This is not surprising since, as we have already argued, our sixth order model describes the two-skyrmion configuration as an axially symmetric system. It is clear that this contradicts the experimental picture where all nuclei are thought to have a shell-like structure.

As a concluding remark let us note that it is a well know problem that the binding energies predicted by the Skyrme model are too large. One usually argues that quantising the model will somewhat solve this problem. Our modification of the Skyrme model has not improved the situation and the binding energy is even stronger when we include a sixth order term. On the other hand the radius of the classical solutions of the Skyrme model are too small compared to experimental

	Experiment		Numerical solutions	
B	Energy (MeV)	Ratio	Skyrme Ratio	Sk6 Ratio
1	939	-	-	-
2	1876.1	1.99798	1.9009	1.8395
3	2809.374	2.99188	2.7650	2.7103
4	3728.35	3.97055	3.6090	3.5045
5	4668.795	4.97209	4.5000	4.3780

Table 3.1: Experimental energy ratio, $E_B/E_{B=1}$, and values obtained for the numerical solutions. The experimental values (MeV) correspond to isotopes with minimum mass [44].

	Experiment		Numerical solutions	
B	Radius (fm)	Ratio	Skyrme Ratio	Sk6 Ratio
1	0.72	-	-	-
2	1.9715	2.73819	1.3549	1.308
3	1.59	2.2083	1.5080	1.5570
4	1.49	2.06944	1.6850	1.7420
5	-	-	1.8890	1.9250

Table 3.2: Experimental radius ratio, $R_B/R_{B=1}$ and values obtained for the numerical solutions. The experimental values (fm) correspond to nuclei with minimum mass [7, 48, 45, 47].

results. The additional sixth order term seems to remedy the situation since, with the exception of the $B = 2$ configurations, all other multi-skyrmion solutions are broader when this term is dominant, thus improving the theoretical values of the matter radius.

Chapter 4

The harmonic map approximation

4.1 Introduction

In the previous chapter we studied some of the classical properties of the sixth order Skyrme model (2.34) using numerical methods to solve the corresponding Euler-Lagrange equations (2.40) (or (3.3)). Although this approach has the advantage of providing us with quantitatively correct results, it is mainly limited by the large computing power required for such complicated problems, thus restraining us from more detailed investigations. In this chapter we will try to extend our understanding of the extended Skyrme model (2.34) by considering a different, more analytical approach.

Recently, it has been shown by Houghton et al. [14] that multi-skyrmion solutions of the pure Skyrme model in $SU(2)$ can be approximated quite well if one uses the so called *rational maps* ansatz to describe the Skyrme fields. Their calculations showed that configurations with $B \leq 9$ that are constructed using this approximation have the same symmetries as the true solutions. In addition, the minimum energy of these static skyrmions is only a few percent higher than the corresponding numerical values. This ansatz was later generalised in terms of harmonic maps by Ioannidou et al [15] in order to approximate solutions of the $SU(N)$ Skyrme model. The advantage of both approximations is that they simplify the differential equations of the Skyrme model significantly and thus, one no longer anticipates the problem of solving the full three-dimensional system. Hence, using such semi-analytical methods one is able to study the Skyrme model systematically in a manner that is both qualitatively correctly and easier to implement.

In what follows, we will present both the rational and harmonic maps ansatz in greater detail and discuss some of their properties. We will then use them to

approximate multi-skyrmion configurations for our extended Skyrme model. As in the previous chapter, we are going to treat the coefficient of the extra sixth order term as a free parameter of the model and we will calculate the energy and radius ratios of these configurations with the single skyrmion. Our study will concentrate on the $SU(2)$ and $SU(3)$ versions of the model (2.34). We will examine static solutions with topological charge $B \leq 9$ for $SU(2)$ and with $B \leq 6$ for $SU(3)$. This will reveal a number of interesting properties of these skyrmions under the rational and harmonic map approximation. Finally, we will compare our results with the ones we obtained numerically in the previous chapter and we will determine whether this is a good approximation for the extended model as well.

4.2 Rational and harmonic map ansatz

As has been mentioned previously, in the most general case, the Skyrme field $U(\vec{x}, t)$ takes values in $SU(N)$ and satisfies the boundary condition $U \to I$ when $|\vec{x}| \to \infty$, where I is the unit matrix. In this description, the three dimensional Euclidean space $\mathbb{R}^3$ is compactified into the three dimensional unit sphere S^3 and hence, U corresponds to mappings from $S^3 \mapsto SU(N)$. If we restrict ourselves to $SU(2)$, any skyrmion solution will be a map from S^3 to $SU(2)$ and since $SU(2)$ is isomorphic to S^3 we will have that $U(\vec{x}, t) : S^3 \mapsto S^3$.

The rational map ansatz, as introduced by Houghton et al. [14], is an approximation of multi-skyrmion solutions using rational maps between Riemann spheres. In general, these rational maps $R(z)$ of degree N are holomorphic functions, *i.e.* they only depend on z, such that $R : S^2 \mapsto S^2$ and have the form

$$R(z) = \frac{p(z)}{q(z)}. \tag{4.1}$$

The polynomials p and q must be of maximum degree N and they must have no common factors.

Consider now a point $\mathbf{x} \in \mathbb{R}^3$ given in spherical coordinates (r, θ, ϕ). It is convenient for what follows, to map the angular coordinates (θ, ϕ) to the complex plane $(\xi, \bar{\xi})$ using the stereographic projection which is defined as $\xi = \tan(\theta/2)\, e^{(i\varphi)}$ and is shown schematically in Figure 4.1.

If we assume that a rational map $R(\xi)$, given by expression (4.1), is a map from a two dimensional sphere, which is centered at the origin of $\mathbb{R}^3$, to an S^2 submanifold

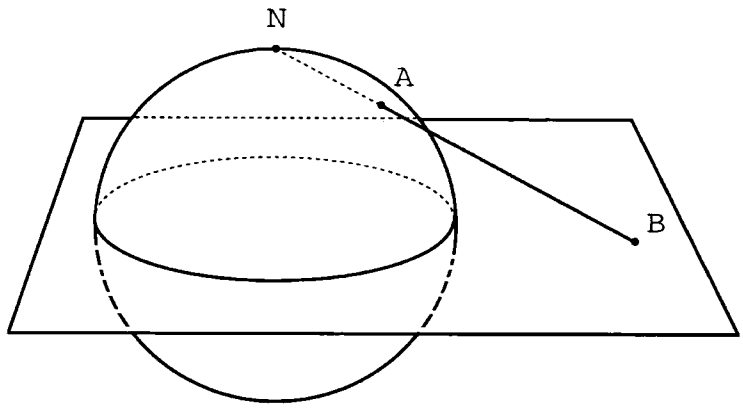

Figure 4.1: Stereographic projection of the unit sphere S^2 to the complex plane $(\xi, \bar{\xi})$. The point A on the sphere is mapped to the point B on the complex plane via the 'north' pole N.

of $SU(2) \equiv S^3$, then we can describe the static field configurations $U(r, \xi)$ using the rational map ansatz [14],

$$U(r,\xi) = \exp\left[ig(r)\frac{1}{1+|R|^2}\begin{pmatrix} 1-|R|^2 & 2\bar{R} \\ 2R & |R|^2-1 \end{pmatrix}\right]. \tag{4.2}$$

The real function $g(r)$ is the usual profile function and in order for U to be well defined at the origin we require that $g(r)$ satisfies the boundary conditions $g(0) = \pi$ and $g(\infty) = 0$, like in (2.8). If we plug the ansatz (4.2) to the general expression of the topological charge B,

$$B = \frac{1}{24\pi^2}\int_{R^3} d\vec{x}^{\,3}\ \varepsilon^{ijk}\, Tr(\partial_i U U^{-1}\ \partial_j U U^{-1}\ \partial_k U U^{-1}), \tag{4.3}$$

then it is quite straightforward to show that B is equal to the degree of the rational map $R(\xi)$, *i.e.* $B = N$. In addition, if we consider a general $SU(2)$ matrix,

$$\begin{pmatrix} \zeta & \eta \\ -\bar{\eta} & \bar{\zeta} \end{pmatrix} \qquad \text{with} \qquad |\zeta|^2 + |\eta|^2 = 1, \tag{4.4}$$

then, the Möbius transformation

$$R(\xi) \mapsto \frac{\zeta R(\xi) + \eta}{-\bar{\eta} R(\xi) + \bar{\zeta}}, \tag{4.5}$$

that acts globally on $R(\xi)$, corresponds to a rotation of the Skyrme field, *i.e.* it can be considered as an isospin rotation of U. Finally, for the single skyrmion, where

$B = N = 1$, the simplest map is $R(\xi) = \xi$ and in this case the ansatz (4.2) is just the hedgehog ansatz given previously in equation (2.7).

The main advantage of approximating the Skyrme fields using rational maps is that, in this way, the energy of the Skyrme model (2.2) simplifies significantly and one can minimise the angular part, given by $R(\xi)$, and the radial part, given by $g(r)$, separately. This can be illustrated by plugging expression (4.2) into the Lagrangian of the Skyrme model (2.2) and deriving the dimensionless energy $\tilde{E}_R$, [1]

$$\tilde{E}_R = \frac{1}{3\pi} \int dr \quad \left(g_r^2 r^2 + 2N \sin^2 g \, (1 + g_r^2) + \mathcal{I} \frac{\sin^4 g}{r^2} \right), \tag{4.6}$$

where the $\mathcal{I}$ is given by,

$$\mathcal{I} = \frac{1}{4\pi} \int d\xi \, d\bar{\xi} \, \frac{2i}{(1 + |\xi|^2)^2} \left(\frac{1 + |\xi|^2}{1 + |R|^2} \frac{dR}{d\xi} \right)^4 . \tag{4.7}$$

From (4.6) and (4.7) we see that the integration over the radius r and the angular part $(\xi, \bar{\xi})$ has decoupled. Hence, a solution of a given baryon charge, B, can be approximated by considering first, the most general rational map $R(\xi)$ of degree B and then minimise the integral $\mathcal{I}$ with respect to the parameters of R. The map determined in this way is unique up to an arbitrary rotation. Given the minimum value for $\mathcal{I}$, one can then minimise the effective energy by solving the Euler-Lagrange equation for the profile function g. This is a one-dimensional problem as for in the single skyrmion solution and it can be solved numerically with great accuracy using for example the shooting method. As it has been shown by Houghton et al. [14], the maps that minimise the integral $\mathcal{I}$ for $B \leq 9$ describe skyrmions that have the same symmetries as the actual solutions and the total energy of these configurations is only 1 or 2 percent higher than the numerical values. Hence, the rational map ansatz manages to approximate the solutions of the pure Skyrme model quite well and within this context one can study the properties of skyrmions in a simple and qualitatively correct way.

As we mentioned at the beginning of this section, the rational map ansatz is restricted to the $SU(2)$ Skyrme model and thus the question of whether we can use a similar approximation for $SU(N)$ arises naturally. In practice, one can always obtain solutions for the Skyrme model in $SU(N)$ by simply embedding the $SU(2)$ ones into a given higher symmetry group. Similarly, all $SU(2)$ skyrmions that

[1] For reasons of simplicity we have kept similar notation to [14].

are constructed using an approximation like the rational map ansatz, can also be embedded into $SU(N)$ and to the present day it seems that these skyrmions are the minimum energy configurations. In other words, non-trivial solutions which are not $SU(2)$ embeddings seem to be local rather than global minima of the energy[2]. Nevertheless, the possibility of obtaining skyrmions in $SU(N)$ that have different symmetries to their $SU(2)$ embeddings is always an interesting subject to explore. Towards this direction, Ioannidou et al. [15] generalised the rational map ansatz to $SU(N)$ by using harmonic maps. To give a brief summary of this generalisation we start by noting that the rational map ansatz can equivalently be expressed in the form

$$U(r,\xi) = \exp\left[2ig(r)\left(P(\xi,\bar{\xi}) - \frac{1}{2}I\right)\right], \tag{4.8}$$

where $g(r)$ is again the real profile function depending only on r, I is just the 2×2 identity matrix and P is a 2×2 projector that it is defined by the property $P^2 = P = P^\dagger$. The angular dependence of U comes from the projector P. If we assume that it has the form

$$P(V) = \frac{V \otimes V^\dagger}{|V|^2}, \tag{4.9}$$

where $V(\xi)$ is an analytic (*i.e.* it only depends on ξ) 2-component complex vector with entries polynomials in ξ of degree N, then P is a rational map $P : S^2 \mapsto \mathbb{CP}^1$. Expressions (4.2) and (4.8) are equivalent and as before, the topological charge B is equal to the degree of the map P, *i.e.* $B = N$. For $B = 1$ the vector $V = (1, \xi)^t$ reduces equation (4.8) to the familiar hedgehog ansatz.

The rational maps P are a special case of harmonic maps from $S^2 \mapsto \mathbb{CP}^{N-1}$ [51]. These maps are solutions of the $\mathbb{CP}^{N-1}$ σ model which is described by the Lagrangian density

$$L_{\mathbb{CP}^{N-1}} = Tr\left(\partial_\mu P\, \partial^\mu P\right), \tag{4.10}$$

where P is given by expression (4.9), but in this general case V is an N-component complex vector. The Euler-Lagrange equation of this model is

$$\left[\partial_\xi \partial_{\bar{\xi}} P, P\right] = 0. \tag{4.11}$$

[2]A comparison between the $SU(2)$, $SU(3)$ and generally $SU(N)$ minimum energy skyrmions can be found in [15, 49]. More details can also be found in [50] where all recent developments on this subject are being discussed.

Since the entries of the vector V are only functions of the complex variable ξ, *i.e.* V is analytic, the projector P also satisfies the first order self-dual equations [51]

$$P\,\partial_\xi P = 0 \qquad \text{and} \qquad \partial_\xi P\,P = \partial_\xi P. \tag{4.12}$$

Note that when $N = 2$, it can be shown [51] that the model (4.10) reduces to the well-known $O(3)$ σ model which is nothing but the quadratic term of the Skyrme model (3.2) in two dimensions

$$\mathcal{L}_\sigma = |\phi_\mu|^2 \tag{4.13}$$

with the constraint $|\phi|^2 = 1$, where $\phi \in S^2$.

Assuming that an ansatz based on the harmonic maps $S^2 \mapsto \mathbb{CP}^{N-1}$ is a 'natural' generalisation of the rational map ansatz, then our $SU(N)$ field can be expressed as [15]

$$\begin{aligned} U(r,\xi) &= e^{2ig(r)\left(P(\xi,\bar{\xi})-I/N\right)} \\ &= e^{-2ig(r)/N}\,\left[I + (e^{2ig(r)} - 1)P(\xi,\bar{\xi})\right]. \end{aligned} \tag{4.14}$$

It is important to remark at this point that (4.14) is not the most general approximation we can consider. The reason is that $SU(N)$ has $N^2 - 1$ dimensions, whereas the N-component complex vector, V, that describes the projector P in $SU(N)$ has $2N - 1$ degrees of freedom. In the next chapter we will exploit further generalisations of this ansatz by adding more projectors in (4.14). However, in what follows we will restrict ourselves to the simplest case of the single projector, P (4.9).

Substituting the ansatz (4.14) in the dimensionless energy of the pure Skyrme model we get [15]

$$\tilde{E}_H = \frac{1}{3\pi}\int dr\ \left(A_N\, g_r^2\, r^2 + 2\mathcal{N}\,\sin^2 g\,(1 + g_r^2) + \mathcal{I}\,\frac{\sin^4 g}{r^2}\right) \tag{4.15}$$

where

$$\begin{aligned} A_N &= \frac{2}{N}(N-1), \\ \mathcal{N} &= \frac{i}{2\pi}\int d\xi\, d\bar{\xi}\,\mathrm{Tr}\left(|\partial_\xi P|^2\right), \\ \mathcal{I} &= \frac{i}{4\pi}\int d\xi\, d\bar{\xi}\,(1+|\xi|^2)^2\,\mathrm{Tr}\left([\partial_\xi P,\,\partial_{\bar{\xi}} P]^2\right). \end{aligned} \tag{4.16}$$

The integral $\mathcal{N}$ is nothing but the energy of the two-dimensional Euclidean $\mathbb{CP}^{N-1}$ σ model that we have already mentioned (4.10). Hence, by using the ansatz (4.14)

to approximate the Skyrme fields, we have included in the solutions of the model all holomorphic maps (or self-dual solutions)[3] from $S^2 \mapsto \mathbb{CP}^{N-1}$. In addition, if the projector is given by (4.9), then the energy $\mathcal{N}$ is equal to the degree of the harmonic map and equal to the baryon number

$$B = \frac{i}{2\pi} \int d\xi \, d\bar{\xi} \, \mathrm{Tr} \left(P \left[\partial_{\bar{\xi}} P, \, \partial_{\xi} P \right] \right). \tag{4.17}$$

In other words, the topological charge of the Skyrme model harmonic map ansatz is just the topological charge of the $\mathbb{CP}^{N-1}$ model, *i.e.* it is equal to the highest degree of the polynomials in ξ among the components of $V = f(\xi)$.

The integral $\mathcal{I}$ in (4.15) is independent of r and it can be minimised with respect to the parameters of the harmonic maps. To do so, one first considers the most general map of degree B in $SU(N)$, by assuming that the N-component vector, $V = f(\xi)$, has the form

$$f = \begin{pmatrix} \xi^B + \alpha_{B-1}\,\xi^{B-1} + \ldots + \alpha_1\,\xi \\ \beta_{B-1}\,\xi^{B-1} + \beta_{B-2}\,\xi^{B-2} + \ldots + \beta_1\,\xi + \beta_0 \\ \gamma_{B-2}\,\xi^{B-2} + \gamma_{B-3}\,\xi^{B-3} + \ldots + \gamma_1\,\xi + \gamma_0 \\ \vdots \end{pmatrix}, \tag{4.18}$$

where we have used the $SU(N)$ invariance of the model to set $\alpha_B = 1$ and $\alpha_0 = 0$. All coefficients can be taken to be complex except β_{B-1}, which can be considered to be real. We see therefore that finding minimum energy configurations is equivalent to finding the appropriate map that minimises the integral $\mathcal{I}$. There are a number of numerical methods that can be used for this problem like the *downhill simplex* method[4]. Having found the minimum value of the integral $\mathcal{I}$, we can easily solve the corresponding Euler-Lagrange equations that are given by

$$g_{rr}\left(1 + 2\mathcal{N}\frac{3\sin^2 g}{4r^2}\right) + 2\frac{g_r}{r} + \frac{3\sin 2g}{4r^2}\left[\mathcal{N}(g_r^2 - 1) - \mathcal{I}\frac{\sin^2 g}{r^2}\right] = 0. \tag{4.19}$$

As it has been shown by Ioannidou et al. in [15] the non trivial maps that give minimum energy configurations in $SU(3)$ have different symmetries from their $SU(2)$ embeddings but their energy is not a global minimum. Unfortunately, these configurations cannot be compared with any true solutions since, as we have already

[3] An extensive review on these classical solutions of the $\mathbb{CP}^{N-1}$ model can be found in [51] and also in [50].

[4] For details on this and other methods see chapter 10 of [52].

seen in the previous chapter, the only solutions that have been found numerically are the ones of the $SU(2)$ model.

In what follows we will study solutions of the extended Skyrme model (2.34) for both the $SU(2)$ and $SU(3)$ cases and hence, we will use the ansatz (4.14) to approximate the Skyrme fields.

4.3 Extended sixth order Skyrme model in the harmonic map approximation

In this and the following sections we will investigate the properties of the extended sixth order Skyrme model (2.34) under the harmonic map ansatz.

We start our analysis by first substituting the ansatz (4.14) into expression (2.39) and thus obtaining the general energy in dimensionless units

$$\begin{aligned}\tilde{E} &= \frac{1}{3\pi}\int dr\,\Big(A_N\, g_r^2\, r^2 + 2\mathcal{N}\sin^2 g\,(1+(1-\lambda)g_r^2)\\ &\quad +(1-\lambda)\mathcal{I}\,\frac{\sin^4 g}{r^2} + \lambda\mathcal{I}\,\frac{\sin^4 g}{r^2}\,g_r^2 + \frac{2}{3}\,\lambda\,\mathcal{M}\,\frac{\sin^6 g}{r^4}\Big),\end{aligned} \tag{4.20}$$

where

$$\begin{aligned}A_N &= \frac{2}{N}(N-1),\\ \mathcal{N} &= \frac{i}{2\pi}\int d\xi\, d\bar{\xi}\,\mathrm{Tr}\left(|\partial_\xi P|^2\right),\\ \mathcal{I} &= \frac{i}{4\pi}\int d\xi\, d\bar{\xi}\,(1+|\xi|^2)^2\,\mathrm{Tr}\left([\partial_\xi P,\,\partial_{\bar{\xi}} P]^2\right),\\ \mathcal{M} &= \frac{i}{8\pi}\int d\xi\, d\bar{\xi}\,(1+|\xi|^2)^4\,\mathrm{Tr}\left([\partial_\xi P,\,\partial_{\bar{\xi}} P]^3\right).\end{aligned} \tag{4.21}$$

The integrals $\mathcal{N}$, $\mathcal{I}$ are the same as the ones derived for the pure Skyrme model. Moreover, like $\mathcal{I}$, the integral $\mathcal{M}$ is also independent of r and it can be minimised with respect to the parameters of the harmonic map. However, we will show that the $\mathcal{M}$ integral is identically zero and hence, only $\mathcal{I}$ needs to be minimised, something that has already been done in [14, 15, 50].

To prove that $\mathcal{M}$ vanishes, we need to use some properties of the projector, P, which is given by

$$P(f) = \frac{f\otimes f^\dagger}{|f|^2}, \tag{4.22}$$

and $\partial f/\partial\bar{\xi} = 0$. As we have seen in the previous section, since f is analytic, $P(f)$ satisfies the first order self-dual equations

$$PP_\xi = 0 \qquad \text{and} \qquad P_\xi P = P_\xi, \tag{4.23}$$

where P_ξ denotes the derivative of P with respect to ξ. From (4.23) we have

$$PP_\xi P = 0 \quad \text{and thus} \quad P_\xi^2 = 0. \tag{4.24}$$

Using (4.24) we notice that

$$\begin{aligned} Tr[P_\xi, P_{\bar{\xi}}]^n &= Tr(P_\xi P_{\bar{\xi}} - P_{\bar{\xi}} P_\xi)^n \\ &= Tr\left((P_\xi P_{\bar{\xi}})^n + (-1)^n (P_{\bar{\xi}} P_\xi)^n\right) \\ &= (1 + (-1)^n)\, Tr\left((P_\xi P_{\bar{\xi}})^n\right), \end{aligned} \tag{4.25}$$

proving that

$$Tr[P_\xi, P_{\bar{\xi}}]^n = 0 \quad \text{for} \quad n \quad \text{odd}, \tag{4.26}$$

and thus, $\mathcal{M}$ in (4.21) is identically zero. All angular dependence and therefore the symmetry of a given configuration, comes from the angular integrals $\mathcal{I}$ and $\mathcal{M}$. Hence, we see that in the harmonic map ansatz the multi-skyrmion configurations of the usual and the extended Skyrme model have the same symmetries. This was also observed in the previous chapter when we obtained the true solutions of the extended Skyrme model. Thus, we can conclude that the harmonic map approximation provides qualitatively correct results for the sixth order Skyrme model as well.

By treating the $\mathcal{N}$ and $\mathcal{I}$ as two parameters we can then minimise the energy $\tilde{E}$ by solving the following Euler-Lagrange equations for g

$$\begin{aligned} g_{rr}\left(1 + 2\mathcal{N}\frac{1-\lambda}{A_N}\frac{\sin^2 g}{r^2} + \mathcal{I}\frac{\lambda}{A_N}\frac{\sin^4 g}{r^4}\right) + \frac{2}{r}g_r\left(1 - \mathcal{I}\frac{\lambda}{A_N}\frac{\sin^4 g}{r^4}\right) \\ + \frac{1}{A_N}\frac{\sin 2g}{r^2}\left(\mathcal{N}\left((1-\lambda)g_r^2 - 1\right) + \mathcal{I}\frac{\sin^2 g}{r^2}(\lambda g_r^2 - 1 + \lambda)\right) = 0. \end{aligned} \tag{4.27}$$

Again, this is a one-dimensional equation and it can be solved numerically with great accuracy. Before we use the above results to study the solutions of the extended Skyrme model (2.34) for both the $SU(2)$ and $SU(3)$ cases, let us first consider the $SU(2)$ pure Sk6 model in the harmonic maps approximation, *i.e.* assume that

$\lambda = 1$ and $A_N = 1$ in (4.20) and (4.27). By considering the minimum values of the integral $\mathcal{I}$ [14] (see Table 4.1) we solve equation (4.27) and plot the profile function $g(r)$, Figure 4.2, and the energy profile, Figure 4.3, of skyrmions with topological charge $B = 2..9$. The harmonic maps that minimise $\mathcal{I}$ are discussed in detail in the following section.

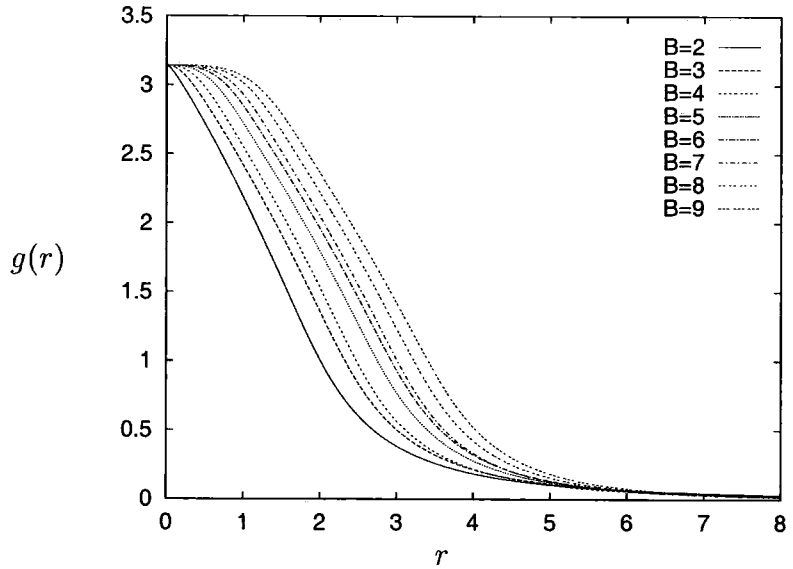

Figure 4.2: The profile function $g(r)$ of the Sk6 model for $B = 2...9$.

These two figures are similar to the ones obtained for the pure Skyrme model [14]; the profile functions $g(r)$ in Figure 4.2 are shifted to the right when the topological charge B increases, thus indicating an increase in size. The latter can also be observed in Figure 4.3 where the profiles of the energy density spread out for large B.

4.4 Energy and radius ratio in $SU(2)$

In this section, we analyse how the properties of multi-skyrmion configurations in the rational map approximation depend on the parameter λ. For this purpose we will calculate the energy and radius ratios as a function of λ. This is the same approach as in the case of the true solutions that we examined in the previous chapter. However, since the Euler-Lagrange equations (4.27) only depend on r, we

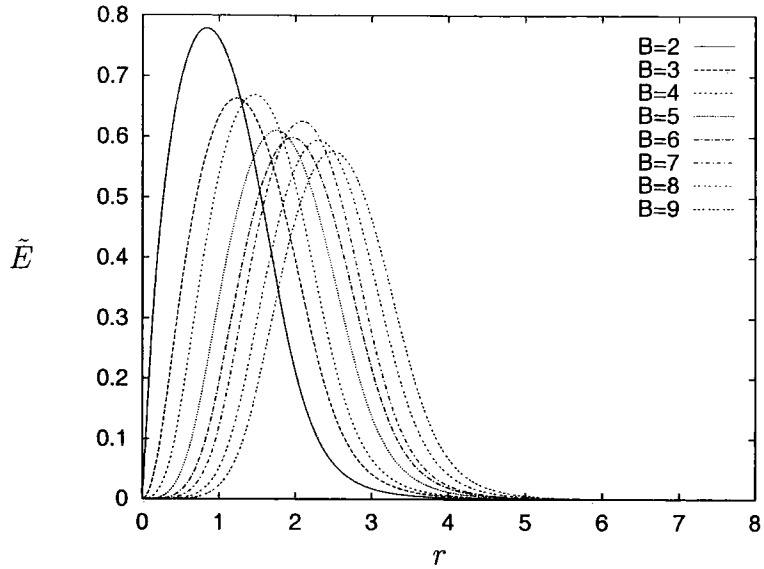

Figure 4.3: Energy profiles for $B = 2...9$.

will be able to obtain minimum energy skyrmions using the shooting method and thus our results will have very good accuracy.

At this stage we would like to remind the reader that $\lambda = 0$ corresponds to the pure Skyrme model while $\lambda = 1$ is equivalent to the pure Sk6 model. Moreover, the energy and radius ratios only depend on λ, *i.e.* the mixing between the two higher order terms.

The harmonic maps that minimise the integral $\mathcal{I}$ for skyrmions with $B \leq 9$ have already been found in [14] and we present them in Table 4.1. The symmetries of these static configurations are the same as the numerical solutions. In particular, besides the first five skyrmions, with symmetries shown in Figures 3.3 and 3.9, the $B = 6, 7, 8$ and 9 skyrmions in the harmonic map ansatz have the same symmetries as the numerical solutions, D_{4d}, Y_h, D_{6d} and D_{4d} respectively. This subject is explored in great detail in [14, 42, 43] where one can also find plots of constant baryon density that demonstrate these specific symmetries visually.

Since we have already checked in section 4.3 that the angular dependence of the pure and the extended Skyrme model are the same, we will treat the integral $\mathcal{I}$ as a parameter and use its corresponding values for a given baryon number, B, from Table 4.1.

$SU(2)$		
B	Harmonic Map $f(\xi)$	$\mathcal{I}$
1	$(\xi, 1)^t$	1
2	$(\xi^2, 1)^t$	5.81
3	$\left(\xi\,(\xi^2 - \sqrt{3}i),\ \sqrt{3}i\,\xi^2 - 1\right)^t$	13.58
4	$\left(\xi^4 + 2\sqrt{3}i\xi^2 + 1, \xi^4 - 2\sqrt{3}i\xi^2 + 1\right)^t$	20.65
5	$(\xi\,(\xi^4 + b\xi^2 + a),\ a\,\xi^4 - b\xi^2 + 1)^t$, $a = 3.07\,,\ b = 3.94$	35.75
6	$(\xi^2\,(0.16\,i\,\xi^6 + 1), \xi^4 + 0.16\,i)^t$	50.76
7	$(\xi\,(\xi^6 + \beta\xi^4 + 7\xi^2 - \beta),\ \beta z^6 - 7\xi^4 - \beta\xi^2 - 1)^t$, $\beta = \pm 7/\sqrt{5}$	60.87
8	$(\xi^2\,(0.14\,\xi^6 + 1), \xi^6 - 0.14)^t$	85.63
9	$\begin{pmatrix} 5\,i\,\delta\xi^6 - 9\xi^4 + 3\,i\,\delta\xi^2 + 1 + \gamma\xi^2\,(\xi^6 - i\,\delta\xi^4 - \xi^2 + i\,\delta) \\ \xi^3(-\xi^6 - 3i\,\delta\xi^4 + 9\xi^2 - 5\,i\,\delta) + \gamma\xi(-i\,\delta\xi^6 + \xi^4 + i\,\delta\xi^2 - 1) \end{pmatrix}$, $\gamma = -1.98, \delta = \sqrt{3}$	112.83
5*	$(\xi(\xi^4 - 5), -5\xi^4 + 1)^t$	52.05
5**	$(\xi^5, 1)^t$	84.425

Table 4.1: Harmonic maps $f(\xi)$ minimising the angular integral $\mathcal{I}$ for $SU(2)$ [14]. The 5* and 5** configurations denote saddle points that we also consider.

4.4.1 Minimum energy configurations

We first examine the skyrmion configurations with $B \leq 9$ that are believed to be global minima of the target space. They are described by the harmonic maps of Table 4.1 and their energy and radius ratios are shown in Figures 4.4 to 4.11.

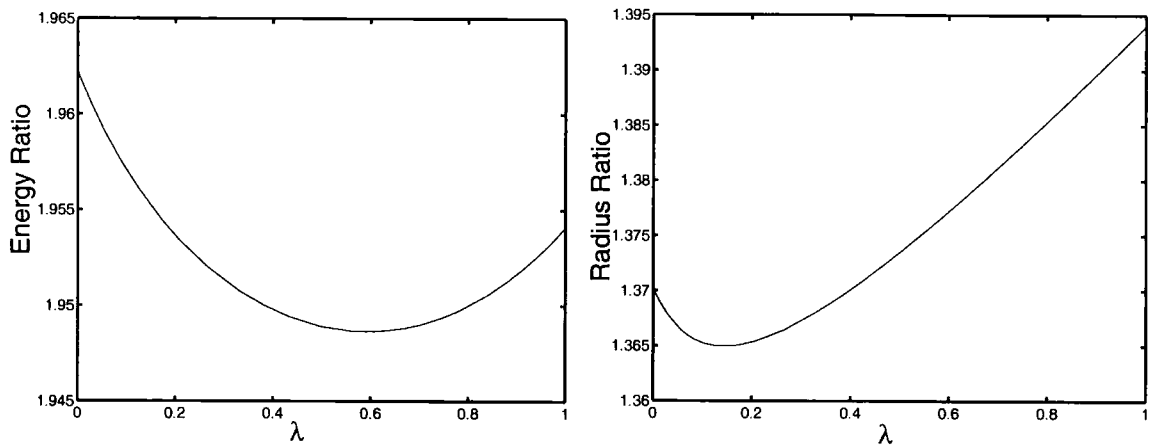

Figure 4.4: $\tilde{E}$ and $\tilde{R}$ ratio of $B = 2/B = 1$ as a function of λ for the $SU(2)$ harmonic map ansatz.

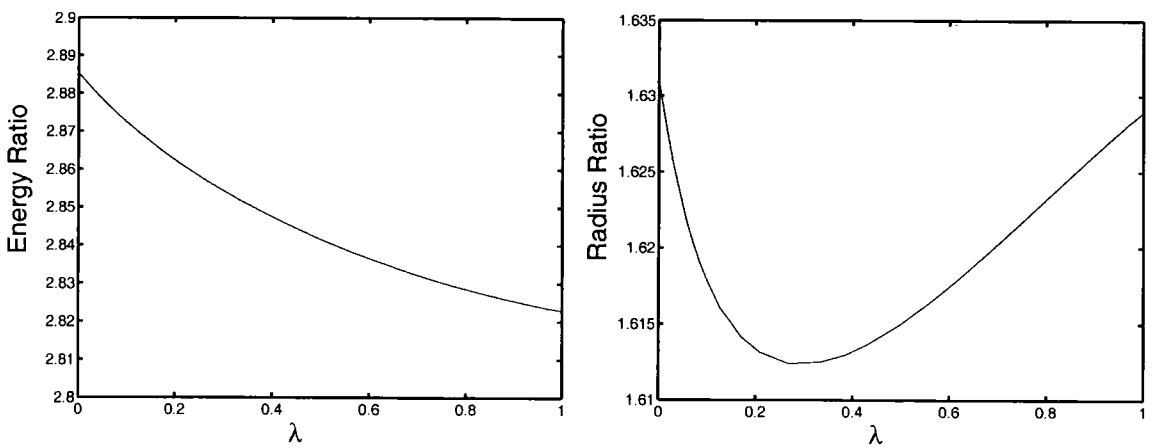

Figure 4.5: $\tilde{E}$ and $\tilde{R}$ ratio of $B = 3/B = 1$ as a function of λ for the $SU(2)$ harmonic map ansatz.

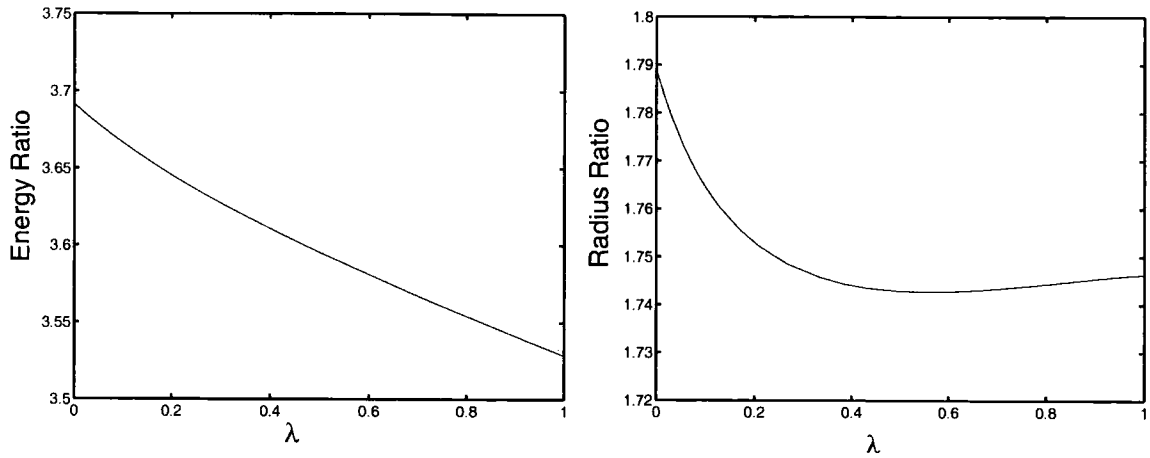

Figure 4.6: $\tilde{E}$ and $\tilde{R}$ ratio of $B = 4/B = 1$ as a function of λ for the $SU(2)$ harmonic map ansatz.

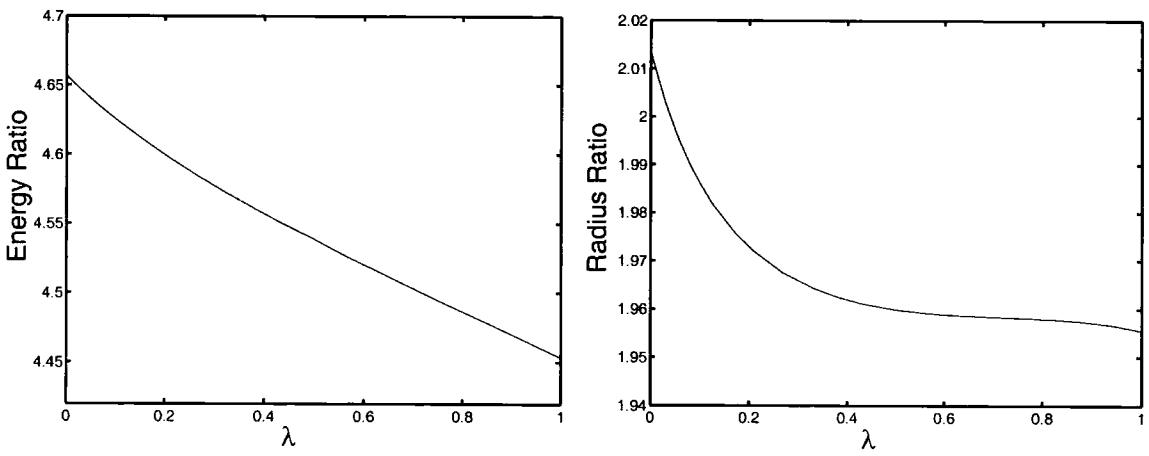

Figure 4.7: $\tilde{E}$ and $\tilde{R}$ ratio of $B = 5/B = 1$ as a function of λ for the $SU(2)$ harmonic map ansatz.

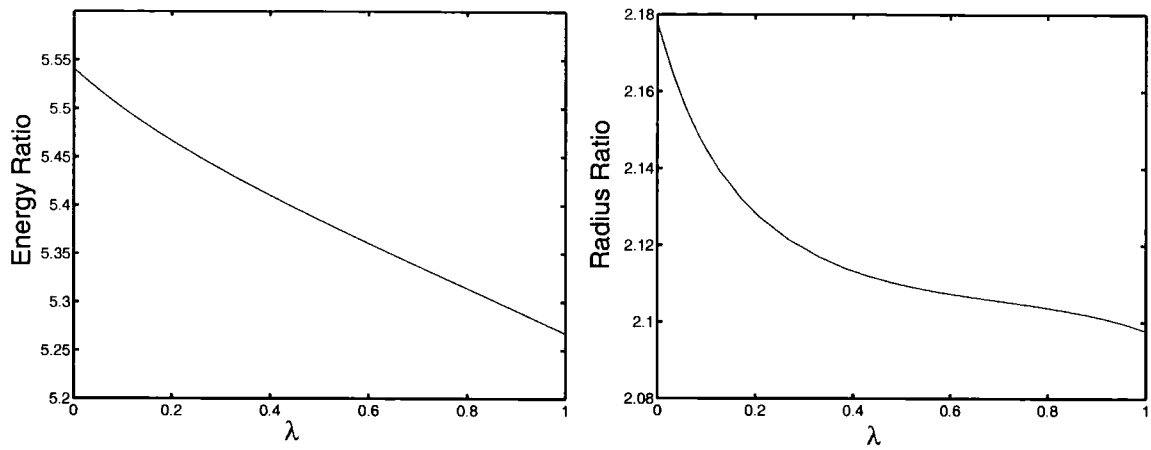

Figure 4.8: $\tilde{E}$ and $\tilde{R}$ ratio of $B = 6/B = 1$ as a function of λ for the $SU(2)$ harmonic map ansatz.

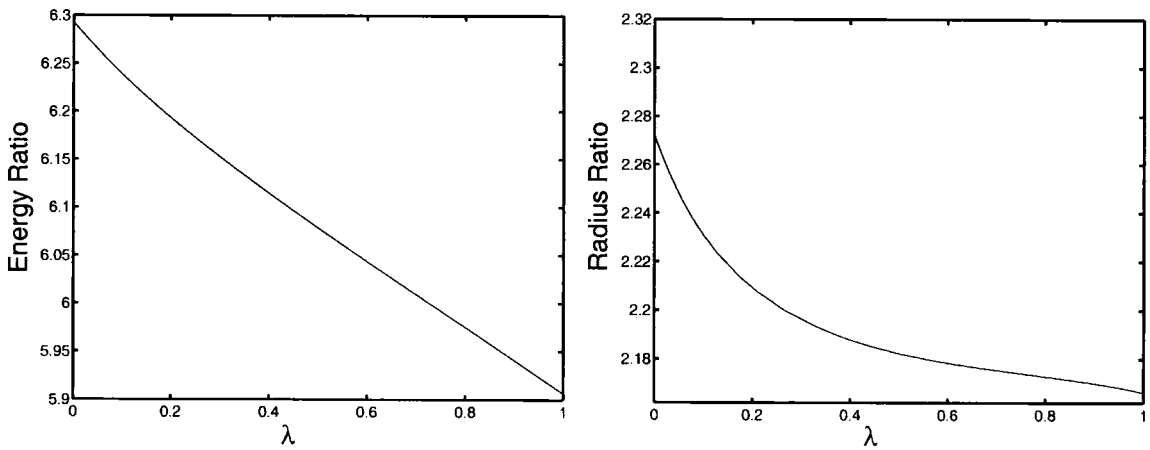

Figure 4.9: $\tilde{E}$ and $\tilde{R}$ ratio of $B = 7/B = 1$ as a function of λ for the $SU(2)$ harmonic map ansatz.

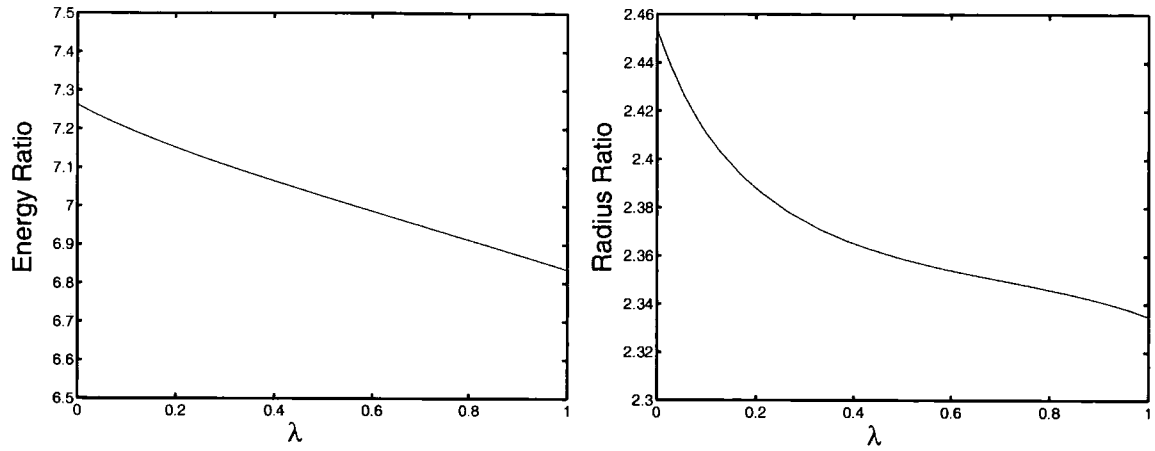

Figure 4.10: $\tilde{E}$ and $\tilde{R}$ ratio of $B = 8/B = 1$ as a function of λ for the $SU(2)$ harmonic map ansatz.

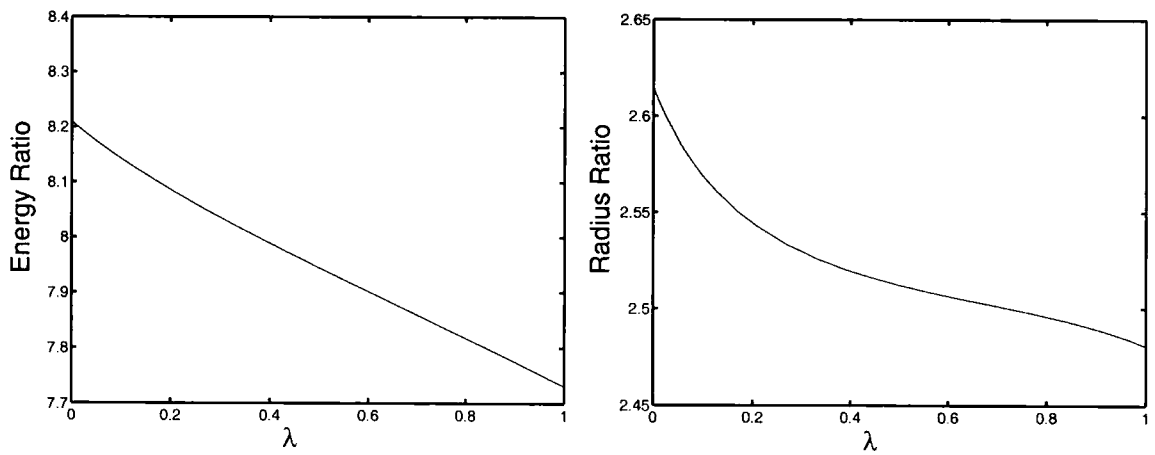

Figure 4.11: $\tilde{E}$ and $\tilde{R}$ ratio of $B = 9/B = 1$ as a function of λ for the $SU(2)$ harmonic map ansatz.

When comparing these results with the numerical solutions, we notice first of all that the energy ratio predicted by the ansatz is always too large. Apart from this, the prediction for the energy is rather good, except for the case $B = 2$ where the energy difference between the numerical solution and the rational map ansatz is 7 times as large for the Sk6 model than for the pure Skyrme model. This will be made even more clear in the last section where we will compare the asymptotic values of the model with the corresponding numerical solutions.

In addition, we observe that, unlike Figures 3.5 to 3.8 of the true solutions, the Figures obtained for the harmonic map approximation, exhibit local minima for $B = 2..4$ [5]. Moreover, both the energy and radius ratio graphs seem to be quite similar in shape when $B \geq 6$ and they have no local minima or maxima.

The radius ratio obtained with the harmonic map ansatz is always too large when compared with the radius ratio of the exact solution. For $B = 2$, the radius ratio increases with λ and the error only gets worse as λ increases. The case $B = 3$ is rather surprising, as the radius ratio has a deep local minimum around the value $\lambda = 0.3$; this is where the relative error is the smallest, otherwise the relative error is smaller for the pure Sk6 model than for the pure Skyrme model. The cases $B = 4..9$ are very similar: the radius ratios decrease when λ increases and the error for the pure Sk6 model is very small especially when $B = 4$.

We can thus conclude that the harmonic map ansatz produces good approximations to the solutions of the generalised Skyrme model and the error is in most cases smaller for the pure Sk6 model than for the pure Skyrme model, the only exception being the case $B = 2$.

4.4.2 Saddle point configurations

So far we have examined the behaviour of the model for harmonic maps that minimise the angular integral $\mathcal{I}$ and correspond to minimum energy configurations. We next consider harmonic maps that correspond to saddle points of the energy for $B = 5$. The reason for selecting these solutions is that their binding energies are much larger than the experimental values and it would be interesting to see their behaviour at larger energies. For this purpose, we have considered the two harmonic

[5] As mentioned when we were analysing the graphs of the $B = 5$ true solution, the small local minimum observed in that case is most probably a numerical artifact.

maps, $B = 5^*$ and $B = 5^{**}$, given in Table 4.1. The first has octahedral symmetry whereas the second gives a toroidal Skyrme field. In general, rational maps that are expressed as $R(z) = z^B$ correspond to multi-skyrmion configurations that always have axial symmetry [14].

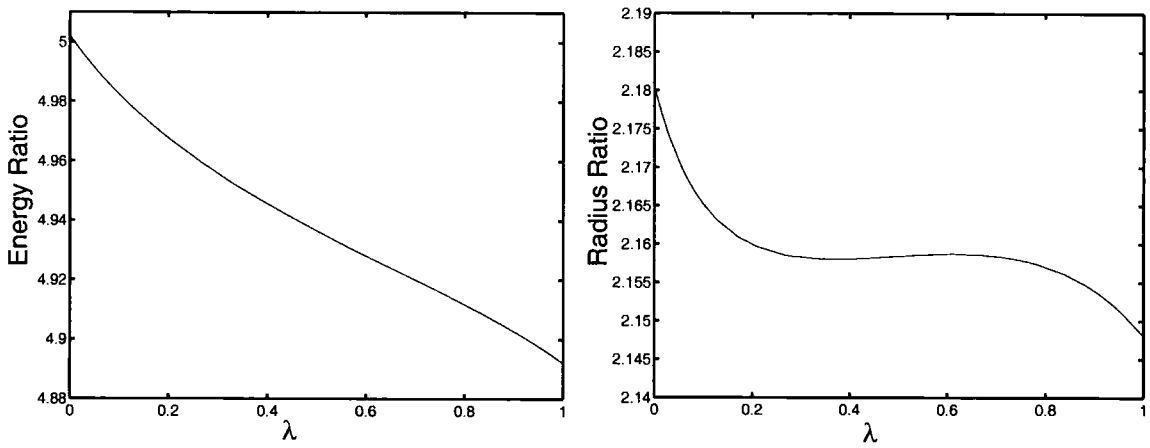

Figure 4.12: $\tilde{E}$ and $\tilde{R}$ ratio of $B = 5^*/B = 1$ as a function of λ for the $SU(2)$ harmonic map ansatz.

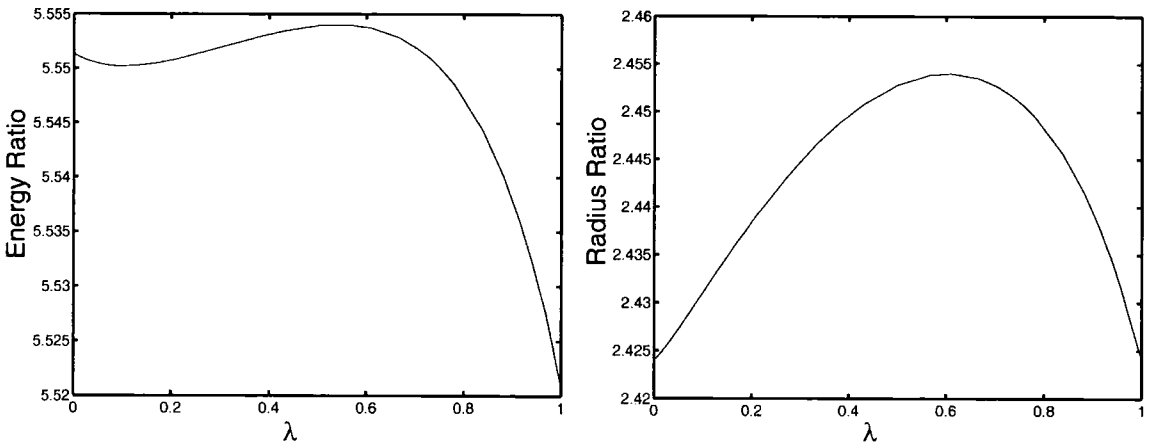

Figure 4.13: $\tilde{E}$ and $\tilde{R}$ ratio of $B = 5^{**}/B = 1$ as a function of λ for the $SU(2)$ harmonic map ansatz.

For the case of $B = 5^*$, shown on Figure 4.12, we see that the binding energy

is slightly larger than 5 for the pure Skyrme model and that it decreases when the strength of the sixth order term increases, going through the experimental value 4.97 when $\lambda \approx 0.1$.

The second case, shown in Figure 4.13, is the only example where we have a global maximum for the energy and radius ratios. Notice that the maximum value of both ratios is obtained for $\lambda \simeq 0.6$, *i.e.* when the two terms are comparable to each other.

4.5 Energy and radius ratio in $SU(3)$

In this section we look at the harmonic map configurations for the $SU(3)$ models. The harmonic maps that we use, together with the corresponding values of $\mathcal{I}$, are given in Table 4.2 and can be found in [15, 50].

$SU(3)$		
B	Harmonic Map $f(\xi)$	$\mathcal{I}$
1	$(\xi, 1)^t$	1
2	$(\xi^2, \sqrt{2}\,\xi, 1)^t$	4
3	$(\xi^3, 1.576\xi, \sqrt{2}^{-1})^t$	10.51
4	$(\xi^4, 2.7191\xi^2, 1)^t$	18.05
5	$(\xi^5 - 2.7\xi, 2\,\xi^4 + 1, 9/2\,\xi^3)^t$	27.26
6	$(\xi^6 + 3\xi, 1 - 3\xi^5, 7.06\,\xi^3)^t$	37.33

Table 4.2: Harmonic maps $f(\xi)$ minimising the angular integral $\mathcal{I}$ for $SU(3)$ [15, 50].

The single $SU(3)$ skyrmion is the well-known hedgehog ansatz and is just an embedding of the $SU(2)$ solution. Moreover, the minimising map for $B = 3$ has been found in [50] and gives a slightly smaller value for the integral $\mathcal{I}$ than the map that was identified in [15]. In this last reference it was suggested that the minimising map should be: $f(\xi) = (\sqrt{2}\xi^3, 2.23\xi, 1)^t$ and the corresponding value for $\mathcal{I}$ was found to be 10.65. However, this last map is not the global minimum of the $B = 3$ configuration but rather a saddle point.

It is useful to note at this point that the numerical constant A_N appearing in (4.20) and (4.27) is now equal to 4/3. We should also stress that these configurations approximate solutions that are believed to be saddle points of the energy. Their energy is larger than the corresponding $SU(2)$ embeddings and they have different symmetries as well which can be found in [15, 50].

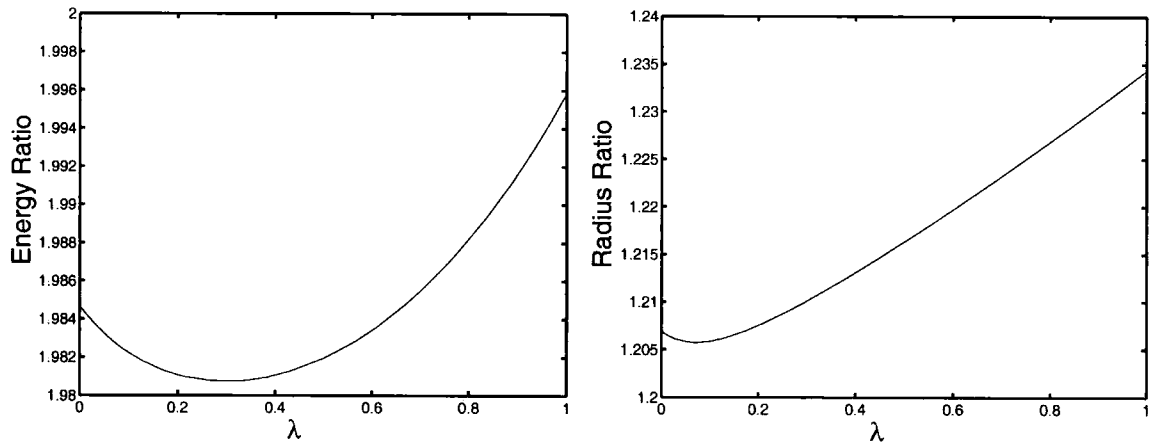

Figure 4.14: $\tilde{E}$ and $\tilde{R}$ ratio of $B = 2/B = 1$ as a function of λ for the $SU(3)$ harmonic map ansatz.

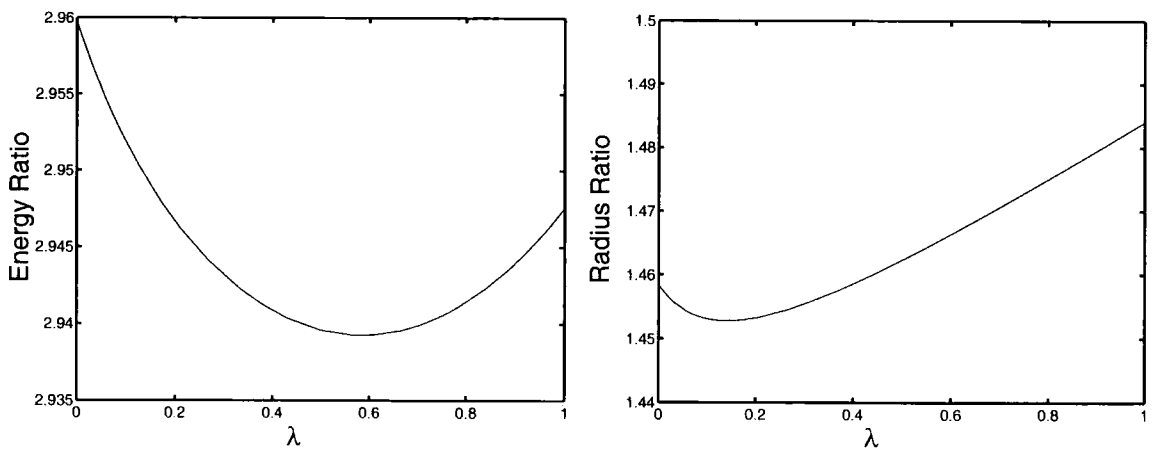

Figure 4.15: $\tilde{E}$ and $\tilde{R}$ ratio of $B = 3/B = 1$ as a function of λ for the $SU(3)$ harmonic map ansatz.

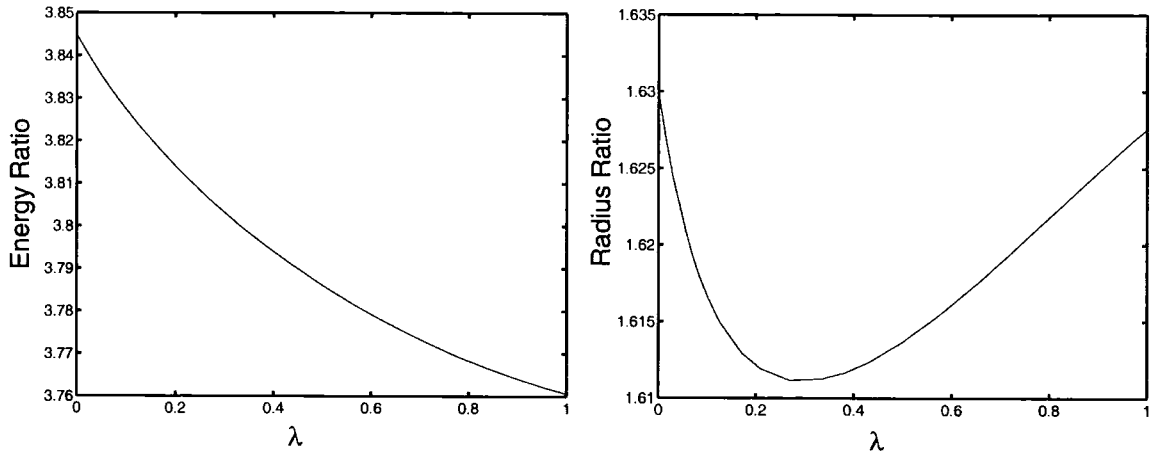

Figure 4.16: $\tilde{E}$ and $\tilde{R}$ ratio of $B = 4/B = 1$ as a function of λ for the $SU(3)$ harmonic map ansatz.

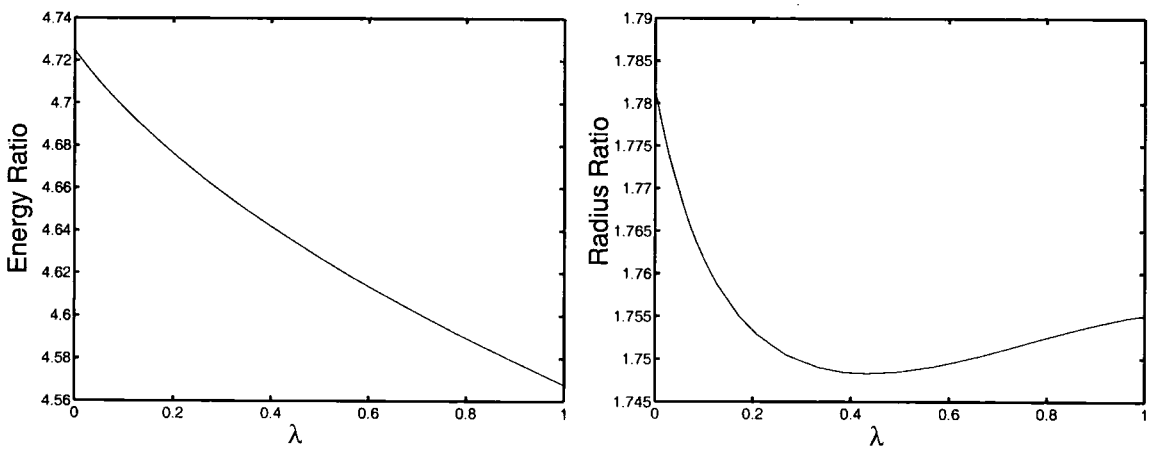

Figure 4.17: $\tilde{E}$ and $\tilde{R}$ ratio of $B = 5/B = 1$ as a function of λ for the $SU(3)$ harmonic map ansatz.

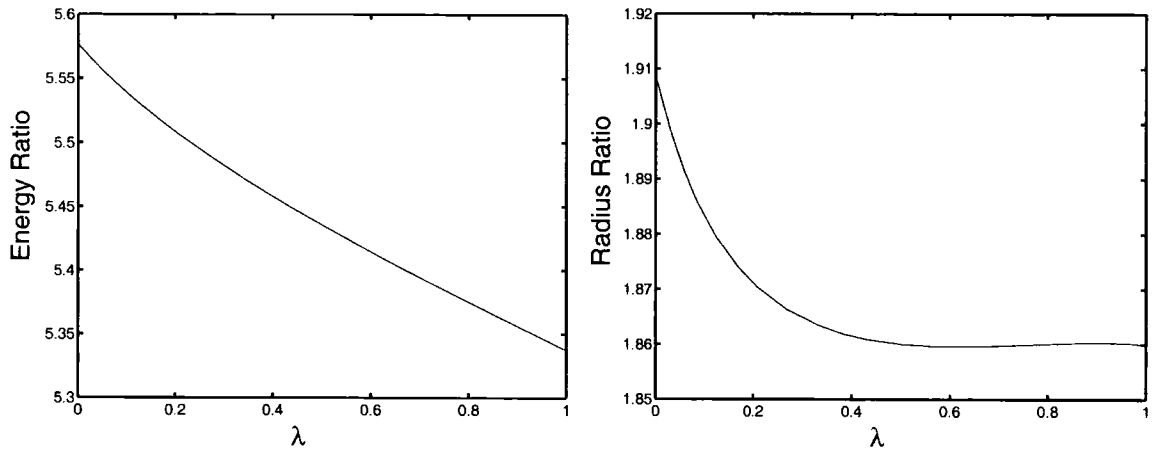

Figure 4.18: $\tilde{E}$ and $\tilde{R}$ ratio of $B = 6/B = 1$ as a function of λ for the $SU(3)$ harmonic map ansatz.

From Figures 4.14 to 4.18 we observe that that unlike the $SU(2)$ model, the energy of the $B = 2$ solutions increases with λ. For a given B and a fixed value of λ, the energy ratio of these configurations is always larger than the energy ratio of the corresponding $SU(2)$ solutions, while on the other hand, the radius ratios is always smaller.

It is also interesting to note that the λ dependence of the energy and radius ratios obtained for a given B looks very much like the curve obtained for the $SU(2)$ model for $B - 1$ Skyrmions. This can be explained by performing the change of variable $r \to rk$, where

$$k^2 = \frac{(1-\lambda)}{2}\left(1 + \sqrt{1 + \frac{4\lambda}{A_N(1-\lambda)^2}}\right) \tag{4.28}$$

and rewrite (4.20) as

$$\tilde{E} = \frac{A_N k}{3\pi}\int dr\Bigg(A_N\, g_r^2 r^2 + 2\mathcal{N}'\sin^2 g\,\left(1 + (1-\lambda')g_r^2\right) + (1-\lambda')\mathcal{I}'\frac{\sin^4 g}{k^2 r^2} + \lambda'\mathcal{I}'\frac{\sin^4 g}{r^2}\, g_r^2\Bigg) \tag{4.29}$$

where $\mathcal{N}' = \mathcal{N}/A_N$, $\mathcal{I}' = \mathcal{I}/A_N$, and $\lambda' = \lambda/k^4$. The function $k(\lambda)$ monotonically decreases from $k(0) = 1$ to $k(1) = A_N^{-1/4} = 0.931$ and so it is relatively close to 1 for all values of λ.

$SU(2)$		$SU(3)$			
N	$\mathcal{I}$	N	$\mathcal{I}$	$\mathcal{N}'$	$\mathcal{I}'$
2	5.81	3	10.65	2.25	7.98
3	13.58	4	18.05	3	13.54
4	20.65	5	27.26	3.75	20.44
5	37.75	6	37.33	4.5	28

Table 4.3: $\mathcal{N}'$ and $\mathcal{I}'$ for the $SU(3)$ ansatz.

In Table 4.3, we give the values of $\mathcal{N}'$ and $\mathcal{I}'$ for the $SU(3)$ ansatz and we notice that the $SU(3)$ solutions for $B = 4$ and $B = 5$ are closely related to the $SU(2)$ solutions for $B = 3$ and $B = 4$ respectively.

4.6 Comparison with numerical solutions

Having examined the λ dependence of the energy and radius ratios of the sixth order Skyrme model in the harmonic map ansatz (Figures 4.4 to 4.18), in this section we want to compare our results with the true solutions. Let us emphasise one more time that the harmonic map ansatz describes only an approximation and not the actual solution of the model. Hence, we cannot compare the skyrmion configurations of this chapter directly with experimental data.

In Tables 4.4 and 4.5 we present the asymptotic values of the energy and radius ratios, *i.e.* the values for $\lambda = 0$ and $\lambda = 1$, for both the $SU(2)$ and $SU(3)$ versions of the model. We compare these values with the $SU(2)$ numerical solutions that we found in the previous chapter.

For the energy ratio we see that the values predicted by the harmonic map approximation are always too high and as mentioned previously, the largest error is observed for the $B = 2$ configuration. On the other hand, as B increases we see that the relative error becomes smaller. This is not surprising since, as previously noted for the $SU(2)$ pure Skyrme model, the harmonic map ansatz seems to approximate the true solutions of the model better for large B. As expected, for the $SU(3)$ version

	$SU(2)$ Numerical Solutions		$SU(2)$		$SU(3)$	
B	Skyrme Ratio	Sk6 Ratio	Skyrme Ratio	Sk6 Ratio	Skyrme Ratio	Sk6 Ratio
2	1.9009	1.8395	1.96223	1.95407	1.98468	1.99585
3	2.7650	2.7103	2.88541	2.82888	2.95974	2.94756
4	3.6090	3.5045	3.69164	3.52850	3.84491	3.76064
5	4.5000	4.3780	4.65685	4.45345	4.72485	4.56766
6	-	-	5.54105	5.26743	5.57660	5.33739
7	-	-	6.29299	5.90659	-	-
8	-	-	7.26286	6.83536	-	-
9	-	-	8.20935	7.73077	-	-

Table 4.4: Energy ratio, $E_B/E_{B=1}$, for the $SU(2)$ numerical solutions, and the $SU(2)$ and $SU(3)$ harmonic map ansatz configurations.

	$SU(2)$ Numerical Solutions		$SU(2)$		$SU(3)$	
B	Skyrme Ratio	Sk6 Ratio	Skyrme Ratio	Sk6 Ratio	Skyrme Ratio	Sk6 Ratio
2	1.3549	1.308	1.37023	1.39403	1.20691	1.234384
3	1.5080	1.5570	1.63107	1.62894	1.45842	1.483996
4	1.6850	1.7420	1.78911	1.746286	1.63002	1.62755
5	1.8890	1.9250	2.013822	1.95551	1.78149	1.75505
6	-	-	2.178298	2.09768	1.909141	1.859916
7	-	-	2.272394	2.16623	-	-
8	-	-	2.454491	2.33477	-	-
9	-	-	2.614928	2.48059	-	-

Table 4.5: Radius ratio, $R_B/R_{B=1}$, for the $SU(2)$ numerical solutions, and the $SU(2)$ and $SU(3)$ harmonic map ansatz configurations.

of the model the values of the energy ratio are always larger than the corresponding $SU(2)$ embeddings. Moreover, we notice that as in the actual solutions of the model, the additional sixth order term in the harmonic map ansatz increases the binding energies. The only exception being the $B = 2$ case in $SU(3)$.

Similarly, from Table 4.5, we see that the sixth order term makes the skyrmions narrower except for $B = 2$ in $SU(2)$ and $B = 2, 3$ in $SU(3)$. It is also noticeable that the values of the radius ratio in $SU(3)$ are always much smaller that the corresponding ones in $SU(2)$. This implies that the skyrmion configurations in $SU(3)$ are narrower in comparison to their $SU(2)$ embeddings.

As a concluding remark, we note that the harmonic map ansatz provides us with a rather good approximation of the multi-skyrmion solutions of the extended Skyrme model. It predicts the symmetries of these configurations correctly, at least for $B \leq 5$. In addition, the values of the total energy and radius, obtained using this ansatz, are good approximations of the true solutions, and in many cases even better, for the extended model than for the pure Skyrme model.

Chapter 5

Spherically symmetric solutions in $SU(N)$

5.1 Introduction

Until now, our study of the sixth order Skyrme model (2.34) has mainly concentrated on finding static solutions that are global minima of the energy functional (2.35) and as we argued in chapter 3, one can only obtain such solutions numerically. In this chapter we will explore the possibility of constructing topologically non trivial solutions in $SU(N)$ using analytical methods. Although these solutions will be saddle points, *i.e.* they will have higher energy than the solutions we have found previously, their properties are quite interesting from a mathematical point of view.

In our construction we will follow the method that is described in [49] and is based on the harmonic map ansatz (4.14). In the previous chapter we showed that this ansatz can be used to approximate minimum energy solutions of the pure Skyrme model quite well. Under this approximation, the angular dependence of the $SU(N)$ Skyrme fields is described by a harmonic map, P, of the form (4.22) whereas the radial dependence is given by a profile function $g(r)$. However, as has been proven in [49], if we include in this ansatz further projectors, P_i, which are constructed in a very special way, then we obtain exact solutions for the pure Skyrme model in $SU(N)$. These solutions are all spherically symmetric and although they are local minima (or saddle points) rather than global minima, they correspond to bound states of skyrmions.

In what follows, we will consider the same generalised harmonic map ansatz and will also try to construct radially symmetric solutions for the extended sixth order Skyrme model. We will show that for this model the multi-projector ansatz can provide us with exact solutions in $SU(3)$. However, we will prove that due to an additional constraint that is coming from the extra sixth order term, this method

does not work for the general $SU(N)$ model. Nevertheless, this generalised ansatz can still be used to construct low-energy bound states in $SU(N)$. As we shall see, these configurations have some quite interesting properties.

5.2 Generalisation of the harmonic map ansatz in $SU(N)$

Our starting point will be the one-projector harmonic map ansatz that we introduced in the previous chapter,

$$\begin{aligned} U(r,\theta,\varphi) &= e^{2if(r)(P(\xi,\bar{\xi})-I/N)} \\ &= e^{-2if(r)/N}\left(I+(e^{2if(r)}-1)P(\xi,\bar{\xi})\right). \end{aligned} \tag{5.1}$$

We remind the reader that the profile function $f(r)$ describes the radial dependence of the field U and the projector P describes the angular part. In addition, P is a harmonic map from S^2 to $\mathbb{CP}^{N-1}$, *i.e.* a solution of the $\mathbb{CP}^{N-1}$ model, and satisfies the Euler-Lagrange equation

$$\left[\partial_\xi\partial_{\bar{\xi}}P, P\right] = 0. \tag{5.2}$$

As we have mentioned previously, when the projector P is of the form

$$P(h) = \frac{h\otimes h^\dagger}{|h|^2}, \tag{5.3}$$

where the complex vector $h \in C^N$ is holomorphic

$$\frac{\partial h}{\partial\bar{\xi}} = 0, \tag{5.4}$$

then P also satisfies the first order self-dual equations

$$P\,\partial_\xi P = 0 \qquad \text{and} \qquad \partial_\xi P\,P = \partial_\xi P. \tag{5.5}$$

Besides the map (5.3), there are further solutions of the $\mathbb{CP}^{N-1}$ model that can be constructed in a very special way. To illustrate how this is done, we need to introduce an operator P_+ which acts on any complex vector $u \in C^N$ and is defined as

$$P_+u = \partial_\xi u - u\,\frac{u^\dagger\,\partial_\xi u}{|u|^2}. \tag{5.6}$$

If we take a holomorphic vector $h(\xi)$, we can define $P_0^+ h = h$ and by induction

$$V_k = P_+^k h = P_+(P_+^{k-1} h). \tag{5.7}$$

Using these N-component vectors, we can then construct a sequence of solutions (or else projectors) of the $\mathbb{CP}^{N-1}$ model as follows:

$$P_k = P(P_+^k h) = \frac{V_k V_k^\dagger}{|V_k|^2} = \frac{P_+^k h (P_+^k h)^\dagger}{|P_+^k h|^2}, \qquad k = 0, \ldots, N-1. \tag{5.8}$$

It is clear that the first projector P_0 of the above sequence is the one previously defined in (5.3).

It can be proven that the harmonic maps (5.8) are solutions of the general second order equations (5.2). The details of this proof can be found in [51] and in Appendix B we repeat it for reasons of completeness.

From (5.8), we see that the action of the operator P_+ can be understood as a transformation from one solution of the $\mathbb{CP}^{N-1}$ model, to another [51]. Notice also, that any projector P_k for $k \geq 1$, which is constructed like (5.8), no longer satisfies the self-dual equations (5.5). This follows quite easily from the following properties of the vectors $P_+^k h$ [51, 49]:

$$\begin{aligned} (P_+^k h)^\dagger P_+^l h &= 0, \quad \text{if } k \neq l, \\ \partial_{\bar{\xi}} (P_+^k h) &= -P_+^{k-1} h \frac{|P_+^k h|^2}{|P_+^{k-1} h|^2}, \\ \partial_\xi \left(\frac{P_+^{k-1} h}{|P_+^{k-1} h|^2} \right) &= \frac{P_+^k h}{|P_+^{k-1} h|^2}. \end{aligned} \tag{5.9}$$

These properties hold only if we assume that h is holomorphic. They also imply that the harmonic projectors P_k are mutually orthogonal [51], *i.e.* they satisfy the following relations

$$\begin{aligned} P_k P_j &= \delta_{kj} P_k, \\ \sum_{k=0}^{N-1} P_k &= 1. \end{aligned} \tag{5.10}$$

Using all the above, we can define a generalised multi-projector ansatz [49] as

$$\begin{aligned} U &= exp\{ig_0(P_0 - \frac{I}{N}) + ig_1(P_1 - \frac{I}{N}) + \cdots + ig_{N-2}(P_{N-2} - \frac{I}{N})\} \\ &= e^{-ig_0/N}(I + A_0 P_0)\, e^{-ig_1/N}(I + A_1 P_1) \ldots\, e^{-ig_{N-2}/N}(I + A_{N-2} P_{N-2}), \end{aligned} \tag{5.11}$$

where $g_k(r)$ are $N-1$ unknown profile functions and $A_k = e^{ig_k} - 1$. From the orthogonality property (5.10) we see that the projector P_{N-1} can always be written as a linear combination of the remaining projectors and hence, we do not consider it in the description of U. Moreover, for the ansatz to be well defined, the profile functions $g_k(r)$ must be a multiple of 2π at the origin and at infinity.

In what follows, we will use this ansatz to construct spherically symmetric solutions for the pure and the extended sixth order Skyrme model.

There is one final remark to be made at this point. In the previous chapter we argued that if we do not consider the radial dependence from $g(r)$, then the one projector ansatz, defined in (5.1), depends on the $2N-1$ real functions of the harmonic map. However, a general $SU(N)$ field has N^2-1 degrees of freedom and hence, using this approximation we cannot explore the whole target space of $SU(N)$. To improve this ansatz, one can consider further projectors that do not depend on each other. By assuming that these projectors are mutually orthogonal, *i.e.* they satisfy equations (5.10), we ensure that the field U has N^2-1 degrees of freedom[1]. In order to obtain minimum energy solutions, one needs to consider the most general form for all maps and minimise them with respect to their parameters simultaneously. This has been done in [50] for $SU(3)$. However, this generalisation is much more difficult to handle even numerically. Hence, we will restrict ourselves to the multi-projector ansatz (5.11), where all harmonic maps are constructed from the sequence (5.8). It is clear that in this approximation the fields U have at most $2N-1$ degrees of freedom.

5.3 Constructing radially symmetric skyrmions in $SU(N)$

Having defined the generalised multi-projector ansatz in (5.11), we proceed by expressing the general Euler-Lagrange equations of the model (2.40) in the usual spherical coordinates (r, θ, ϕ). This will prove useful for the calculations that will follow.

[1] In general, a harmonic map P_N in $\mathbb{CP}^{N-1}$ is described by a C^N vector. A vector orthogonal to that is a C^{N-1} vector and hence it describes a harmonic map that is a solution of the $\mathbb{CP}^{N-2}$ model, *i.e.* a map with $2N-3$ degrees of freedom.

We have,

$$\partial_r \left\{ r^2 R_r + \frac{1-\lambda}{4}\left(A_{\theta r\theta} + \frac{1}{\sin^2\theta} A_{\varphi r\varphi} \right) + \frac{1}{16}\lambda \left[\frac{1}{\sin^2\theta} \left(B_{\theta\theta\varphi r\varphi} + B_{\varphi\varphi\theta r\theta} \right) \right] \right\}$$
$$+ \frac{1}{\sin\theta}\,\partial_\theta \left\{ \sin\theta + \left[R_\theta + \frac{1-\lambda}{4}\left(A_{r\theta r} + \frac{1}{r^2\sin^2\theta} A_{\varphi\theta\varphi} \right) \right] \right.$$
$$\left. + \frac{\lambda}{16\, r^2 \sin^2\theta} \left(B_{rr\varphi\theta\varphi} + B_{\varphi\varphi r\theta r} \right) \right\} + \frac{1}{\sin^2\theta}\,\partial_\varphi \left\{ R_\varphi + \frac{1-\lambda}{4}\left(A_{r\varphi r} + \frac{1}{r^2} A_{\theta\varphi\theta} \right) \right.$$
$$\left. + \frac{\lambda}{16\, r^2} \left(B_{rr\theta\varphi\theta} + B_{\theta\theta r\varphi r} \right) \right\} = 0, \tag{5.12}$$

where

$$A_{jij} \equiv \Big[R_j,\, [R_i,\, R_j] \Big] \qquad \text{and} \qquad B_{jjkik} \equiv \Big[R_j,\, [R_j, R_k]\, [R_i, R_k] \Big]. \tag{5.13}$$

At this stage we would like to remind the reader that, as before, the parameter $\lambda \in [0,1]$ is dimensionless and denotes the mixing between the two higher order terms, the Skyrme and the sixth order term. It is fairly easy to show that

$$R_r = i \sum_{j=0}^{N-2} \dot{g}_j \left(P_j - \frac{I}{N} \right), \tag{5.14}$$

where $\dot{g}_j$ is the derivative of $g_j(r)$ with respect to r. In addition, if we map the polar angles (θ, ϕ) to the complex coordinates $(\xi, \bar{\xi})$ using the stereographic projection, $\xi = \tan(\theta/2) e^{i\phi}$, we have

$$R_\xi = \sum_{i=1}^{N-1} \left[e^{i(g_i - g_{i-1})} - 1 \right] \frac{V_i\, V_{i-1}^\dagger}{|V_{i-1}|^2}\,, \tag{5.15}$$

and the derivatives with respect to θ and φ are given by

$$\partial_\theta = \frac{1+|\xi|^2}{2\sqrt{|\xi|^2}} \left(\xi\, \partial_\xi + \bar{\xi}\, \partial_{\bar{\xi}} \right), \qquad \partial_\varphi = i \left(\xi\, \partial_\xi - \bar{\xi}\, \partial_{\bar{\xi}} \right). \tag{5.16}$$

Substituting the above into equations (5.12) we get

$$\partial_r\left[r^2R_r+(1-\lambda)\frac{(1+|\xi|^2)^2}{8}\left(A_{\bar{\xi}r\xi}+A_{\xi r\bar{\xi}}\right)\right]+\frac{(1+|\xi|^2)^2}{2}\left((R_{\bar{\xi}})_{\xi}+(R_{\xi})_{\bar{\xi}}\right)$$
$$+(1-\lambda)\frac{(1+|\xi|^2)^3}{8r^2}\left(\xi\,A_{\xi\xi\bar{\xi}}-\bar{\xi}\,A_{\bar{\xi}\xi\bar{\xi}}\right)+(1-\lambda)\frac{(1+|\xi|^2)^4}{16r^2}\left(\left[A_{\xi\xi\bar{\xi}}\right]_{\bar{\xi}}-\left[A_{\bar{\xi}\xi\bar{\xi}}\right]_{\xi}\right)$$
$$+(1-\lambda)\frac{(1+|\xi|^2)^2}{8}\left(\left[A_{r\bar{\xi}r}\right]_{\xi}+\left[A_{r\xi r}\right]_{\bar{\xi}}\right)+\frac{\lambda}{16}\Bigg\{\partial_r\left[\frac{(1+|\xi|^2)^4}{4}\left(B_{\bar{\xi}\xi\bar{\xi}r\bar{\xi}}-B_{\xi\xi\bar{\xi}r\bar{\xi}}\right)\right]$$
$$+\frac{(1+|\xi|^2)^2}{4r^2}\left(\partial_{\bar{\xi}}\left[(1+|\xi|^2)^2\,B_{rr\xi\xi\bar{\xi}}\right]-\partial_{\xi}\left[(1+|\xi|^2)^2\,B_{rr\bar{\xi}\xi\bar{\xi}}\right]\right)$$
$$+\frac{(1+|\xi|^2)^2}{2|\xi|^2\,r^2}\left(\xi\partial_{\xi}\left[\frac{(1+|\xi|^2)^2}{4|\xi|^2}(-\xi\xi\xi B_{\xi\xi r\xi r})\right]+\bar{\xi}\partial_{\bar{\xi}}\left[\frac{(1+|\xi|^2)^2}{4|\xi|^2}(-\bar{\xi}\bar{\xi}\bar{\xi}B_{\bar{\xi}\bar{\xi}r\bar{\xi}r})\right]\right)$$
$$+\frac{(1+|\xi|^2)^2}{8r^2}\Bigg(\partial_{\xi}\Big[(1+|\xi|^2)^2(B_{\xi\bar{\xi}r\bar{\xi}r}+B_{\bar{\xi}\xi r\bar{\xi}r}-B_{\bar{\xi}\bar{\xi}r\xi r})\Big]$$
$$+\partial_{\bar{\xi}}\Big[(1+|\xi|^2)^2(-B_{\xi\xi r\bar{\xi}r}+B_{\xi\bar{\xi}r\xi r}+B_{\bar{\xi}\xi r\xi r})\Big]\Bigg)\Bigg\}=0. \quad (5.17)$$

As has been shown in [49], one can construct topologically non-trivial solutions for the usual Skyrme model, *i.e.* solutions of equations (5.17) when $\lambda = 0$, by considering the following spherically symmetric holomorphic vector

$$V_0 = h = (h_0, h_1, \ldots, h_{N-1})^t, \quad (5.18)$$

where

$$h_k = \xi^k\sqrt{C_k^{N-1}}, \quad (5.19)$$

and where C_k^{N-1} denotes the binomial coefficients. To illustrate this construction, in the next section we briefly present some of the calculations performed in [49] for the pure Skyrme model. We then apply the same method to the extended Skyrme model and determine whether it works equally well.

5.3.1 Solutions for the pure Skyrme model

In this section, we will only consider the terms of equations (5.17) that come from the pure Skyrme model and hence, we will ignore all terms which are proportional to $\lambda/16$, *i.e.* we will set $\lambda = 0$ in the equation (5.17).

We start by noting

$$[R_\xi, R_{\bar\xi}] = -\sum_{i=1}^{N-1} a_i^2 \frac{|V_i|^2}{|V_{i-1}|^2}\left(\frac{V_iV_i^\dagger}{|V_i|^2} - \frac{V_{i-1}V_{i-1}^\dagger}{|V_{i-1}|^2}\right), \tag{5.20}$$

$$[R_r, R_\xi] = i\sum_{i=1}^{N-1}(\dot g_i a_i - \dot g_{i-1}a_i)\,\frac{V_iV_{i-1}^\dagger}{|V_{i-1}|^2} = \sum_{i=1}^{N-1} K_i \frac{V_iV_{i-1}^\dagger}{|V_{i-1}|^2}, \tag{5.21}$$

$$[R_r, R_{\bar\xi}] = i\sum_{i=1}^{N-1}(\dot g_i a_i - \dot g_{i-1}a_i)\,\frac{V_{i-1}V_i^\dagger}{|V_{i-1}|^2} = \sum_{i=1}^{N-1} K_i \frac{V_{i-1}V_i^\dagger}{|V_{i-1}|^2}, \tag{5.22}$$

where $a_i = e^{i(g_i - g_{i-1})} - 1$. Using the above we have

$$A_{\xi\xi\bar\xi} = [R_\xi, [R_\xi, R_{\bar\xi}]] = \sum_{i=1}^{N-1}\left(\Gamma_i\frac{|V_{i+2}|^2}{|V_{i+1}|^2} + \Delta_i\frac{|V_{i+1}|^2}{|V_i|^2} + H_i\frac{|V_i|^2}{|V_{i-1}|^2}\right)\frac{V_iV_{i-1}^\dagger}{|V_{i-1}|^2}, \tag{5.23}$$

$$A_{r\bar\xi r} = [R_r, [R_{\bar\xi}, R_r]] = \sum_{i=1}^{N-1}\Theta_i\frac{V_{i-1}V_i^\dagger}{|V_{i-1}|^2}, \tag{5.24}$$

where Γ_i, Δ_i and H_i are functions of $g_k(r)$ and Θ_i also include the derivatives of $g_k(r)$.

One of the most important properties of the vectors $V_k = P_+^k h$ when h has the particular form (5.19) is that

$$\frac{|V_i|^2}{|V_{i-1}|^2} \propto (1+|\xi|^2)^{-2}. \tag{5.25}$$

This was proved in [49] and in Appendix B we present this proof in detail. Using (5.25) and keeping in mind that $\partial_\xi\,(1+|\xi|^2)^{-2} = -2\bar\xi(1+|\xi|^2)^{-3}$, we have that the terms

$$\frac{(1+|\xi|^2)^3}{8r^2}\,\xi\,A_{\xi\xi\bar\xi} \qquad \text{and} \qquad \frac{(1+|\xi|^2)^4}{16r^2}\,[A_{\xi\xi\bar\xi}]_{\bar\xi}, \tag{5.26}$$

in equations (5.17) will mutually cancel out their ξ-dependence coming outside the projectors P_i. The only terms that will 'survive' are terms that involve the derivatives of $\frac{V_iV_{i-1}^\dagger}{|V_{i-1}|^2}$. These terms are proportional to $\sum_{i=1}^{N-1}(1+|\xi|^2)^{-2}(P_i - P_{i-1})\,L_i$, where L_i are functions of $g_k(r)$ only.

Using similar arguments one can show [49] that all the remaining terms for the pure Skyrme model are proportional to either $P_i - P_{i-1}$ or $P_i - \frac{I}{N}$. Moreover, from (5.10) one can eliminate the projector P_{N-1} and as a result equations (5.17) will be the sum of the $N-1$ terms $P_i - \frac{I}{N}$ for $i = 0 \ldots N-2$, with coefficients that depend

only on r. This implies that the Euler-Lagrange equations for the Skyrme model reduce to $N-1$ ordinary differential equations for the profile functions g_i and their solutions, if they exist, will provide us with exact solutions of the $SU(N)$ Skyrme model.

Note that the latter is similar to the $B=1$ skyrmion in $SU(2)$ that we have studied in the previous chapters. There we saw that if we use the hedgehog ansatz (2.7) to describe the fields U, then the angular dependence of the equations of motion vanishes and one is left with an ordinary differential equation of the profile function that depends only on r. The solution of this equation corresponds to an exact solution of the model. We can therefore understand the multi-projector ansatz (5.11) as a generalisation of the hedgehog solution for $B=1$. Any solution obtained using this ansatz, with P_i constructed as (5.8) and V_k given by (5.18), will be an exact spherically symmetric solution in $SU(N)$. In fact, the $B=1$ skyrmion is just the $SU(2)$ special case of these solutions.

5.3.2 Solutions for the extended sixth order Skyrme model

In this section we wish to determine whether we can also construct spherically symmetric solutions for the extended sixth order Skyrme model. Since we have already shown that this is true for the pure Skyrme model, it is sufficient to consider only the extra terms of equations (5.17) that come from the sixth order term, *i.e.* terms that are proportional to $\lambda/16$, and try to factorise their angular dependence similarly.

Our calculations will start from the terms that involve $B_{\bar{\xi}\xi\bar{\xi}r\xi}$ and $B_{\xi\xi\bar{\xi}r\bar{\xi}}$. Using (5.20-5.22) it is straightforward to check that

$$B_{\bar{\xi}\xi\bar{\xi}r\xi} - B_{\xi\xi\bar{\xi}r\bar{\xi}} = \sum_{i=1}^{N-1} \left(b_i \frac{|V_{i-1}|^2}{|V_{i-2}|^2} \frac{|V_i|^2}{|V_{i-1}|^2} + c_i \frac{|V_i|^4}{|V_{i-1}|^4} + d_i \frac{|V_{i+1}|^2}{|V_i|^2} \frac{|V_i|^2}{|V_{i-1}|^2} \right) (P_i - P_{i-1}), \tag{5.27}$$

where b_i, c_i and d_i are functions of g_k only. However, by using the property (5.25) we have that

$$\frac{(1+|\xi|^2)^4}{4} \left(B_{\bar{\xi}\xi\bar{\xi}r\xi} - B_{\xi\xi\bar{\xi}r\bar{\xi}} \right) \propto (P_i - P_{i-1}). \tag{5.28}$$

Hence, we have proven that these two terms are proportional to $P_i - P_{i-1}$. Further-

more, we notice that

$$B_{rr\xi\xi\bar{\xi}} = i\sum_{i=1}^{N-1}\left(e_i\frac{|V_i|^2}{|V_{i-1}|^2}+s_i\frac{|V_{i-1}|^2}{|V_{i-2}|^2}\right)\frac{V_iV_{i-1}^\dagger}{|V_{i-1}|^2}, \tag{5.29}$$

with $e_i = e(g_i)$ and $s_i = s(g_i)$. But in equation (5.17) this term appears as

$$\partial_{\bar{\xi}}\left[(1+|\xi|^2)^2 B_{rr\xi\xi\bar{\xi}}\right] = 2\xi\,(1+|\xi|^2)B_{rr\xi\xi\bar{\xi}} + (1+|\xi|^2)^2\,\partial_{\bar{\xi}}\,(B_{rr\xi\xi\bar{\xi}}). \tag{5.30}$$

As before, we have that $\partial_{\bar{\xi}}\frac{|V_i|^2}{|V_{i-1}|^2} \propto -2\xi\,(1+|\xi|^2)^{-3}$ and the only parts of (5.30) that are non-zero are the ones that involve the derivatives of $\frac{V_iV_{i-1}^\dagger}{|V_{i-1}|^2}$ with respect to $\bar{\xi}$. As these terms are proportional to $\sum_{i-1}^{N-1} C_i(1+|\xi|^2)^{-2}\,(P_i - P_{i-1})$ where $C_i = C(g_i)$, we see that the term $B_{rr\xi\xi\bar{\xi}}$ in (5.17) is also proportional to $(P_i - P_{i-1})$.

Using a similar argument we see that the term in (5.17) involving

$$B_{rr\bar{\xi}\xi\bar{\xi}} = i\sum_{i=1}^{N-1}\left(E_i\frac{|V_i|^2}{|V_{i-1}|^2}+S_i\frac{|V_{i+1}|^2}{|V_i|^2}\right)\frac{V_{i-1}V_i^\dagger}{|V_{i-1}|^2}, \tag{5.31}$$

where $E_i = E(g_i)$ and $S_i = S(g_i)$, is also proportional to $(P_i - P_{i-1})$.

We continue our calculation by considering the terms

$$B_{\xi\xi r\bar{\xi}r} = \sum_{i=1}^{N-1}\left(M_i\frac{|V_{i-1}|^2}{|V_{i-2}|^2}+N_i\frac{|V_i|^2}{|V_{i-1}|^2}\right)\frac{V_iV_{i-1}^\dagger}{|V_{i-1}|^2}, \tag{5.32}$$

$$B_{\xi\bar{\xi}r\xi r} = \sum_{i=1}^{N-1}\left(T_i\frac{|V_i|^2}{|V_{i-1}|^2}+U_i\frac{|V_{i+1}|^2}{|V_i|^2}\right)\frac{V_iV_{i-1}^\dagger}{|V_{i-1}|^2}, \tag{5.33}$$

$$B_{\bar{\xi}\xi r\xi r} = -\sum_{i=1}^{N-1}\left(X_i\frac{|V_{i+1}|^2}{|V_i|^2}+Y_i\frac{|V_{i-1}|^2}{|V_{i-2}|^2}\right)\frac{V_iV_{i-1}^\dagger}{|V_{i-1}|^2}, \tag{5.34}$$

where all $M_i, N_i, T_i, U_i, X_i, Y_i$ are functions of $g_i(r)$ and their derivatives. Looking carefully to terms (5.32), (5.33) and (5.34) we observe that they have a similar structure to term (5.29) and hence, they too factorise in such a way that the $(\xi, \bar{\xi})$ dependence outside the projectors P_i cancels out and the remaining terms are proportional to $(P_i - P_{i-1})$.

Similarly we have the terms

$$B_{\xi\bar{\xi}r\bar{\xi}r} = \sum_{i=1}^{N-1}\left(\tilde{M}_i\frac{|V_i|^2}{|V_{i-1}|^2}\frac{V_iV_{i+1}^\dagger}{|V_i|^2}+\tilde{N}_i\frac{|V_{i+1}|^2}{|V_i|^2}\frac{V_{i-1}V_i^\dagger}{|V_{i-1}|^2}\right), \tag{5.35}$$

$$B_{\xi\bar{\xi}r\xi r} = \sum_{i=1}^{N-1} \left(\tilde{T}_i \frac{|V_i|^2}{|V_{i-1}|^2} + \tilde{U}_i \frac{|V_{i-1}|^2}{|V_{i-2}|^2} \right) \frac{V_{i-1}V_i^\dagger}{|V_{i-1}|^2}, \tag{5.36}$$

$$B_{\bar{\xi}\xi r\xi r} = -\sum_{i=1}^{N-1} \left(\tilde{X}_i \frac{|V_{i+1}|^2}{|V_i|^2} + \tilde{Y}_i \frac{|V_{i-1}|^2}{|V_{i-2}|^2} \right) \frac{V_{i-1}V_i^\dagger}{|V_{i-1}|^2}, \tag{5.37}$$

where again $\tilde{M}_i, \tilde{N}_i, \tilde{T}_i, \tilde{U}_i, \tilde{X}_i, \tilde{Y}_i$ are functions of $g_i(r)$ and their derivatives. These terms have a similar form to term (5.31) and thus, they are also proportional to $(P_i - P_{i-1})$ after appropriate simplification.

So far all terms we have considered are all proportional to $(P_i - P_{i-1})$ as in the case of the pure Skyrme model. We now look at the remaining two terms in (5.17). They involve the expressions

$$B_{\xi\xi r\xi r} = \sum_{i=3}^{N-1} (a_i K_{i-1} K_{i-2} - a_{i-2} K_i K_{i-1}) \frac{V_i V_{i-3}^\dagger}{|V_{i-3}|^2}, \tag{5.38}$$

$$B_{\bar{\xi}\bar{\xi}r\bar{\xi}r} = \sum_{i=3}^{N-1} (a_i K_{i-1} K_{i-2} - a_{i-2} K_i K_{i-1}) \cdot \frac{V_{i-3} V_i^\dagger}{|V_{i-3}|^2}, \tag{5.39}$$

where $K_i = i\left(\dot{g}_i a_i - \dot{g}_{i-1} a_i\right)$ and $a_i = e^{i(g_i - g_{i-1})} - 1$. It is clear that these terms will always give a $\xi, \bar{\xi}$ dependence besides the projectors P_i and hence, if we want (5.17) to reduce to $N-1$ equations that involve only the profile functions g_i then we have to make sure that (5.38) and (5.39) vanish, *i.e.* we must impose the conditions

$$\begin{aligned} & a_i K_{i-1} K_{i-2} - a_{i-2} K_i K_{i-1} = 0 \Rightarrow \\ & a_i a_{i-2} (\dot{g}_{i-2} - \dot{g}_{i-3}) = a_i a_{i-2} (\dot{g}_i - \dot{g}_{i-1}) \Leftrightarrow \\ & \dot{g}_i - \dot{g}_{i-1} = \dot{g}_{i-2} - \dot{g}_{i-3}. \end{aligned} \tag{5.40}$$

This last constraint which is a result of the additional sixth order term, implies that we can only consider two profile functions g_0 and g_1 and that we should thus have only two equations. Unfortunately we have $N-1$ equations which are not compatible with each other, *i.e.* we cannot express them as a linear combination of two equations. All the above imply that the ansatz (5.11) will provide exact solutions of the generalised Skyrme model only for the $SU(2)$ and the $SU(3)$ where we have by definition one and two profile functions g_i respectively. For larger values of N, the ansatz will nevertheless give some low energy radially symmetric configurations.

5.3.3 Energy and topological charge in $SU(N)$

As shown in the previous section, by using ansatz (5.11) one can obtain solutions or low energy bound states – which are not solutions – for the sixth order Skyrme model by solving $N-1$ equations that involve only the functions $g_i(r)$. However, it is much easier to derive these equations by minimising the energy (2.39). For this purpose it is convenient to write the energy density in terms of $(\xi, \bar{\xi})$:

$$E = -\frac{i}{12\pi^2}\int r^2 dr\, d\xi d\bar{\xi}\, Tr\left(\frac{1}{(1+|\xi|^2)^2}R_r^2 + \frac{1}{r^2}|R_\xi|^2 + \frac{1-\lambda}{4r^2}[R_r, R_\xi][R_r, R_{\bar{\xi}}]\right.$$
$$\left. -(1-\lambda)\frac{(1+|\xi|^2)^2}{16r^4}[R_{\bar{\xi}}, R_\xi]^2 + \lambda\frac{(1+|\xi|^2)^2}{64r^4}\Big[[R_r, R_{\bar{\xi}}]\,,\,[R_r, R_\xi]\Big][R_\xi, R_{\bar{\xi}}]\right). \tag{5.41}$$

If we define

$$\begin{aligned} F_i &= g_i - g_{i+1} \qquad \text{for} \quad i = 0, \ldots, N-3, \\ F_{N-2} &= g_{N-2}, \end{aligned} \tag{5.42}$$

as well as

$$W_i = \frac{|V_i|^2}{|V_{i-1}|^2}\left(1-\cos(F_i)\right) \qquad \text{and} \qquad W_{N-1} = \frac{|V_{N-1}|^2}{|V_{N-2}|^2}\left(1-\cos(g_{N-2})\right), \tag{5.43}$$

then the terms in expression (5.41) can be rewritten as

$$Tr\, R_r^2 = \frac{1}{N}\left(\sum_{i=0}^{N-2}\dot{g}_i\right)^2 - \sum_{i=0}^{N-2}\dot{g}_i^2\,, \tag{5.44}$$

$$Tr\,|R_\xi|^2 = -2\sum_{i=1}^{N-1} W_i\,, \tag{5.45}$$

$$Tr\,[R_r, R_\xi][R_r, R_{\bar{\xi}}] = -2\sum_{k=1}^{N-1} W_k\, \dot{F}_{k-1}^2, \tag{5.46}$$

$$Tr\,[R_{\bar{\xi}}, R_\xi]^2 = 4\left(W_1^2 + \sum_{i=1}^{N-2}(W_i - W_{i+1})^2 + W_{N-1}^2\right), \tag{5.47}$$

$$Tr\left[[R_r, R_{\bar{\xi}}]\,,\,[R_r, R_\xi][R_\xi, R_{\bar{\xi}}]\right] = 4\Big(\dot{F}_0^2 W_1^2 + \sum_{i=1}^{N-2}\Big(\dot{F}_{i-1}W_i - \dot{F}_i W_{i+1}\Big)^2 + \dot{F}_{N-2}^2 W_{N-1}^2\Big), \tag{5.48}$$

where $\dot{g}_i = \frac{\partial}{\partial r} g_i$. However, since [49]

$$\frac{|V_k|^2}{|V_{k-1}|^2} = k(N-k)(1+|\xi|^2)^{-2}, \tag{5.49}$$

we see that all the terms in (5.41) are proportional to $(1+|\xi|^2)^{-2}$ and that after integrating out the angular dependence the energy reduces to

$$\begin{aligned} E = \frac{1}{6\pi}\int r^2 dr \Bigg\{ & -\frac{1}{N}\left(\sum_{i=0}^{N-2}\dot{g}_i\right)^2 + \sum_{i=0}^{N-2}\dot{g}_i^2 + \frac{2}{r^2}\sum_{k=1}^{N-1} Z_k + \frac{(1-\lambda)}{2r^2}\sum_{k=1}^{N-1}(\dot{g}_k - \dot{g}_{k-1})^2 Z_k \\ & + \frac{(1-\lambda)}{4r^4}\left(Z_1^2 + \sum_{k=1}^{N-2}(Z_k - Z_{k+1})^2 + Z_{N-1}^2\right) \\ & + \frac{\lambda}{16r^4}\left(\dot{F}_0^2 Z_1^2 + \sum_{k=1}^{N-2}(\dot{F}_{k-1}Z_k - \dot{F}_k Z_{k+1})^2 + \dot{F}_{N-2}^2 Z_{N-1}^2\right)\Bigg\}, \end{aligned} \tag{5.50}$$

where $Z_k = k(N-k)(1-\cos(F_{k-1}))$.

In [49], it was shown that for the pure Skyrme model ($\lambda = 0$), if we consider the fields F_i defined by (5.42), then we can obtain very special solutions by taking $F_0 = F_1 = \cdots = F_{N-2} = F$. In addition, it was observed that when $F(0) = 2\pi$ and $F(\infty) = 0$ this solution of the $SU(N)$ pure Skyrme model has topological charge

$$B = (F - \sin F)_{r=0}^{r=\infty}\sum_{k=0}^{N-2}(k+1)(N-k-1) = \frac{N}{6}(N^2-1). \tag{5.51}$$

The energy of these solutions is exactly equal to $\frac{N}{6}(N^2-1)$ times the energy of the single skyrmion solution. It is easy to show that, if one uses the same ansatz for the sixth order Skyrme model, the profile $f = F_0/2$ satisfies the hedgehog profile equation (3.5) and the energy of the configuration is given by $E(\lambda) = \frac{N}{6}(N^2-1)E_0(\lambda)$ where $E_0(\lambda)$ is the energy of the hedgehog solution for the generalised model. These configurations are not exact solutions, except for the $SU(3)$ model where we have only two profile functions g_0 and g_1 by definition.

By minimising (5.50), one can derive the following equations for the profile functions F_l, $l = 0,..(N-2)$.

$$-\frac{2(l+1)}{N}\sum_{i=0}^{N-2}(i+1)\ddot{F}_i+2\sum_{k=0}^{l}\sum_{i=k}^{N-2}\ddot{F}_i+\frac{(1-\lambda)}{r^2}\ddot{F}_l(l+1)(N-l-1)(1-\cos F_l)+$$
$$\frac{2}{r}\left(-\frac{2(l+1)}{N}\sum_{i=0}^{N-2}(i+1)\dot{F}_i+2\sum_{k=0}^{l}\left(\sum_{i=k}^{N-2}\dot{F}_i\right)\right)+\frac{(1-\lambda)}{2r^2}\dot{F}_l^2(l+1)(N-l-1)\sin F_l+$$
$$-\frac{2}{r^2}(l+1)(N-l-1)\sin F_l-\frac{(1-\lambda)}{r^4}(l+1)^2(N-l-1)^2(1-\cos F_l)\sin F_l+$$
$$\frac{(1-\lambda)}{2r^4}(l+1)(N-l-1)\sin F_l\,[l(N-l)(1-\cos F_{l-1})+(l+2)(N-l-2)(1-\cos F_{l+1})]$$
$$+\frac{\lambda}{8r^4}\Big\{2\,\ddot{F}_l(l+1)^2(N-l-1)^2(1-\cos F_l)^2-\ddot{F}_{l-1}l(l+1)(N-l)(N-l-1)$$
$$(1-\cos F_{l-1})(1-\cos F_l)-\ddot{F}_{l+1}(l+1)(l+2)(N-l-1)(N-l-2)$$
$$(1-\cos F_l)(1-\cos F_{l+1})\Big\}+\frac{-\lambda}{4r^5}\Big\{2\,\dot{F}_l(l+1)^2(N-l-1)^2(1-\cos F_l)^2-\dot{F}_{l-1}$$
$$l(l+1)(N-l)(N-l-1)(1-\cos F_{l-1})(1-\cos F_l)-\dot{F}_{l+1}(l+1)(l+2)(N-l-1)$$
$$(N-l-2)(1-\cos F_l)(1-\cos F_{l+1})\Big\}+\frac{\lambda}{8r^4}\Big\{2\,\dot{F}_l^2(l+1)^2(N-l-1)^2(1-\cos F_l)$$
$$\sin F_l-\dot{F}_{l-1}^2l(l+1)(N-l)(N-l-1)\sin F_{l-1}(1-\cos F_l)-\dot{F}_{l+1}^2(l+1)(l+2)$$
$$(N-l-1)(N-l-2)(1-\cos F_l)\sin F_{l+1}\Big\}=0. \tag{5.52}$$

When $N=3$, the solution of the 2 equations describes an exact solution of the model, while for larger values of N, the ansatz (5.11) corresponds to low energy configurations.

As proved in [15], the topological charge for the configuration (5.11) is given by

$$B=\sum_{k=0}^{N-2}\mathcal{D}_k(F_k-\sin F_k)_{r=0}^{r=\infty}, \tag{5.53}$$

where

$$\begin{aligned}\mathcal{D}_k &= -i\frac{1}{4\pi^2}\int\frac{|P_+^{k+1}h|^2}{|P_+^kh|^2}d\xi d\bar{\xi}\\ &= \frac{1}{2\pi}(k+1)(N-k-1).\end{aligned} \tag{5.54}$$

Each configuration is thus characterised by the boundary conditions for the profile function F_i and we can, without loss of generality, impose the condition $lim_{r\to\infty}F_i(r)=0$. For the configuration to be well defined at the origin we must

also impose a condition of the type

$$F_i(0) \;=\; n_i\, 2\pi, \tag{5.55}$$

where the $n_i \in N$.

In the following sections we will consider the equations (5.52) and obtain exact solutions for $SU(3)$ and low-energy configurations for $SU(4)$. We will also investigate some special cases in $SU(N)$.

5.4 Exact solutions in $SU(3)$

In $SU(3)$, the multi-projector ansatz (5.11) consists of two profile functions $g_0(r)$ and $g_1(r)$ and the constraint (5.40) is always satisfied. Hence, equations (5.52) lead to exact spherically symmetric solutions of the model. In order to describe these solutions it is more convenient to use the profile functions F_i (5.55) which in this case are $F = F_0$ and $g = F_1$. In this notation the energy (5.50) simplifies to

$$\begin{aligned} E \;=\; \frac{1}{6\pi}\int r^2 dr \Big\{ & \frac{2}{3}\left(\dot{g}^2 + \dot{F}^2 + \dot{g}\,\dot{F}\right) + \frac{1}{r^2}\Big((1-\cos F)((1-\lambda)\dot{F}^2 + 4) \\ & + (1-\cos g)((1-\lambda)\dot{g}^2 + 4)\Big) + (1-\lambda)\frac{2}{r^4}\Big((1-\cos F)^2 \\ & - (1-\cos F)(1-\cos g) + (1-\cos g)^2\Big) + \frac{\lambda}{2r^4}\Big(\dot{F}^2\,(1-\cos F)^2 \\ & + \dot{g}^2(1-\cos g)^2 - (1-\cos F)(1-\cos g)\dot{g}\dot{F}\Big)\Big\}. \end{aligned} \tag{5.56}$$

The equations for the two profile functions F and g are then given by

$$\begin{aligned} & \ddot{g} + \frac{1}{2}\ddot{F} + \frac{\dot{F}}{r} + 2\frac{\dot{g}}{r} + \frac{3}{2r^2}\Big((1-\lambda)(1-\cos g)\ddot{g} + \frac{1}{2}\sin g((1-\lambda)\dot{g}^2 - 4)\Big) \\ & + \frac{1}{2}\sin g((1-\lambda)\dot{g}^2 - 4) + (1-\lambda)\frac{3}{2r^4}\big((1-\cos F) - 2(1-\cos g)\big)\sin(g) \\ & + \frac{3\lambda}{8r^4}(1-\cos g)\Bigg(2\big(\sin g\dot{g}^2 + (1-\cos g)(\ddot{g} - 2\frac{\dot{g}}{r})\big) \\ & - \sin F\dot{F}^2 - (1-\cos F)(\ddot{F} - 2\frac{Fr}{r})\Bigg) = 0 \end{aligned} \tag{5.57}$$

$$\ddot{F}+\frac{1}{2}\ddot{g}+2\frac{\dot{F}}{r}+\frac{\dot{g}}{r}+\frac{3}{4r^2}\left(\sin F((1-\lambda)\dot{F}^2-4)+2(1-\lambda)(1-\cos F)\ddot{F}\right)$$
$$-(1-\lambda)\frac{3}{2r^4}(2(1-\cos F)-(1-\cos g))\sin F+\frac{3\lambda}{8r^4}(1-\cos F)\Bigg(12(\sin F\,\dot{F}^2$$
$$+(1-\cos F)(\ddot{F}-2\frac{\dot{F}}{r}))-\sin g\,\dot{g}^2-(1-\cos g)(\ddot{g}-2\frac{\dot{g}}{r}))\Bigg)=0. \tag{5.58}$$

Moreover, the topological charge of the solution will now be

$$B=\frac{1}{\pi}\left((F-\sin F)\,|_{r=0}^{r=\infty}+(g-\sin(g))|_{r=0}^{r=\infty}\right). \tag{5.59}$$

If we take the boundary conditions

$$\begin{aligned} F(0) &= n_F 2\pi \\ g(0) &= n_g 2\pi, \end{aligned} \tag{5.60}$$

where n_F and n_g are integers, we will have that

$$B_{SU(3)}=2(n_f+n_g). \tag{5.61}$$

When n_F and n_g are of opposite signs, we can interpret the solutions as a mixture of skyrmions and anti skyrmions.

In Table 5.1, we give the energy of the hedgehog solution ($B=1$) for the $SU(2)$ model and for the two asymptotic values, $\lambda=0$ and $\lambda=1$. As we have mentioned a number of times in the previous chapters, this solution is an embedded solution of any $SU(N)$ model and it is the solution with the lowest energy. We thus use it as the reference energy for all the other solutions.

$SU(2)$		Energy	
n_g	B	$E(0)$	$E(1)$
1	1	1.2315	0.9395

Table 5.1: Topological charge and energy of the hedgehog $SU(2)$ solution.

In Table 5.2 we present the properties of the different solutions for the $SU(3)$ models. The first two columns specify the boundary condition of the solution, and

$SU(3)$			Total Energy		Relative Energy	
n_F	n_g	B	$E(0)$	$E(1)$	$E_B(0)/(\|B\|E_1(0))$	$E_B(1)/(\|B\|E_1(1))$
1	1	4	4.928	3.758	1	1
1	0	2	2.377	1.819	0.965	0.968
0	1	2	2.377	1.819	0.965	0.968
1	-1	2-2	3.862	3.191	0.784	0.849

Table 5.2: Topological charge and energy of some $SU(3)$ solutions.

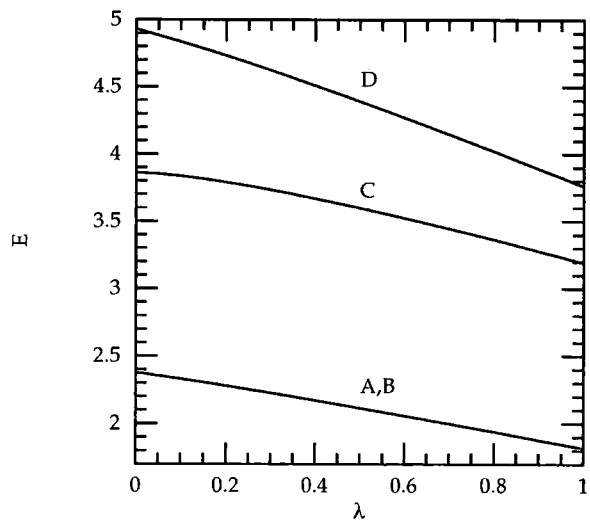

Figure 5.1: Energy of the $SU(3)$ solution for the boundary condition (A) $n_F = 0, n_g = 1$, (B) $n_F = 1, n_g = 0$, (C) $n_F = 1, n_g = -1$, (D) $n_F = 1, n_g = 1$.

the third column gives the topological charge of that solution. In column 4 and 5 we give the energy of the solutions for the pure Skyrme model and the pure Sk6 model while columns 6 and 7 give the corresponding relative energy per skyrmion, that is the energy divided by the energy of the single skyrmion and the total number of skyrmions. For the solutions corresponding to the superposition of skyrmions and anti-skyrmions, we define the total number of skyrmions as the total number of skyrmions and anti-skyrmions.

From Table 5.2 we see that with the exception of the first case, where $n_g = 1, n_F = 1$, all other solutions are more bound for the pure Skyrme model, *i.e.* they have relatively smaller energy per skyrmion in comparison with the pure Sk6 model. This is even true for the solution with topological charge $B = 0$. In addition, we observe that the configurations with $n_g = 0, n_F = 1$ and $n_g = 1, n_F = 0$ correspond to the same solutions modulo an internal rotation. This last symmetry of the model is characteristic of the pure Skyrme model and as pointed out in [49], it follows from the invariance of

$$Z_k = k(N-k)(1-\cos(F_{k-1})), \tag{5.62}$$

that appears in (5.50), under the interchange

$$F_k \leftrightarrow F_{N-k-2} \qquad \text{for} \qquad k = 0, \ldots, N-2. \tag{5.63}$$

Since the extra terms in the energy (5.50), that come from the additional sixth order term, are also proportional to Z_k^2 we see that the general model is also invariant under the symmetry (5.63). The latter can also be seen in Figure 5.1 where we have plotted the energy of the 3 different types of solution as a function of λ.

5.5 Radially symmetric skyrmions in $SU(4)$

In the last two sections we saw that the ansatz (5.11) describes an exact solution of the sixth order model, with $\lambda \neq 0$, only for the $SU(3)$ model. However, for $SU(N)$ with $N \geq 4$, if we assume that the fields U are described by $N-1$ profile functions, *i.e.* if we do not consider the constraint (5.40), then this approximation will still produce low energy configurations. In particular, when λ is small, we can expect the ansatz to be very close to an exact solution. In this section we look at some

configurations of the $SU(4)$ model. For this model, we have three profile functions F_0, F_1 and F_2 and the energy for the general ansatz (5.11) is explicitly given by

$$E = \frac{1}{6\pi}\int r^2 dr \Bigg\{ \frac{1}{4}\left(3\dot{F}_0^2 + 4\dot{F}_1^2 + 3\dot{F}_2^2 + 4\dot{F}_0\dot{F}_1 + 4\dot{F}_1\dot{F}_2 + 2\dot{F}_0\dot{F}_2\right) + \frac{2}{r^2}\left[3(1-\cos F_0)\right.$$
$$\left. +4(1-\cos F_1)+3(1-\cos F_2)\right] + (1-\lambda)\Big(\frac{1}{2r^2}\left[3\dot{F}_0^2(1-\cos F_0)+4\dot{F}_1^2(1-\cos F_1)+\right.$$
$$\left.3\dot{F}_2^2(1-\cos F_2)\right] + \frac{1}{2r^4}\left\{9\,(1-\cos F_0)^2 + 16\,(1-\cos F_1)^2 + 9\,(1-\cos F_2)^2\right.$$
$$\left.-12(1-\cos F_0)(1-\cos F_1) - 12(1-\cos F_1)(1-\cos F_2)\right\}\Big)$$
$$+\frac{\lambda}{8r^4}\Big(9\dot{F}_0^2(1-\cos F_0)^2 + 16\dot{F}_1^2(1-\cos F_1)^2 + 9\dot{F}_2^2(1-\cos F_2)^2$$
$$\left.-12F_0F_1(1-\cos F_0)(1-\cos F_1) - 12F_1F_2(1-\cos F_1)(1-\cos F_2)\Big)\right\}, \qquad (5.64)$$

from which we can derive the following equations

$$\left(\frac{3\lambda(1-\cos F_0)^2}{2r^4} + \frac{2(1-\lambda)(1-\cos F_0)}{r^2} + 1\right)\ddot{F}_0 + \frac{1}{3}\ddot{F}_2$$
$$+\left(\frac{2}{3} - \frac{\lambda(1-\cos F_0)(1-\cos F_1)}{r^4}\right)\ddot{F}_1 - \frac{4\sin F_0}{r^2} + \frac{6\,\dot{F}_0 + 4\dot{F}_1 + 2\dot{F}_2}{3r}$$
$$+\frac{(1-\lambda)\dot{F}_0^2\sin F_0}{r^2} + (1-\lambda)\frac{\sin F_0}{r^4}(4(1-\cos F_1) - 6(1-\cos F_0))$$
$$+\lambda\frac{(1-\cos F_0)}{r^4}\left(\frac{3}{2}\,\dot{F}_0^2\sin F_0 - \dot{F}_1^2\sin F_1\right)$$
$$-\lambda\frac{(1-\cos F_0)}{r^5}\Big(3\dot{F}_0(1-\cos F_0) - 2\,\dot{F}_1(1-\cos F_1)\Big) = 0, \qquad (5.65)$$

$$\left(\frac{1}{2} - \frac{3\lambda(1-\cos F_0)(1-\cos(F_1)}{4r^4}\right)\ddot{F}_0 + \left(\frac{1}{2} - \frac{3\lambda(1-\cos F_1)(1-\cos F_2)}{4r^4}\right)\ddot{F}_2$$
$$+\left(1 + \frac{2\lambda(1-\cos F_1)^2}{r^4} + \frac{2(1-\lambda)(1-\cos F_1)}{r^2}\right)\ddot{F}_1$$
$$+\frac{(1-\lambda)\dot{F}_1^2\sin F_1}{r^2} + \frac{\dot{F}_0 + 2\,\dot{F}_1 + \dot{F}_2}{r} - 4\frac{\sin F_1}{r^2} +$$
$$(1-\lambda)\frac{\sin F_1}{r^4}\Big(3(1-\cos F_0) + 3(1-\cos F_2) - 8(1-\cos F_1)\Big)$$
$$-\frac{\lambda}{r^5}(1-\cos F_1)\Big(4\,\dot{F}_1(1-\cos F_1) - \frac{3}{2}\,\dot{F}_0(1-\cos F_0) - \frac{3}{2}\,\dot{F}_2(1-\cos F_2)\Big)$$
$$+\frac{\lambda}{r^4}(1-\cos F_1)\left(2\,\dot{F}_1^2\sin F_1 - \frac{3}{4}\dot{F}_0^2\sin F_0 - \frac{3}{4}\dot{F}_2^2\sin F_2\right) = 0$$
$$(5.66)$$

and

$$\left(\frac{2}{3}-\frac{\lambda(1-\cos F_1)(1-\cos F_2)}{r^4}\right)\ddot{F}_1+\Big(\frac{3\lambda(1-\cos F_2)^2}{2r^4}+1$$
$$+\frac{2(1-\lambda)(1-\cos F_2)}{r^2}\Big)\ddot{F}_2+\frac{1}{3}\ddot{F}_0+\frac{2\dot{F}_0+4\dot{F}_1+6\,\dot{F}_2}{3r}-4\frac{\sin F_2}{r^2}$$
$$+\frac{(1-\lambda)\dot{F}_2^2\sin F_2}{r^2}+(1-\lambda)\frac{\sin F_2}{r^4}\left(4(1-\cos F_1)-6(1-\cos F_2)\right)$$
$$-\lambda\frac{(1-\cos F_2)}{r^5}\Big(3\,\dot{F}_2(1-\cos F_2)-2\,\dot{F}_1(1-\cos F_1)\Big)$$
$$+\lambda\frac{(1-\cos F_2)}{r^4}\left(\frac{3}{2}\,\dot{F}_2^2\sin F_2-\dot{F}_1^2\sin F_1\right)=0. \tag{5.67}$$

Describing the boundary condition for the profile functions as before, *i.e.* $F_i(0) = n_i 2\pi$, the topological charge is given by

$$B = 3n_0 + 4n_1 + 3n_2. \tag{5.68}$$

In Table 5.3 we present the energy values of various types of configurations when $\lambda = 0$ and $\lambda = 1$. We notice that, as in the $SU(3)$ model, when $\lambda = 0$, the solutions are symmetric under the exchange $F_0 \leftrightarrow F_2$, but that the sixth order term breaks the symmetry. This results in a difference of energy between the configuration with $(n_0 = 0, n_1 = 0, n_2 = 1)$ and $(n_0 = 1, n_1 = 0, n_2 = 0)$ as well as between the configurations with $(n_0 = 1, n_1 = 1, n_2 = 0)$ and $(n_0 = 0, n_1 = 1, n_2 = 1)$.

$SU(4)$				Total Energy		Relative Energy	
n_0	n_1	n_2	B	$E(0)$	$E(1)$	$E_B(0)/(\lvert B\rvert E_1(0))$	$E_B(1)/(\lvert B\rvert E_1(1))$
0	0	1	3	3.51739	2.66653	0.95210	0.94598
1	0	0	3	3.51739	2.72915	0.95210	0.96819
0	1	0	4	4.78807	6.33322	0.97204	1.68507
1	0	1	6	7.22464	6.04604	0.97780	1.07244
1	1	0	7	8.45219	6.62998	0.98052	1.00802
0	1	1	7	8.45219	7.28058	0.98052	1.10694
1	1	1	10	12.311	9.39605	1	1

Table 5.3: Topological charge and energy of some $SU(4)$ configurations.

Let us stress one important point. If we observe carefully the values of the energy for the configuration with $(n_1 = 1, n_1 = 1, n_2 = 1)$ in Table 5.3, we see that it describes a state of ten skyrmions that has energy exactly ten times the energy of the hedgehog configuration for all values of λ. This configuration corresponds to taking

$$F_0 = F_1 = F_2 = F \Leftrightarrow g_0 = 2g_1 = 3g_2. \tag{5.69}$$

In sections 1.3.1 and 1.3.2 we examined the construction of spherically symmetric solutions using the general ansatz (5.11). There we argued that the special configuration (5.69) describes an exact solution of the pure Skyrme model with baryon number $B = \frac{N}{6}(N^2-1)$. Therefore, for $SU(4)$, where $B = 10$, this solution will have energy ten times the energy of the single skyrmion. Hence, one can easily assume that the configuration with $(n_1 = 1, n_1 = 1, n_2 = 1)$ is also an exact solution for the general sixth order model since its energy is always ten times the energy of $B = 10$ for any value of λ. However, this assumption is misleading because this special case (5.69) does not satisfy the constraint (5.40) and thus, the angular dependence does not cancel out of the general equations of motion (5.17). Hence, in order to obtain exact solutions for the sixth order model, one has to ensure that all constraints are satisfied before any equation is derived from the energy (5.50). In a different case the ansatz will correspond to an approximation and not to a solution of the model.

Another observation that can be made from Table 5.3 is that the configurations with baryon number $B = 4, 6$ and 7 correspond to bound states when $\lambda = 0$ (as expected) but when λ increases the relative energy per skyrmion becomes larger than one and clearly these are no longer bound states. We also see that the largest relative energy per skyrmion is obtained for $(n_0 = 0, n_1 = 1, n_2 = 0)$. The latter can also be seen in Figure 5.2 where we present the curve for the energy of the configurations as a function of λ.

In the same Figure one can also see how the sixth order term breaks the symmetry $F_0 \leftrightarrow F_2$ between the configurations with $(n_0 = 0, n_1 = 0, n_2 = 1)$ and $(n_0 = 1, n_1 = 0, n_2 = 0)$ and between the configurations with $(n_0 = 1, n_1 = 1, n_2 = 0)$ and $(n_0 = 0, n_1 = 1, n_2 = 1)$.

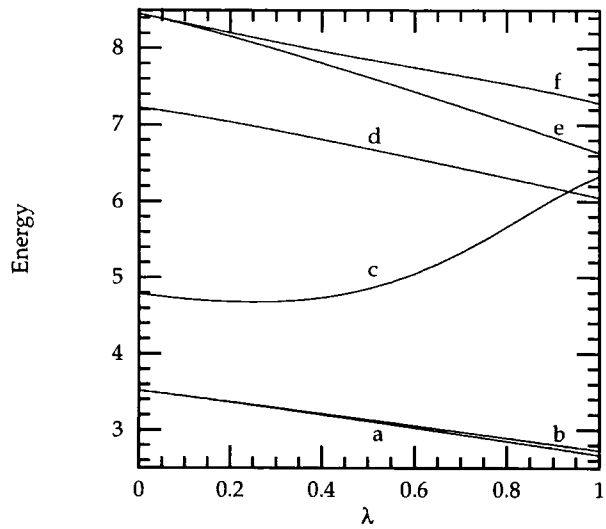

Figure 5.2: Energy density of the $SU(4)$ multi-projector ansatz (a) $n_0 = 0, n_1 = 0, n_2 = 1$; (b) $n_0 = 1, n_1 = 0, n_2 = 0$; (c) $n_0 = 0, n_1 = 1, n_2 = 0$; (d) $n_0 = 1, n_1 = 0, n_2 = 1$; (e) $n_0 = 1, n_1 = 1, n_2 = 0$; (f) $n_0 = 0, n_1 = 1, n_2 = 1$.

5.6 Low energy configurations in $SU(N)$

In the previous sections we inserted the ansatz (5.11) into the full equation for the $SU(N)$ model and we found that we had only two independent profile functions g_0 and g_1. There we argued that for $N \geq 4$ these equations do not decouple and hence, this ansatz only provides solutions for the $SU(3)$ model. In addition, we have explored the case of the $SU(4)$ model and investigated the properties of various low energy configurations that can be constructed by the general ansatz (5.11) without imposing the constraint (5.40). In this section we will use this general ansatz in order to compute low energy configurations in $SU(N)$. In particular we will consider the reduced ansatz defined by (5.11) together with the constraint $g_i = g_{i+2}$. If we define

the profiles $F = g_0 - g_1$ and $g = g_{N-2}$ then the energy (5.50) becomes

$$\begin{aligned}\tilde{E} &= \frac{1}{6\pi}\int r^2 dr\Big\{\frac{N-1}{N}\dot{g}^2 + K_1\dot{F}^2 + K_2\dot{g}\dot{F} + \frac{1}{2r^2}\Big[(1+\frac{N}{6}(N^2-7)) \\ &(1-\cos F)\Big((1-\lambda)\dot{F}^2+4\Big) + (N-1)(1-\cos g)\Big((1-\lambda)\dot{g}^2+4\Big)\Big] \\ &+(1-\lambda)\frac{N-1}{2r^4}\Big[\frac{1}{6}(N-2)(N+9)(1-\cos F)^2 + (N-1)(1-\cos g)^2 \\ &-2\,(N-2)(1-\cos F)(1-\cos g)\Big] \\ &+\frac{\lambda}{8r^4}\Big[\frac{1}{6}(N-2)(N^2+20N-45)(1-\cos F)^2\dot{F}^2 + (N-1)^2(1-\cos g)^2\dot{g}^2 \\ &-2(-1)^{N-1}(N-1)(N-2)(1-\cos F)(1-\cos g)\dot{g}\dot{F}\Big]\Big\}, \end{aligned} \tag{5.70}$$

where

$$K_1 = \begin{cases} \frac{N^2-4}{4N} & N \text{ even} \\ \frac{N^2-1}{4N} & N \text{ odd} \end{cases} \quad \text{and} \quad K_2 = \begin{cases} \frac{2-N}{N} & N \text{ even} \\ \frac{N-1}{N} & N \text{ odd} \end{cases}. \tag{5.71}$$

From (5.70) we can derive the following equations for F and g

$$\begin{aligned} &2\frac{N-1}{N}\ddot{g} + K_2\ddot{F} + 2K_2\frac{\dot{F}}{r} + 4\frac{N-1}{N}\frac{\dot{g}}{r} + \frac{N-1}{r^2}\Big((1-\lambda)(1-\cos g)\ddot{g} \\ &+\frac{1}{2}\sin g\,\big((1-\lambda)\dot{g}^2-4\big)\Big) + (1-\lambda)\frac{N-1}{r^4}\sin g\Big((N-2)(1-\cos F) \\ &-(N-1)(1-\cos g)\Big) + \frac{\lambda}{4r^4}(N-1)(1-\cos g)\Bigg((N-1)\big[\sin g\dot{g}^2 \\ &+(1-\cos g)(\ddot{g}-2\frac{\dot{g}}{r})\big] + (N-2)(-1)^N(\sin F\dot{F}^2 + (1-\cos F)(\ddot{F}-2\frac{\dot{F}}{r}))\Bigg) = 0 \end{aligned} \tag{5.72}$$

and

$$\begin{aligned} &2K_1\ddot{F} + K_2\ddot{g} + 4K_1\frac{\dot{F}}{r} + 2K_2\frac{\dot{g}}{r} \\ &+\frac{1}{12r^2}(N^3-7N+6)\Big(\sin F((1-\lambda)\dot{F}^2-4) + 2(1-\lambda)(1-\cos F)\ddot{F}\Big) \\ &-(1-\lambda)\frac{1}{r^4}(N-1)(N-2)\sin F\left(\frac{1}{6}(N+9)(1-\cos F) - (1-\cos g)\right) \\ &\frac{\lambda}{4r^4}\Bigg(\frac{1}{6}(N^3+18N^2-85N+90)(1-\cos F)\Big(\sin F\dot{F}^2 \\ &+(1-\cos F)(\ddot{F}-2\frac{\dot{F}}{r})\Big) + (-1)^N(N-2)(N-1)(1-\cos F)\Big(\sin g\dot{g}^2 \\ &+(1-\cos g)(\ddot{g}-2\frac{\dot{g}}{r})\Big)\Bigg) = 0. \end{aligned} \tag{5.73}$$

Moreover, one can easily show that the baryon number is related to the boundary values for F and g by the following expression

$$B = \frac{1}{2\pi}\left(\left(\frac{N}{4}+(-1)^N(1-\frac{3}{4}N)\right)(F-\sin F)|_{r=0}^{r=\infty} + (N-1)(g-\sin g)|_{r=0}^{r=\infty}\right). \quad (5.74)$$

When solving the equations (5.72) and (5.73) for the profiles g and F we used various boundary conditions and found that in order to get configurations corresponding to a bound state, *i.e.* a configuration with an energy per skyrmion smaller the energy of the hedgehog solution, we need to take $n_F = 0$ and $n_g = 1$. The energies found are given in Table 5.4.

		Total Energy		Relative Energy	
Model	B	$E(0)$	$E(1)$	$E_B(0)/(\lvert B\rvert E_1(0))$	$E_B(1)/(\lvert B\rvert E_1(1))$
$SU(3)$	2	2.377	1.819	0.965	0.968
$SU(4)$	3	3.624	2.759	0.981	0.979
$SU(5)$	4	4.811	3.632	0.977	0.966
$SU(6)$	5	6.015	4.518	0.977	0.962

Table 5.4: Topological charge and energy for the reduced ansatz with $n_F = 0$ and $n_g = 1$.

In Figures 5.3 and 5.4 we present the profile and the energy density for different values of N and for $\lambda = 0.5$. We observe that the energy density has the shape of a hollow sphere of radius $r = 0.7\sqrt{N}$. The profile g has the same shape for all values of N but is shifted to the right as N increases. The profile F on the other hand is also shifted as the shell radius increases, but its amplitude decreases like $1/N^2$. Notice that in Figure 5.4, the profiles for $N = 100$ and $N = 200$ have been multiplied by 100 to make them visible. For other values of λ the graphs look very much the same except that the shell radius and width are slightly different. The conclusions, however, remain the same.

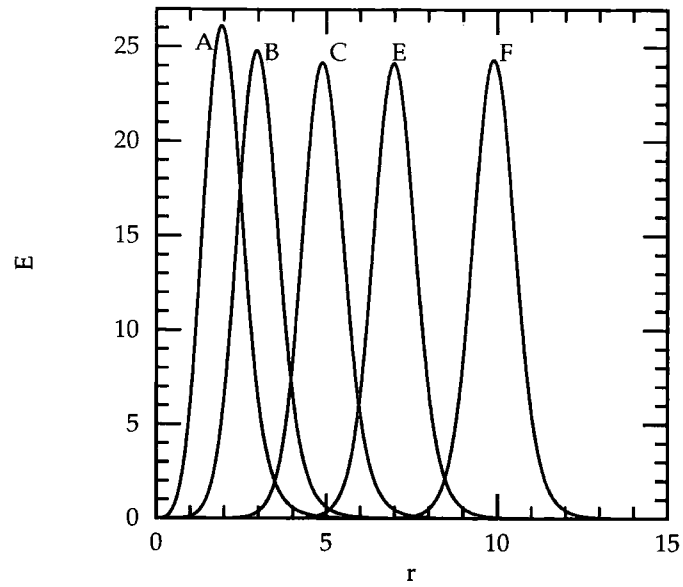

Figure 5.3: Energy density of the multi-projector solution with $n_F = 0$, $n_g = 1$, $\lambda = 0.5$. (A) N=10, (B) N=20, (C) N=50, (D) N=100, (E) N=200.

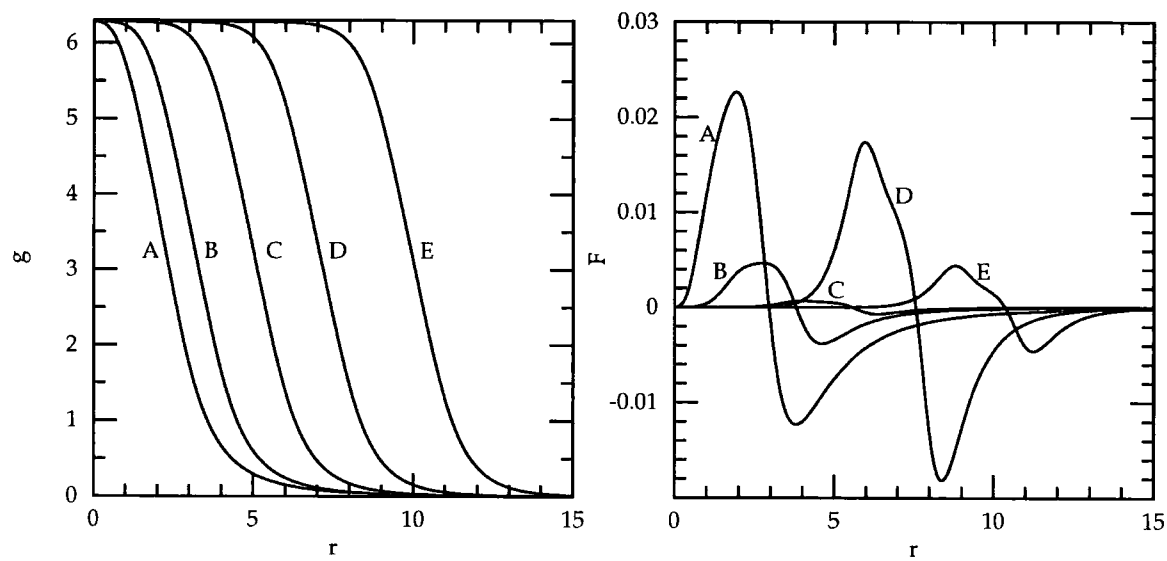

(a) (b)

Figure 5.4: (a) profile g and (b) profile F of the multi-projector solution with $n_F = 0$, $n_g = 1$, $\lambda = 0.5$. (A) g & F for N=10, (B) g & F for N=20, (C) g & F for N=50, (D) g & $(100 \times F)$ for N=100, (E) g & $(100 \times F)$ for N=200.

Figure 5.4.(b) suggests simplifying the ansatz further for large N by taking $F(r) = 0$. This implies that $g_i = g \ \forall i$ and the multi-projector ansatz (5.11) becomes

$$U = \exp\left(-ig(P_{N-1} - I/N)\right), \tag{5.75}$$

where P_{N-1} can also be written as[2]

$$P_{N-1} = \frac{\tilde{h}\tilde{h}^\dagger}{|\tilde{h}|^2}, \tag{5.76}$$

and where $\tilde{h}$ is equal, up to a unitary rotation, to the complex conjugate of the holomorphic vector V_0 defined in (5.18): $\tilde{h} = A\bar{V}_0$ for some $A \in SU(N)$ with $\partial_\xi A = \partial_{\bar{\xi}} A = 0$. This is shown by using the fact that P_{N-1} is an anti-holomorphic projector [51] and that solving (5.49) recursively (see Appendix B) we have

$$|V_k|^2 = \frac{k!(N-1)!}{(N-1-k)!}\ |1 + |\xi|^2|^{N-1-2k}, \tag{5.77}$$

and so $|V_{N-1}|^2 = [(N-1)!]^2\ |1 + |\xi|^2|^{1-N}$.

The topological charge of the anti-holomorphic projector P_{N-1} is equal to $1-N$ and as the profile function is $-g$, the baryon number for this configuration is $N-1$. The ansatz (5.75) is not a solution, but its energy

$$\begin{aligned} E \ = \ & \frac{1}{6\pi}\int r^2 dr \Bigg\{ \frac{N-1}{N}\,\dot{g}^2 + \frac{1}{2r^2} + (N-1)(1-\cos g)((1-\lambda)\dot{g}^2 + 4) \\ & + \frac{1}{2r^4}(N-1)^2(1-\cos g)^2\left((1-\lambda) + \frac{\lambda}{4r^4}\dot{g}^2\right)\Bigg\}, \end{aligned} \tag{5.78}$$

can easily be computed by solving the equation

$$\begin{aligned} & 2g_{rr} + 4\frac{g_r}{r} + \frac{N}{r^2}\Big((1-\lambda)(1-\cos g)g_{rr} + \frac{1}{2}\sin g((1-\lambda)g_r^2 - 4)\Big) \\ & + \frac{\lambda}{4r^4}N(N-1)(1-\cos g)(\sin g g_r^2 + (1-\cos g)(g_{rr} - 2\frac{g_r}{r})) = 0. \end{aligned} \tag{5.79}$$

In Figure 5.5, we present the relative energy, $E(\lambda)/(E_{B=1}(\lambda)(N-1))$, of this configuration as a function of N for different values of λ. We see that this configuration corresponds to a bound state of skyrmions and that the energy per skyrmion decreases with N. The energy of this configuration corresponds to an upper bound

[2]See Appendix B for further details.

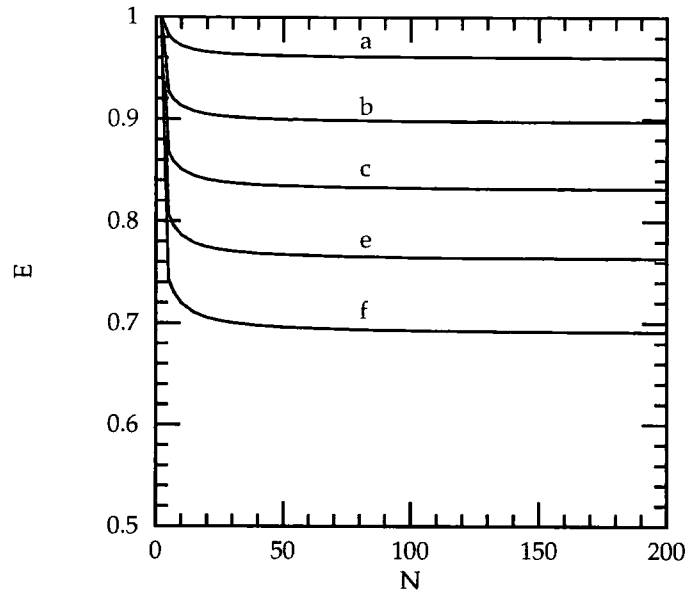

Figure 5.5: Energy $E/(E_{B=1}(N-1))$ of the $SU(N)$, configuration 5.75 for (a) $\lambda = 0$, (b) $\lambda = 0.25$, (c) $\lambda = 0.5$, (e) $\lambda = 0.75$, (f) $\lambda = 1$.

for the energy of the $B = N - 1$ radially symmetric solution of the $SU(N)$ model and these configurations correspond to bound states of skyrmions for all values of N and all values of λ. As every $SU(p)$ solution can be trivially embedded in an $SU(q)$ solution when $p \leq q$ we can claim that for every $B < N$ the $SU(N)$ model has a radially symmetric solution of charge B corresponding to a bound state. With the exception of the hedgehog solutions, these solutions are expected to be unstable when the radial symmetry is broken as their energies are larger than the $SU(2)$ solutions we computed numerically in chapter 3.

Chapter 6

Conclusions and discussion

In this thesis, we have investigated some of the classical properties of an extension of the Skyrme model defined by adding to the Lagrangian a Skyrme-like sixth order term. We have argued that such generalisations of the Skyrme model are motivated by physical as well as by mathematical interest. In our definition of the extended Skyrme model, we introduced a dimensionless coupling constant λ that denotes the mixing between the two higher order terms: the Skyrme and the sixth order term. This parameterisation enabled us to study the dependence of the energy and matter radius of classical solutions with respect to λ.

Our investigation of this model mainly concentrated on computing static multi-skyrmion solutions with topological charge $B = 2..5$ using numerical methods. For the special configuration with $B = 2$ we showed that the minimum energy solution is axially symmetric as in the pure Skyrme model. This enabled us to use an axially symmetric ansatz in order to reduce the equations of the extended model to a two-dimensional system and thus, obtain more accurate results. It also provided us with a way to estimate the accuracy of the numerical methods we used to solve the full three-dimensional system. Overall, we found that the symmetries of multi-skyrmion solutions with $B = 2..5$ are the same as the ones obtained for the pure Skyrme model. By varying the strength of the additional sixth order term, we also computed the energy and radius ratios with the single skyrmion solution for different values of λ. We compared our results with experiment and we showed that in some cases the extended Skyrme model provides us with better theoretical predictions than the pure Skyrme model. In addition, we observed that the extra higher order term makes the multi-skyrmion solutions more bound than in the pure Skyrme model and it also increases their radius, specially for large B.

We then used the harmonic maps ansatz to approximate the above mentioned

solutions. This ansatz, as it was introduced in [14] and in [15], is considered as a rather good approximation of the solutions of the pure Skyrme model. We found that the harmonic maps ansatz works equally well for the sixth order Skyrme model and in some cases even better. To determine this, we firstly plugged this ansatz into the Lagrangian of the extended Skyrme model and showed that the multi-skyrmion configurations of this model have the same symmetries as the ones of the pure Skyrme model thus proving that this approximation provides us with qualitatively correct results at least for $B = 2..5$. We then investigated the energy and radius ratios of these multi-skyrmions by varying the parameter λ. When we compared our results with the true solutions, we found that for certain values of λ, the relative error between the approximate configurations and the corresponding solutions is smaller than the pure Skyrme model.

In addition, we analysed the dependence of the energy and matter radius with respect to λ for multi-skyrmions with topological $B = 6..9$ in $SU(2)$ and $B = 2..6$ in $SU(3)$. Unfortunately, it was not possible to determine the quality of these results since obtaining solutions for configurations with $B > 5$ and for different values of λ, is a time consuming numerical problem that becomes quite complex when B increases. Nevertheless, we showed that under the harmonic maps ansatz, these multi-skyrmions have the same symmetries as the ones of the pure Skyrme model and that the addition of a sixth order makes their energy more bound and decreases their matter radius. We also considered saddle point configurations with $B = 5$ and found that when the two higher order terms, the Skyrme and the sixth order term, are comparable, then the energy and radius ratios become maximum.

Finally we explored the possibility of constructing spherically symmetric solutions in $SU(N)$ using a generalisation of the harmonic maps ansatz that was proposed in [49]. We showed that, unlike the pure Skyrme model, this ansatz works only for the $SU(2)$ and $SU(3)$ extended Skyrme models due to an additional constraint coming from the extra sixth order term. Nevertheless, we argued that this ansatz can still be used to compute low energy configurations of the $SU(N)$ model. In particular, we showed that for every N there is a radially symmetric configuration with topological charge $B < N$ which corresponds to a bound state of skyrmions.

Our analysis of generalised versions of the Skyrme model suggests further investigation on this subject. For instance, in section 2.2.3 we reviewed the construction

of a Skyrme model with an infinite number of higher order terms as proposed by Marleau [10, 11, 37, 12]. However, this model was restricted to the case of the single skyrmion and hence, a further generalisation of this construction to multi-skyrmion configurations in $SU(N)$ is always an interesting possibility. This work is currently under progress and some promising results have already been obtained.

In addition, when we were examining the physical motivation behind the study of extended Skyrme models in chapter 2, we saw that a number of phenomenological arguments suggest that an effective Lagrangian derived from QCD must include further fourth order terms which destabilise the solitons. However, in our definition of an extended Skyrme model, we did not consider these terms since their presence in the Skyrme Lagrangian leads to differential equations with degree higher than two and this is a very difficult problem to solve even numerically. Nevertheless, by using advanced numerical methods and by considerably increasing the amount of computing resources needed, we might be able to systematically study such complicated models and determine whether they can provide us with better theoretical predictions than the original Skyrme model.

We believe that topological solitons and in general, non-linear field theories, are of great mathematical and physical interest, and investigating their properties will always be an exciting subject to explore.

Appendix A

Numerical Methods

In this appendix we describe the numerical methods that we have used throughout this thesis to compute solutions of the extended sixth order Skyrme model.

A.1 Numerical integration of ordinary and partial differential equations

A.1.1 Finite differences method

When defining a function $f(x)$, or equivalently a field $\phi(x)$, on a discrete lattice, we associate this function with each lattice point as

$$f(x) \to f(x_i) = f_i \qquad \text{with} \qquad i = 1, \ldots, N, \tag{A.1}$$

where N is the number of lattice points. For a lattice with regular spacing Δx, we replace the spatial derivatives with their discretised versions using the *finite differences method.* For example, in order to evaluate the first derivative of $f(x)$, we use the central difference operator, defined as

$$\frac{df(x)}{dx} = \frac{f_{i-1} - f_{i+1}}{2\Delta x}. \tag{A.2}$$

Depending on the nature of the numerical problem, one can equivalently use the forward difference operator:

$$\frac{df(x)}{dx} = \frac{f_i - f_{i+1}}{\Delta x}, \tag{A.3}$$

or the backward difference operator:

$$\frac{df(x)}{dx} = \frac{f_{i-1} - f_i}{\Delta x}. \tag{A.4}$$

Similarly, to evaluate the second derivative of f with respect to x, we use the operator:

$$\frac{d^2f(x)}{dx^2} = \frac{f_{i-1} + f_{i+1} - 2f_i}{\Delta x^2}. \tag{A.5}$$

In multi-dimensional problems, where we evaluate multi-variable functions such as $g \equiv g(x_1, x_2, \ldots, x_a)$, we also need to consider their partial derivatives with respect to more than one variable. For example, in two dimensions, we replace the second order mixed derivative of a function $F = F(x, y)$, with the operator

$$\frac{\partial^2 F(x,y)}{\partial x \partial y} = \frac{F_{i+1,j+1} - F_{i+1,j-1} + F_{i-1,j-1} - F_{i-1,j+1}}{4\Delta x \Delta y}, \tag{A.6}$$

where $i = 1, \ldots, N_x$ and $j = 1, \ldots, N_y$. In (A.6), $F_{i,j}$ is the value of the function at each lattice point and $\Delta x, \Delta y$ are the grid spacings in the x and y direction respectively[1].

All the above operators are of order two. One can increase the accuracy of the numerical results by using finite difference operators of higher order precision in Δx. For instance, the first order derivative can be evaluated using,

$$\frac{df(x)}{dx} = \frac{-f_{i+2} + 8f_{i+1} - 8f_{i-1} + f_{i-2}}{12\Delta x} + \mathcal{O}(\Delta x^4). \tag{A.7}$$

However, increasing the precision of the difference operators is not always favourable as it decreases the convergence speed significantly.

A.1.2 Integration methods

To numerically solve an ordinary differential equation (ODE) of first order, given by the general form

$$\frac{df(x)}{dx} = F(x, f(x)), \tag{A.8}$$

we approximate $f(x)$ by expanding $f(x + dx)$ as a Taylor series. For example, up to first order precision in dx, we have

$$\begin{aligned} f(x + dx) &= f(x) + dx\frac{df}{dx} + \mathcal{O}(dx^2) \\ &= f(x) + dxF(x, f) + \mathcal{O}(dx^2). \end{aligned} \tag{A.9}$$

[1] In general, we choose $\Delta x = \Delta y = \Delta$ and $N_x = N_y = N$ for simplicity.

By descretising $f(x)$ on a lattice with spacing Δx, we have

$$f_{i+1} = f_i + \Delta x \; F(x_i, f_i) + \mathcal{O}(\Delta x^2). \tag{A.10}$$

Given the value of the function f at the point x_0, we can evaluate F at this point and thus find f_1 up to first order precision in Δx. If we repeat this procedure N_x times, we can integrate equation (A.10) from x_0 to $x_N = x_0 + N_x \, \Delta x$. This is called the *Euler* method and is the simplest way to approximate a solution for a first order ODE. However, this method is not very accurate since we evaluate $f(x)$ only to first order precision in Δx.

To achieve better accuracy in our numerical results, we use the *4th order Runge-Kutta* method. This method consists of expanding $f(x + dx)$ as a Taylor series up to fourth order precision in dx and evaluate f_{i+1} using the derivative value at the starting point x_i, the final point x_{i+1} and two midpoints. The explicit form of the 4th order Runge-Kutta formula is

$$f_{i+1} = f_i + \frac{\Delta x}{6} \left(k_1 + 2\,k_2 + 2\,k_3 + k_4\right) + \mathcal{O}(\Delta x^5), \tag{A.11}$$

where

$$\begin{aligned} k_1 &= F(x_i, f_i), \\ k_2 &= F(x_i + \frac{\Delta x}{2}, f_i + \frac{k_1}{2}), \\ k_3 &= F(x_i + \frac{\Delta x}{2}, f_i + \frac{k_2}{2}), \\ k_4 &= F(x_i + \Delta x, f_i + k_3). \end{aligned} \tag{A.12}$$

The Runge-Kutta method is much more accurate than the Euler method and is preferred in the majority of numerical problems. Improved versions of the Runge-Kutta method that use adaptive step size can further increase the accuracy of the integration (see for example chapter 16 of reference [52]). However, for our numerical problems the formula (A.11) provides us with sufficient accuracy.

The Runge-Kutta method can also be applied to higher order differential equations. In general, any ODE of order n can be reduced to a set of n coupled first order differential equations. For example, the equation

$$\frac{d^2 f(x)}{dx^2} = F\left(x, f(x), \frac{df(x)}{dx}\right), \tag{A.13}$$

can equivalently be rewritten as a system of two first order equations as

$$\begin{aligned} \frac{df(x)}{dx} &= g(x), \\ \frac{dg(x)}{dx} &= F\Big(x, f(x), g(x)\Big). \end{aligned} \tag{A.14}$$

A.1.3 The shooting method

When solving a differential equation numerically, it is often required to impose a set of boundary conditions that must be satisfied by the solution at specific points of the integration interval. For example, consider the problem of finding the minimum energy of a one dimensional system. In other words, minimise the functional

$$E = \int_{r_0}^{r_0+L} dr\ \mathcal{E}[r, f(r), f'(r)], \tag{A.15}$$

where $f(r)$ must satisfy the boundary conditions: $f(r_0) = A$ and $f(r_0 + L) = B$. Using the principle of least action, this problem is equivalent to solving the second order Euler-Lagrange differential equation, which is given by the general form

$$\frac{d}{dr}\left(\frac{d\mathcal{E}}{df'}\right) - \frac{d\mathcal{E}}{df} = 0. \tag{A.16}$$

As mentioned previously, this second order ODE can be reduced to a system of two coupled first order ODEs which must also satisfy the two boundary conditions.

The problem of solving (A.16) numerically, is called a *two point boundary value* problem and can be approached by two different ways. One can start by imposing the values of all independent variables at one boundary point and integrate all ODEs in order to match the other boundary condition. Alternative we can use an initial configuration and try to adjust it so that it satisfies the finite differences equation and the two boundary conditions simultaneously. We will explore the latter case in the following section.

The shooting method consists of transforming the two point boundary value problem into an initial value problem. Given the value of the function $f(r)$ at the first boundary point, r_0, we try different values of the derivative $\frac{df(r_0)}{dr}$ until the boundary value $f(r_0 + L)$ is satisfied. This is shown schematically in Figure A.1.

For the integration of the ODEs we use the 4th order Runge-Kutta method that we saw in the previous section.

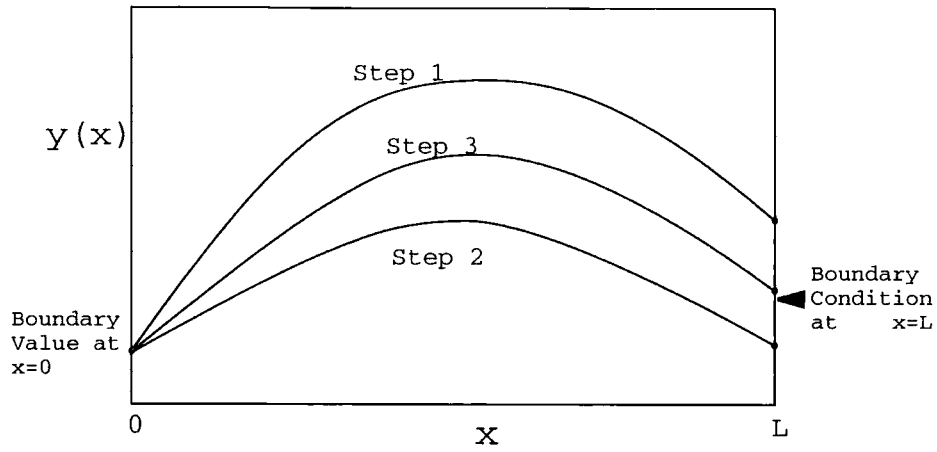

Figure A.1: The shooting method. Using the initial values of $y(x)$ at the first boundary point we adjust the first derivative of $y(x)$ in order to meet the second boundary condition.

We applied the shooting method to find the minimum energy solution of the extended sixth order Skyrme model in the case of the single skyrmion and to obtain minimum energy configurations of multi-skyrmions in the harmonic map ansatz. In both cases, the Euler-Lagrange equation that needs to be solved is one dimensional and has boundary conditions at $r = 0$ and at $r = \infty$, *i.e.* it is a two point boundary value problem.

The advantage of using the shooting method in this type of numerical problems, is that it has large convergence speed and thus enables us to use a large number of integration points in order to obtain very accurate results. For the profile functions of the hedgehog ansatz or the harmonic map ansatz, we were forced to use an interval $r \in [0, 80]$ to get an accurate value for the matter radius as well as up to 160000 lattice points. In all these cases, we compared the solutions obtained with grids of different sizes and different number of points to ensure that our results are not affected by edge effects, especially when computing the matter radius.

The disadvantage of the shooting method is that it can only be applied to one dimensional numerical problems. For higher dimensional problems, one needs to use a different approach.

A.1.4 Relaxation methods

The relaxation method consists of solving a two point (or many point) boundary value problem by using an initial configuration and iterate the system until a solution is found, which must also satisfy all boundary conditions. Consider, for example, the Euler-Lagrange equation (A.16) and rewrite it as a diffusion equation,

$$\frac{df(r,t)}{dt} = \frac{d^2f(r,t)}{dr^2} - F\left(r, f(r,t), \frac{df(r,t)}{dr}\right), \tag{A.17}$$

where the coefficient of the leading term, $\frac{d^2f(r,t)}{dr^2}$, is dimensionless. In the limit where $t \to \infty$, $\frac{df(r,t)}{dt}$ goes to 0 and $f(r)$ satisfies the equation

$$0 = \frac{d^2f(r)}{dr^2} - F\left(r, f(r), \frac{df(r)}{dr}\right). \tag{A.18}$$

In other words, for large t, the initial configuration of f is said to *relax* to a solution of equation (A.18) which also satisfies all boundary conditions. We show this method in Figure A.2 schematically.

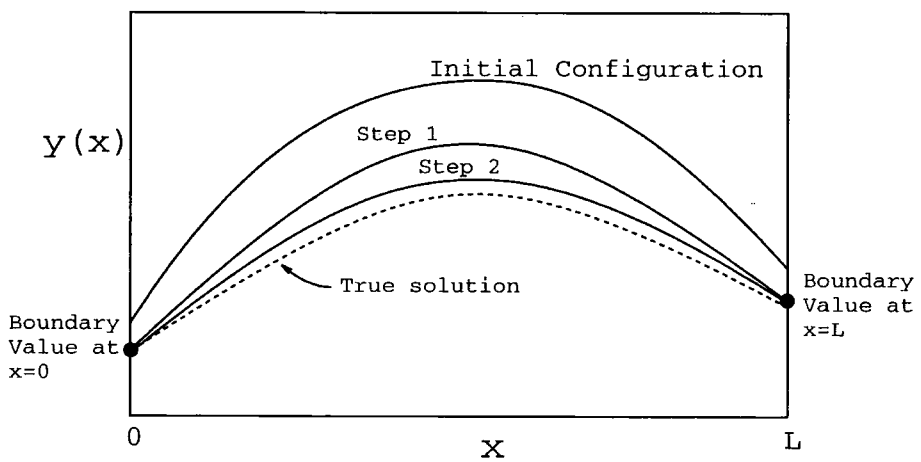

Figure A.2: Relaxation method. We use an initial configuration (guess) of $y(x)$, that does not need to satisfy the two boundary conditions. We then relax the system until $y(x)$ simultaneously satisfies the finite differences equation, to a desired accuracy, and the boundary conditions at $x = x_0$ and $x = L$.

When applying the relaxation method to a numerical program, we replace equation (A.17) by its discretised version and integrate it using the Euler method. Using a higher precision integration method, like the 4th order Runge-Kutta method, is not necessary as we are interested in the asymptotic limit of the solution. Finding

an initial configuration that is close to the solution of the system is always important as it can decrease the number of iteration steps significantly.

Although the main advantage of the relaxation method is that it can be applied to multi-dimensional problems, it has the disadvantage of converging quite slowly. To increase the convergence speed, we use a modified version of this method, the *Successive Over-Relaxation* method (SOR) [52], which consists of using a convergence factor ω in (A.17):

$$\frac{df(r,t)}{dt} = \omega \left[\frac{d^2 f(r,t)}{dr^2} - F\left(r, f(r,t), \frac{df(r,t)}{dr}\right)\right], \tag{A.19}$$

where $0 < \omega < 2$. Determining the optimum value for ω is quite difficult, especially for complicated differential equations such as the ones arising from the Skyrme model. In general, we use an initial value around 1 and we choose the best value for our numerical problem by trial and error. We found that in the case of the extended Skyrme model, ω should be slightly higher than 1, but we had to adjust this value for each multi-skyrmion configuration.

We used the SOR method to obtain solutions of the extended Skyrme model for multi-skyrmions with $B = 2..5$ and for different values of the parameter λ. For boundary conditions, we imposed the vacuum value of the field on the edges of the grid.

When computing the energy and the matter radius for each configuration, we found that our results are affected by two main sources of inaccuracy. The first is the finiteness of the field which increases the value of the energy by distorting the field slightly. The second is that the value of the energy is systematically underestimated by the finite differences method which we use to discretise the differential equations. Although one could expect that these two effects cancel each other, it is very difficult to estimate their order of magnitude.

One way to reduce the edge effects, is to compute the same solutions on grids of different sizes, but keep the lattice spacing, $\Delta x = L/N$ constant. By looking at how the energy changes as a function of the size, it is possible to find a value of L for which the edge effects are relatively small. For the solutions of the extended Skyrme model with $B = 2..5$ we chose a box ranging from -8 to 8 in all directions and used grids of 100, 120 and 140 lattice points. To estimate the relative error, we computed the topological charge, Q, since we already know that it must take integer values from 2 to 5. We found that, after extrapolation, this error varied between 0.5 % and

0.1%. In addition, the values we obtained for the energy per Q of the pure Skyrme model, after extrapolation, all fit within 0.15% the value of E/Q that was found by Battye and Sutcliffe [43] using different numerical methods. For the matter radius we used the same method. However, the integrand of this quantity decreases slowly towards infinity and hence, it is more sensitive to edge effects. We believe that the overall behaviour of the radius ratio as a function of the parameter λ, Figures 3.5 to 3.8, can be trusted, although some fine details might be numerical artifacts.

In the case of the $B = 2$ skyrmion, we used an axially symmetric configuration and solved the Euler-Lagrange differential equations in a two dimensional grid. This enabled us to increase the accuracy of our results by using larger grids and more lattice points. We used a grid defined by $z \in [-20, 20]$ and $r \in [0, 20]$ with lattice spacing $\Delta x = 0.05$. We found that, in this case, the relative error was smaller than 0.1%. Moreover, the value of the energy of the pure Skyrme model that we obtained in this way, fits the one that was found in reference [43] within 0.04%. We compared these results with the ones we obtained by solving the three dimensional system for $B = 2$ and found that the difference between the two energies was less than 0.1%, thus validating the numerical methods used.

Appendix B

Properties of the harmonic projectors P_k

In this appendix, we prove in detail some of the properties of the harmonic projectors P_k which we used in chapter 5.

We start by recalling that the projector $P = P(\xi, \bar{\xi})$, where $(\xi, \bar{\xi})$ are the usual complex coordinates, is defined as a harmonic map from $S^2 \mapsto \mathbb{CP}^{N-1}$. In other words, we assume that P is a classical solution of the two dimensional $\mathbb{CP}^{N-1}$ σ model [51] and hence, it satisfies the Euler-Lagrange equation

$$\left[\partial_\xi \partial_{\bar{\xi}} P, P\right] = 0. \tag{B.1}$$

If the projector P has the special form

$$P_0(h) = \frac{h \otimes h^\dagger}{|h|^2}, \tag{B.2}$$

where the vector $h \in C^N$ is holomorphic, *i.e.*

$$\frac{\partial h}{\partial \bar{\xi}} = 0, \tag{B.3}$$

then P_0 is also a solution of the first order self-dual equations

$$P_0\, \partial_\xi P_0 = 0 \qquad \text{and} \qquad \partial_\xi\, P_0\, P_0 = \partial_\xi P_0. \tag{B.4}$$

As we already mentioned in chapter 5, it is possible to construct further solutions of the $\mathbb{CP}^{N-1}$ model through Gramm-Schmidt orthogonalisation procedure. To do so, we need to introduce the operator P_+ which acts on any complex vector $u \in C^N$ as

$$P_+ u = \partial_\xi u - u\, \frac{u^\dagger\, \partial_\xi u}{|u|^2}. \tag{B.5}$$

If we take a holomorphic vector $h(\xi)$, with $P_0^+ h = h$, we can define by induction the N-component vectors

$$V_k = P_+^k h = P_+(P_+^{k-1} h), \qquad k = 0, \ldots, N-1, \tag{B.6}$$

where $V_N = P_+^N h = 0$. Using these vectors, we then construct a sequence of solutions of the $\mathbb{CP}^{N-1}$ σ model as follows

$$P_k = P(P_+^k h) = \frac{V_k V_k^\dagger}{|V_k|^2} = \frac{P_+^k h (P_+^k h)^\dagger}{|P_+^k h|^2}, \qquad k = 0, \ldots, N-1, \tag{B.7}$$

As the vectors V_k (B.6) are mutually orthogonal, *i.e.*

$$(P_+^k h)^\dagger P_+^l h = 0, \quad \text{if } k \neq l, \tag{B.8}$$

the corresponding projectors P_k will satisfy the orthogonality relations

$$P_k P_j = \delta_{kj} P_k \qquad \text{and} \qquad \sum_{k=0}^{N-1} P_k = 1. \tag{B.9}$$

In addition, when h is holomorphic, the following properties of the vectors V_k hold:

$$\partial_{\bar\xi} \left(P_+^k h\right) = -P_+^{k-1} h \frac{|P_+^k h|^2}{|P_+^{k-1} h|^2} \tag{B.10}$$

and

$$\partial_\xi \left(\frac{P_+^{k-1} h}{|P_+^{k-1} h|^2} \right) = \frac{P_+^k h}{|P_+^{k-1} h|^2}. \tag{B.11}$$

To prove property (B.10) we start by noting that when the vectors V_k have the form (B.6), then it quite easy to show that

$$|V_k|^2 = \left(\partial_{\bar\xi} V_{k-1}^\dagger\right) V_k. \tag{B.12}$$

From the orthogonality property (B.8) we have that $V_{k-1}^\dagger V_k = 0$ and hence,

$$\partial_{\bar\xi} \left(V_{k-1}^\dagger V_k\right) = \left(\partial_{\bar\xi} V_{k-1}^\dagger\right) V_k + V_{k-1}^\dagger \left(\partial_{\bar\xi} V_k\right) \;=\; 0. \tag{B.13}$$

If we multiply (B.13) from the left with V_{k-1} and use (B.12), we have

$$\begin{aligned} |V_{k-1}|^2 \left(\partial_{\bar\xi} V_k\right) &= -V_{k-1} |V_k|^2, \qquad \text{or equivalently} \\ \partial_{\bar\xi} V_k &= -V_{k-1} \frac{|V_k|^2}{|V_{k-1}|^2}, \end{aligned} \tag{B.14}$$

proving property (B.10).

To prove (B.11) we start from the left hand side

$$\partial_\xi \left(\frac{V_{k-1}}{|V_{k-1}|^2} \right) = \frac{\left(\partial_\xi V_{k-1}\right) |V_{k-1}|^2 - V_{k-1} \left(\partial_\xi V_{k-1}^\dagger\right) V_{k-1} - V_{k-1} V_{k-1}^\dagger \left(\partial_\xi V_{k-1}\right)}{|V_{k-1}|^4} \tag{B.15}$$

and by using the hermitian conjugate of (B.14) and the orthogonality property (B.8) we have

$$\begin{aligned}\partial_\xi\left(\frac{V_{k-1}}{|V_{k-1}|^2}\right) &= \frac{1}{|V_{k-1}|^2}\left(\partial_\xi V_{k-1} - \frac{V_{k-1}V_{k-1}^\dagger\,(\partial_\xi V_{k-1})}{|V_{k-1}|^2}\right)\\ &= \frac{V_k}{|V_{k-1}|^2}.\end{aligned} \tag{B.16}$$

Having constructed these special projectors P_k using the vectors V_k we would like to show that they are indeed solutions of the $\mathbb{CP}^{N-1}$ model (see [51] and references therein). We start by noting that the Gramm-Schmidt orthogonalisation procedure implies that the vectors V_k are constructed by the sequence of the holomorphic vectors

$$h,\ \partial_\xi h,\ \partial_\xi^2 h, \ldots,\ \partial_\xi^k h,\ \ldots \tag{B.17}$$

Let us define the normalised vectors obtained by the Gramm-Schmidt orthogonalisation of the sequence (B.17) as

$$a_1,\ a_2,\ \ldots,\ a_k, \ldots,\ a_N. \tag{B.18}$$

Consider now the a_k element of (B.17) and construct the projector

$$P = a_k\, a_k^\dagger. \tag{B.19}$$

We can also construct another projector Q as follows

$$Q = \sum_{i=1}^{k-1} a_i\, a_i^\dagger. \tag{B.20}$$

The projector, Q, can be thought of as a solution of the grassmannian model $G(k-1,N)$ (see reference [51] for further details). A grassmannian model $G(M,N)$ is the generalisation of the two dimensional $\mathbb{CP}^{N-1}$ σ model in terms of $N \times M$ matrix fields. When $M = 1$ these fields become N-component complex vectors and thus $G(M,N)$ reduces to the $\mathbb{CP}^{N-1}$ model. A solution of the $G(M,N)$ model can be obtained using a set of M linearly independent holomorphic vectors which are properly orthonormalised [51]. Since Q is constructed by such vectors (sequence (B.18)), we can consider it as a solution of $G(k-1,N)$ which satisfies the first order self-dual equations of this model (by analogy to the $\mathbb{CP}^{N-1}$ model). In other words,

$$\partial_{\bar\xi} Q\, Q = 0. \tag{B.21}$$

Similarly, the projector $P+Q$ is a solution of the self-dual equations of the $G(k,N)$ grassmannian model, *i.e.*

$$\left(\partial_{\bar{\xi}}(P+Q)\right)\,(P+Q)=0. \tag{B.22}$$

From the orthogonality properties (B.8),(B.10) and (B.11) it is easy to check that

$$\partial_{\bar{\xi}}a_j = a_{j-1}a_{j-1}^{\dagger}(\partial_{\bar{\xi}}a_j) + a_j a_j^{\dagger}(\partial_{\bar{\xi}}a_j) \tag{B.23}$$

and

$$\partial_{\xi}a_j = a_{j+1}a_{j+1}^{\dagger}(\partial_{\xi}a_j) + a_j a_j^{\dagger}(\partial_{\xi}a_j). \tag{B.24}$$

Using relations (B.23) and (B.24) we have that

$$\left(\partial_{\bar{\xi}}P\right)Q=0 \tag{B.25}$$

and

$$P\left(\partial_{\xi}Q\right)=\partial_{\xi}Q, \tag{B.26}$$

$$\left(\partial_{\bar{\xi}}Q\right)P=\partial_{\bar{\xi}}Q. \tag{B.27}$$

Substituting (B.25) and (B.27) to equation (B.22) we have

$$\left(\partial_{\bar{\xi}}P\right)\,P+\partial_{\bar{\xi}}Q=0 \tag{B.28}$$

and by hermitian conjugation,

$$P\left(\partial_{\xi}P\right)+\partial_{\xi}Q=0. \tag{B.29}$$

If we differentiate (B.28) with ∂_{ξ} and (B.29) with $\partial_{\bar{\xi}}$ and subtract them, we get

$$\left[\partial_{\xi}\partial_{\bar{\xi}}P,P\right]=0, \tag{B.30}$$

proving that the projector, P, is a solution of the Euler-Lagrange equations of the $\mathbb{CP}^{N-1}$ σ model.

There is one important remark that can be made at this point. The last vector V_{N-1} of the sequence (B.6) is, up to a unitary isorotation, equal to the complex conjugate of the vector h and hence, the projector P_{N-1} is an anti holomorphic projector. To prove this, we note that $V_N = P_+^N h = 0$ and by using properties (B.10) and (B.11) it is very easy to check that

$$P_{N-1}\left(\partial_{\bar{\xi}}\,P_{N-1}\right)=0 \tag{B.31}$$

Equation (B.31) implies that P_{N-1} satisfies the complex conjugate of the first order self-dual equations (B.4). However, as was previously mentioned, of the sequence of solutions of the $\mathbb{CP}_{N-1}$ model, only the holomorphic projector P_0 satisfies the self-dual equations. Hence, we can conclude that P_{N-1} is an anti holomorphic projector, *i.e.* it can be written in the form

$$P_{N-1} = \frac{\tilde{h}\tilde{h}^\dagger}{|\tilde{h}|^2}, \tag{B.32}$$

where $\tilde{h}$ is equal to the complex conjugate of h, up to an overall factor.

Finally there is another important property of the projectors P_k that we have used in chapter 5 in order to construct spherically symmetric solutions of the pure and the extended Skyrme model in $SU(N)$. There, we saw that this construction crucially depends on choosing the holomorphic vector h to be of the special form

$$h = (h_0, h_1, \ldots, h_{N-1})^t, \tag{B.33}$$

where

$$h_k = \xi^k \sqrt{C_k^{N-1}}, \tag{B.34}$$

and where C_k^{N-1} denotes the binomial coefficients. In this case,

$$\frac{|V_i|^2}{|V_{i-1}|^2} \propto (1 + |\xi|^2)^{-2}. \tag{B.35}$$

Using this last property, we saw that the angular dependence of the Euler-Lagrange equations of the model vanishes. As a result, one is left with $N-1$ ordinary differential equations that involve only the profile functions $g_i(r)$. Hence, the solutions of these equations, if they exist, are exact solutions of the $SU(N)$ model.

Property (B.35) was proved by Ioannidou et al. [49] using induction and in what follows we give this proof for reasons of completeness.

We start by noting that when the components of h are given by the form (B.34) then it is very easy to check that

$$|h|^2 = (1 + |\xi|^2)^{N-1}. \tag{B.36}$$

For the first projector $V_1 = P_+ h$ we have

$$V_1 = (\partial_\xi h) - \frac{hh^\dagger (\partial_\xi h)}{|h^2|}, \tag{B.37}$$

and hence,

$$\begin{aligned} |V_1|^2|h|^2 &= |h|^2|\partial_\xi h|^2 - \left|\partial_\xi |h|^2\right|^2 \\ &= (N-1)(1+|\xi|^2)^{N-3}|h|^2, \end{aligned} \tag{B.38}$$

or equivalently

$$|V_1|^2 = (N-1)(1+|\xi|^2)^{N-3}. \tag{B.39}$$

We now assume that $|V_k|^2 = \alpha(1+|\xi|^2)^{N-2k-1}$ and calculate $|V_{k+1}|^2$. We have that

$$V_{k+1} = (\partial_\xi V_k) - \frac{V_k V_k^\dagger (\partial_\xi V_k)}{|V_k^2|} \tag{B.40}$$

and hence,

$$|V_{k+1}|^2|V_k|^2 = |V_k|^2|\partial_\xi V_k|^2 - \left|\partial_\xi |V_k|^2\right|^2. \tag{B.41}$$

In addition,

$$\begin{aligned} V_k^\dagger (\partial_\xi V_k) &= \partial_\xi |V_k|^2 - \left(\partial_\xi V_k^\dagger\right) V_k \\ &= \partial_\xi |V_k|^2, \end{aligned} \tag{B.42}$$

where we used the complex conjugate of property (B.10) and the orthogonality of the projectors. From (B.42) we have that

$$\begin{aligned} |\partial_\xi V_k|^2 &= \partial_\xi \partial_{\bar\xi} |V_k|^2 - V_k^\dagger \partial_\xi \partial_{\bar\xi} V_k \\ &= \partial_\xi \partial_{\bar\xi} |V_k|^2 + \frac{|V_k|^4}{|V_{k-1}|^2}, \end{aligned} \tag{B.43}$$

where we also used the orthogonality properties (B.8) and (B.11). By substituting (B.43) to (B.41) we finally have

$$|V_{k+1}|^2 = \partial_\xi \partial_{\bar\xi} |V_k|^2 + \frac{|V_k|^4}{|V_{k-1}|^2} - \frac{\left|\partial_\xi |V_k|^2\right|^2}{|V_k|^2}. \tag{B.44}$$

and by assuming that $|V_{k-1}|^2 = \beta(1+|\xi|^2)^{N-2k+1}$, we get

$$|V_{k+1}|^2 = \gamma\,(1+|\xi|^2)^{N-2k-3}, \tag{B.45}$$

where $\gamma = \alpha(N-2k-1) + \frac{\alpha^2}{\beta}$. If we use induction again for (B.45), then it is quite easy to check that

$$|V_k|^2 = \frac{k!(N-1)!}{(N-1-k)!}\,(1+|\xi|^2)^{N-1-2k}, \tag{B.46}$$

proving that indeed

$$\frac{|V_i|^2}{|V_{i-1}|^2} \propto (1+|\xi|^2)^{-2}. \tag{B.47}$$

Bibliography

[1] I. Floratos and B.M.A.G. Piette. 'Multi-skyrmion solutions for the sixth order Skyrme model'. *hep-th/***0103126**, *To be published in Phys. Rev.*, **D 64**, (2001).

[2] I. Floratos and B.M.A.G. Piette. 'Spherically symmetric solutions of the 6th order $SU(N)$ Skyrme models'. *To be published in J. Math. Phys.*, (2001).

[3] T. H. R. Skyrme. 'A unified field theory of mesons and baryons'. *Nucl. Phys.*, **31**:556, (1962).

[4] G. 't Hooft. 'A planar diagram theory for strong interactions'. *Nucl. Phys.*, **B72**:461, (1974).

[5] E. Witten. 'Baryons in the $1/N$ expansion'. *Nucl. Phys.*, **B160**:57, (1979).

[6] E. Witten. 'Current algebra, baryons, and quark confinement'. *Nucl. Phys.*, **B223**:433, (1983).

[7] G.S. Adkins, C.R. Nappi, and E. Witten. 'Static properties of nucleons in the Skyrme model'. *Nucl. Phys.*, **B228**:552, (1983).

[8] G.S. Adkins and C.R. Nappi. 'Stabilization of chiral solitons via vector mesons'. *Phys. Lett.*, **137B**:251, (1984).

[9] A. Jackson, A.D. Jackson, A.S. Goldhaber, G.S. Brown, and L.C. Castillo. 'A modified skyrmion'. *Phys. Lett.*, **B154**:101, (1985).

[10] L. Marleau. 'The Skyrme model and higher order terms'. *Phys. Lett.*, **B235**:141, (1990).

[11] S. Dubé and L. Marleau. 'Phenomenological implications of a generalized Skyrme model'. *Phys. Rev.*, **D 41**:1606, (1990).

[12] L. Marleau. 'All orders skyrmions'. *Phys. Rev.*, **D 45**:1776, (1992).

[13] M.A. Halasz, R.D. Amado, and P. Protopapas. 'Two skyrmion dynamics with omega mesons'. *Phys. Rev.*, **D 61**:074022, (2000).

[14] C. J. Houghton, N. S. Manton, and P. M. Sutcliffe. 'Rational maps, monopoles and skyrmions'. *Nucl. Phys.*, B **510**:507, (1998).

[15] T.Ioannidou, B.Piette, and W.J.Zakrzewski. '$SU(N)$ skyrmions and harmonic maps'. *J.Math.Phys.*, **40**:6353, (1999).

[16] V.G. Makhankov, Y.P. Rybakov, and V.I. Sanyuk. *The Skyrme Model.* Springer-Verlag, (1993).

[17] M. Gell-Mann and Y. Neeman. *The Eightfold Way.* W.A. Benjamin, Inc, New York, (1964).

[18] O.W. Greenberg. 'Spin and unitary-spin independence in a paraquark model for baryons and mesons'. *Phys. Rev. Lett.*, **13**:598, (1995).

[19] M. Han and Y. Nambu. 'Three-triplet model with double $SU(3)$ symmetry'. *Phys. Rev.*, **B139**:1006, (1995).

[20] H.D. Politzer. 'Reliable perturbative results for strong interactions'. *Phys. Rev. Lett.*, **30**:1346, (1973).

[21] D.J. Gross and F. Wilczek. 'Ultraviolet behaviour of non abelian gauge theories'. *Phys. Rev. Lett.*, **30**:1373, (1973).

[22] D.J. Gross and F. Wilczek. 'Asymptotically free gauge theories I '. *Phys. Rev.*, **D8**:3633, (1973).

[23] D.J. Gross and F. Wilczek. 'Asymptotically free gauge theories II'. *Phys. Rev.*, **D9**:(1973), 980.

[24] M.E. Peskin and D.V. Schroeder. *An Introduction to Quantum Field Theory.* Addison-Wesley, (1995).

[25] L.H. Ryder. *Quantum Field Theory.* Cambridge University Press, (1996).

[26] F. Halzen and A.D. Martin. *Quarks and Leptons: An introductory course in Modern Particle Physics.* Wiley, (1984).

[27] J.B. Zuber and R. Stora (Eds). *Les Houches 1982, Recent Advances in Field Theory and Statistical Mechanics.* North-Holland Physics Publishing, (1982).

[28] E. Witten. 'The $1/N$ expansion in atomic physics'. *Recent developments in Gauge Theories, (ed) G 't Hooft et al (New York: Plenum)*, page 403, (1980).

[29] P.G. Drazin and R.S. Johnson. *Solitons: an introduction.* Cambridge University Press, (1989).

[30] R.H. Hobart. 'On the instability of a class of unitary field models'. *Proc. Phys. Soc. London*, **82**:201, (1963).

[31] G.H. Derrick. 'Comments on nonlinear wave equations as models for elementary particles'. *J. Math. Phys.*, **5**:1252, (1964).

[32] E.B. Bogomol'nyi. 'Stability of classical solutions'. *(Engl. Trans.) Sov. J. Nucl. Phys.*, **24**:449, (1976).

[33] T.H.R. Skyrme. 'A nonlinear field theory'. *Proc. Roy. Soc. London*, **A260**:127, (1961).

[34] C. J. Aitchison, C. M. Fraser, and P. J. Miron. 'Effective lagrangian for skyrmion physics'. *Phys. Rev.*, D **33**:1994, (1986).

[35] A. A. Adrianov. 'Bosonization in four dimensions due to anomalies and an effective lagrangian for pseudoscalar mesons'. *Phys. Lett.*, **157B**:425, (1985).

[36] A. A. Adrianov and Y.V. Novozhilov. 'Chiral bosonization in non abelian gauge theories'. *Phys. Lett.*, **153B**:422, (1985).

[37] L. Marleau. 'Modifying the Skyrme model: pion mass and higher derivatives'. *Phys. Rev.*, **D 43**:885, (1991).

[38] L. Marleau. 'A generating function for all orders skyrmions'. *Phys. Rev.*, **D 63**:036007, (2001).

[39] J.A. Neto. 'A note in the Skyrme model with higher derivative terms'. *hep-ph/**9402257**, J. Phys.*, **G 20**:1527, (1994).

[40] N.S.Manton. 'Is the $B = 2$ skyrmion axially symmetric ?'. *Phys. Lett.*, **B 192**:177, (1987).

[41] J.J.M. Verbaarschot. 'Axial symmetry of bound baryon number two solution of the Skyrme model'. *Phys. Lett.*, **B 195**:235, (1987).

[42] R.A.Battye and P. M. Sutcliffe. 'Symmetric skyrmions'. *Phys.Rev.Lett.*, **79**:363, (1997).

[43] R.A.Battye and P. M. Sutcliffe. 'Skyrmions, fullerenes and rational maps'. *hep-ph/***0103026**, (2001).

[44] B.L.Cohen. *Concepts of Nuclear Physics.* McGraw Hill Series in Fundamentals of Physics, (1971).

[45] I.Tanihata *et al.* 'Measurements of interaction cross sections and radii of He isotopes'. *Phys. Lett.*, **B160**:380, (1985).

[46] I.Tanihata *et al.* 'Measurements of interaction cross sections and nuclear radii in the light p-shell region'. *Phys. Rev. Lett.*, **55**:2676, (1985).

[47] P.Egelhof. 'Nuclear structure studies by direct reactions with radioactive beams'. *Acta Physica Polonica*, B **30**:487, (1999).

[48] J.Martorell, D.W.L.Sprung, and D.C.Zheng. 'Deuteron polarizability shifts and the deuteron matter radius'. *Phys. Rev.*, C **51**:1127, (1995).

[49] T.Ioannidou, B.Piette, and W.J.Zakrzewski. 'Spherically symmetric solutions of the $SU(N)$ Skyrme models'. *J.Math.Phys.*, **40**:6223, (1999).

[50] P. M. Sutcliffe and W.J.Zakrzewski. *'Skyrmions from Harmonic Maps'.* H. Aratyn and A.S.Sorin (eds.), Integrable Hierarchies and Modern Physical Theories, Kluwer Academic Publishers. Printed in the Netherlands, 2001, pages 215-241.

[51] W.J. Zakrzewski. *Low Dimensional Sigma models.* IOP, (1989).

[52] W.H.Press, S.A.Teukolsky, W.T.Vetterling, and B.P.Flannery. *Numerical Recipes in C, Second edition.* Cambridge University Press, (1992).